SURFACE DISCHARGE OF HEATED WATER

by

H. Stefan,
N. Hayakawa,
and
F.R. Schiebe

University of Minnesota
St. Anthony Falls Hydraulic Laboratory
Mississippi River at 3rd Avenue S.E.
Minneapolis, Minnesota 55414

for the

Office of Research and Monitoring
ENVIRONMENTAL PROTECTION AGENCY

Project #16130 FSU

December 1971

EPA Review Notice

This report has been reviewed by the Environmental Protection Agency and approved for publication. Approval does not signify that the contents necessarily reflect the views and policies of the Environmental Protection Agency nor does mention of trade names or commercial products constitute endorsement or recommendation for use.

PREFACE

The dissipation of heat from cooling water rejected by power generating plants has become a problem of great concern because of its ecological impact. Research efforts in the area of thermal pollution, thermal addition, calefaction, or whatever name may be used have been tremendously increased over the past decade. The St. Anthony Falls Hydraulic Laboratory has participated in these efforts, and several reports on related topics have preceded this one.

This volume is divided into three parts, each of which contains its own conclusions and recommendations, table of contents, series of figures and tables, and list of bibliographical references. The parts are as follows:

Part I: "Three-Dimensional Jet-Type Surface Plumes in Theory and in the Laboratory," by H. Stefan (Project Report No. 126, St. Anthony Falls Hydraulic Laboratory, University of Minnesota, December 1971), pages I-i through I-129 plus Appendices A and B.

Part II: "The Two-Dimensional Buoyant Surface Jet and the Internal Hydraulic Jump," by H. Stefan and N. Hayakawa (Project Report No. 127, St. Anthony Falls Hydraulic Laboratory, University of Minnesota, August 1971), pages II-i through II-55.

Part III: "Field Measurements in a Three-Dimensional Jet-Type Surface Plume," by H. Stefan and F. R. Schiebe (Project Report No. 128, St. Anthony Falls Hydraulic Laboratory, University of Minnesota, December 1971), pages III-i through III-35.

From these titles it is clear that the report deals with one particular aspect of the very complex thermal pollution problem. Emphasis is on flow, entrainment, and dilution of heated water effluents near surface outlets. The results are of significance for open-cycle operating systems and may also find application in the operation of cooling ponds and mixing chambers.

Part I: Three-Dimensional Jet-Type Surface Plumes in Theory and in the Laboratory

by

H. Stefan

December 1971

ABSTRACT

The steady flow of heated water from a channel into a reservoir or lake has been studied analytically and experimentally. A three-dimensional buoyant-jet-type model has been developed to predict the main trajectory, velocity, and temperature distributions in that portion of the plume in which the flow is dominated by the momentum and the buoyancy of the discharge and has free boundaries. The interaction between turbulent mixing, buoyant spreading, and surface cooling, which are crucial for the development of any thermal plume, can be illustrated with the aid of the model. The effects of weak cross currents and weak wind on the development of a surface plume are also incorporated into the model. The model does not apply to heated water discharges which cling to a shoreline due to a particular shoreline configuration or to wind or current conditions. The effects of cold water wedge penetration into an outlet channel can be accommodated by the model.

Experimental results on temperature and velocity distributions in free-jet-type three-dimensional thermal plumes have been used to verify some of the assumptions made in the numerical model, particularly those regarding Gaussian velocity and temperature distributions and lateral spread coefficients. In addition, the measurements have been used to illustrate changes in total flow rate, total heat storage, and dimensions of a surface plume. The distribution of temperatures, velocities, and Richardson numbers in an experimental surface plume has been illustrated using different types of contour plots. There is reasonable agreement between the results of the experiments and the proposed analytical prediction method.

CONTENTS

LIST OF FIGURES AND TABLES

LIST OF SYMBOLS AND UNITS

a	Standard deviation of velocity distribution in vertical plane through main trajectory [ft]
b	Standard deviation of velocity distribution at water surface [ft]
C	Drag coefficient [-]
C	Heat content [BTU]
c_1, c_2, c_3	Coefficients related to various functions for entrainment coefficient [-]
c_4	Coefficient designating turbulent spread of non-buoyant, circular, submerged jet [-]
c_5	Coefficient designating buoyancy induced lateral spread of plume [-]
c_6	= exp (-0.5)
c_7	Coefficient related to initial spread of contour of plume
c_p	Specific heat of water [BTU slugs^{-1} $^{o}F^{-1}$]
D	Drag force [lbs]
D_o	Hydraulic diameter of discharge channel [ft]
d	Depth [ft]
d_o	Depth at discharge channel [ft]
F	densimetric Froude number [-]
F	Force [lbs]
f_1, f_2, f_3, f_4, f_5	Values of specified integrals [-]

g	Acceleration of gravity (32.2 ft sec^{-2})
H	Heat flux [BTU sec^{-1}]
K	Entrainment coefficient [-]
K_s	Surface heat transfer coefficient [BTU ft^{-2} $^oF^{-1}$ hr^{-1}]
k	Constant concentration [-]
M	Momentum flux [lbs]
m	Number limiting depth of plume [-]
N	Number of steps
N_p	Number of positive values in a profile [-]
n	Number limiting width of plume [-]
Q	Volumetric flow rate [ft^3 sec^{-1}]
R	Radius of curvature of plume in horizontal plane [ft]
Re	Reynolds number
Ri	Richardson number
r	Distance from and perpendicular to main trajectory [ft]
s	Distance from virtual origin along main trajectory [ft]
T	Temperature [^oF]
t	Time [sec]
U_o	Average discharge velocity [ft sec^{-1}]
U_s	Constant stream or current velocity [ft sec^{-1}]
u	Flow velocity tangent to main trajectory [ft sec^{-1}]
v	Flow velocity perpendicular to main trajectory [ft sec^{-1}]
W	Wind velocity [ft sec^{-1}]
w_o	Width of discharge channel [ft]
x	Coordinate in direction perpendicular to current [ft]
y	Coordinate in direction of current [ft]
z	Depth [ft]

α	Angle between plume trajectory and current [degrees]
β	Angle between wind and current [degrees]
δ	Halfwidth to depth ratio of plume [-]
ϵ	Error
λ	Similarity parameter [-]
μ	Dynamic viscosity [lb sec ft^{-2}]
ϱ	Density of water [slugs ft^{-3}]
τ	Wind shear stress [lb ft^{-2}]
ϕ	Spread angle of contour [degrees]

Subscripts

a	air
c	contour
D	drag
E	equilibrium
e	experimental
f	friction
h	horizontal
i	control volume
i	element along main trajectory
j	element along vertical profile
ℓ	lake or ambient
n	net value
o	initial value
o	neutrally buoyant (for K only)
r	in r-direction
s	in s-direction
T	temperature
th	theoretical
u	velocity
v	vertical
w	wind

Superscript * differential with reference to ambient water

SECTION I

CONCLUSIONS

The study reported in Part I deals with the steady flow of heated water from a channel into a reservoir or lake. A three-dimensional buoyant-jet-type analytical model has been developed and compared with laboratory data. The model is based on the observation that a heated water surface discharge is initially dominated by the momentum and the buoyancy of the discharge. The absence of solid boundaries and the unhindered spread of the heated water are essential. The model will predict the main trajectory, the depth, and the width of the plume and the centerline velocities and temperatures in the plume. The model includes the effect of cold water wedge penetration into an outlet channel.

The method of calculation is such that the geometrical extent of the flow field which can be legitimately covered by a jet-type model (the nearfield) becomes apparent from the results. The experimental data which are reported and analyzed have been valuable as a guide to a physically meaningful analytical description of the flow. A spread parameter was used and its possible magnitude derived from experimental data.

Results obtained with the analytical model and from experiments show substantial initial dilution of effluents even when buoyancy and stratification are strong.

SECTION II

RECOMMENDATIONS

It is recommended that the effects of solid boundaries and strong winds on thermal plumes be further investigated both analytically and experimentally. A substantial change in the flow and turbulent mixing processes is induced when heated water is injected into strong cross currents or onshore winds. Further attention should be given to these circumstances.

SECTION III

INTRODUCTION

The possibility of ecological stresses on the aquatic environment produced by discharges of large quantities of heated water from industrial plants, particularly power generating plants, has been discussed by numerous authors. References [1,2,3,4,5]* are examples of such discussions. A large amount of information on the effects of heat on organisms is becoming available, and it indicates that future site selection and operating policy for power plants will be much more complex in the light of their variable impact on water ecology.

Temperature standards have been set by individual states under the guidance and supervision of the federal government. These standards have an important bearing on power plant site selection and mode of operation, especially when the standards are very restrictive. Mixing zones are often allowed near the heated water outfalls. Temperature standards are frequently defined in terms of a temperature increment between an ambient water temperature and the outlet temperature and in terms of a maximum discharge temperature, both of which must be met at the end of the mixing zone. It is therefore necessary to be able to predict in the planning stage the temperature decay in a mixing zone. The present investigation was concerned with that problem.

Heated water can be discharged into a natural body of water in many different ways. Frequently the discharge is from an open channel, and attention will be focused on this case.

*References for Part I are listed on pages I-125 through I-129.

SECTION IV

PREVIOUS STUDIES ON THERMAL PLUMES

The problem of heat dispersion in a body of water has been attacked theoretically, experimentally, and through site studies. A general solution method according to which point temperatures and velocities in all thermal plumes could be calculated has not been found. A few theoretical approaches have been tried, with some success, and laboratory and field measurements have been accumulated and interpreted. More such data will certainly be forthcoming.

Theoretical Studies

The surface plume problem has generally been treated theoretically as either a passive dispersion problem, as in Refs. [6,7,8], or a two-dimensional turbulent jet problem as in Refs. [9,10,11,12]. The plume has also been treated theoretically as a purely buoyant surface jet [13] and as a three-dimensional surface jet [14]. These theories apply to the near field only, where turbulence is generated by shear between discharge and ambient fluid. Both jet-type dispersion and passive dispersion in a free turbulent field are treated with various simplifying assumptions in Ref. [15]. There have also been a number of studies dealing with non-buoyant two- or three-dimensional jet discharges into cross-currents or co-current streams; Refs. [16] and [17] are examples.

Experimental Studies

Experiments with three-dimensional surface discharges of heated water into cold water tanks have produced temperature data in plumes for a great variety of outlet conditions. Numerous case studies have been made of specific power plants, as a recent compilation [18] shows, and there have also been a few investigations dealing with idealized geometrical boundary conditions and more fundamental aspects of plume formation [13,14,16,17,19,20,21,22]. In this context it is also pertinent to cite studies concerned with fresh water flows into saline bodies of water [23,24].

Model studies of specific power plant sites are, of course, useful in dealing with complicated geometrical boundary conditions. Although scale effects on turbulent mixing and entrainment are beyond control, each experimental plume can be considered a plume in its own right. Therefore, laboratory data are as useful as field measurements when they are used to formulate and examine deterministic prediction methods.

Field Measurements

Field measurements usually consist of sets of temperature data [25,26, 27,28,29]. In a few instances, current measurements have been carried out simultaneously [29]. Such measurements are, of course, very useful in the development of prediction techniques, especially if the discharge, ambient water, and meteorological conditions are measured simultaneously.

SECTION V

THEORETICAL STUDY

Concept of Analytical Plume Model

Power plants operating with open cooling water supply systems withdraw the cooling water from natural sources such as rivers, lakes, and the ocean. They use it once and discharge it at elevated temperatures back into the environment. The present study was concerned with the flow and dissipation of heat in the receiving body of water, with emphasis on lakes. The effects of currents and wind, surface cooling, and mixing are combined in a comprehensive numerical model.

Condenser cooling water temperatures generally range from 10° to 35°F above intake temperatures. Flow rates are of the order of from several hundred to several thousand cfs for the largest power plants presently in operation or under construction. When such large quantities of heated water are discharged into a lake, a so-called thermal plume is formed. If the environmental impact of heated water discharges is to be assessed, it is necessary to be able to predict the size of the plume, its temperature, and its flow characteristics.

At the point of discharge, usually at the end of an outlet channel, a heated water plume is basically a turbulent, incompressible jet of very large dimensions. It is characterized by an initial mass flux, momentum flux, buoyancy flux, and energy flux. As the water moves away from the surface outlet into a larger and colder body of water it will display some features which are familiar from high speed jet flows, such as entrainment of surrounding fluid by turbulent mixing. In the absence of both solid boundaries near the jet and external forces, the momentum flux will be conserved. Sometimes the effects of solid boundaries on the jet are felt rather strongly, however, and the conservation of momentum assumption does not apply. As the flow volume increases and the velocities in the jet decrease, the characteristics of the receiving body of water--in particular its currents and its turbulence--will be imprinted more and more on the jet. Eventually the jet flow will be altered to such an extent that the initial characteristics will be unrecognizable.

Simultaneously with the jet's development, the atmosphere has its effect on the thermal plume. There is an energy flux, reversible in direction, across any air-water interface. Usually heat energy is transmitted by evaporation, conduction, convection, and long-wave backradiation from the plume to the atmosphere, with the result that the heat flux carried by the plume decreases with distance from its point of discharge. Sometimes the direction of the heat flux is reversed. The water surface is also where the transfer of mechanical energy provided by wind takes place. Shear stresses at the water surface, wave generation, currents, and turbulence are very closely associated with the action of wind. From field studies it is well known that wind has an influence on the shape and extent of thermal plumes.

A third and very important aspect of thermal plumes is that of buoyancy and stratification. Since the density of fresh water decreases when the temperature is raised above 39.2°F, heated water will generally float when surrounded by colder water. This is also the case when sea water is used as a source of cooling water. Buoyancy will cause lateral spread of a plume beyond that produced by turbulent mixing. It will also tend to reduce or eliminate vertical mixing between a thermal plume and the underlying water. The thermal plume will thus display certain features which are typical for stratified flows.

Experimental studies and field measurements have revealed quite clearly the dual character of thermal plumes as turbulent jets and stratified flows. A simplified mathematical formulation will be given for the heated water plume problem in terms of a buoyant jet flow into a slow cross current under the effects of wind and surface cooling. The model will predict the main trajectory, the depth, the width, and the temperature distribution of the plume as well as the rate of heat dispersion.

Since the geometry of heated water outlet channels and shoreline configurations varies from one discharge to another, it is often advantageous to consider separately an outlet region, a near field, and a far field. In the outlet region, channel and lake shore geometries have a major effect on the flow and mixing in addition to the source characteristics of momentum and buoyancy flux. If the outlet and shore geometries are complicated, it may be necessary to study this zone separately using analytical or numerical methods or even physical model studies. The model which will now be discussed begins at the point from which solid boundaries have a negligible effect on the plume and considers essentially the flow in the near field.

The near field is that portion of the plume in which the dynamics are controlled by the momentum of the discharge and by external forces such as wind, shear, and well defined currents. The far field is that portion of the plume where the heated effluent is dispersed essentially by turbulent mixing and heat transfer mechanisms which are controlled by the overall hydrodynamic and thermodynamic characteristics of the receiving body of water, including specifically large-scale turbulence, existing stratification, and overall velocity patterns.

The theory to be presented considers a three-dimensional half-jet and the essential forces and processes contributing to its development. Since at the present time turbulent flow and transport processes are not understood completely enough to permit an exact solution for the three-dimensional turbulent flow in a thermal plume, the problem is formulated in terms of experimentally supported and mostly well documented semi-empirical relationships. Several of these are drawn from previous studies, but some new ones are also proposed. All relationships together constitute a mathematical model of the thermal plume.

Basic Equations

The theory approximates the real plume by a three-dimensional horizontal half-jet discharging at some angle α_o into an existing current as shown in Fig. 1. A finite shear stress produced by wind is assumed to exist at the water surface. The behavior of the heated water jet in a body of water of infinite extent will be examined. A real outlet is usually located at the shore, and the last assumption will be satisfied only if the current and wind patterns allow the jet to move away from the shoreline. A strong initial momentum and an offshore wind will generally help to produce such a situation.

In the analysis the thermal plume is described in terms of its main trajectory and its velocity and temperature distributions in cross sections perpendicular to the main trajectory. The main trajectory is the streamline through all points with maximum velocity at the water surface. The plume in this study is characterized by velocities and temperatures in excess of those of the surrounding water. The situation is shown schematically in Fig. 2.

The excess velocity and excess temperature distributions in a plane perpendicular to the main trajectory are assumed to be similar to each other when normalized with respect to centerline values (for velocity and temperature) and standard deviations (for distances from the main trajectory), respectively. The practical evaluations will be carried through with Gaussian distributions in both vertical and horizontal directions, although other distributions can be used as well without changing the essence of the procedure. Gaussian profiles approximate experimental data on submerged jets quite well [30,31,32] and have been used before in numerical models [9,11,30]. The velocity distribution is shown schematically in Fig. 2. Temperature and velocity measurements in surface plumes [20,21,22] support to some degree the use of Gaussian distributions in the description of three-dimensional plumes. An analysis of experimental data to this effect will be presented in a later section. Because of the complicated interaction between buoyancy and turbulence in a horizontally stratified flow, it is thought that under close scrutiny the similarity principle does not hold rigorously for the vertical distributions. This serious theoretical defect is fully realized, but appears not to be of overwhelming significance for the overall picture of a plume.

The spread of these Gaussian distributions, as measured by standard deviations, will be different in the horizontal and vertical directions because of buoyancy as evidenced by experimental and field data. The relative velocity and temperature distributions are therefore described by the equations

$$\frac{u^*(s,r,z)}{u^*(s,0,0)} = \exp\left[-\frac{1}{2}\left(\frac{r}{b}\right)^2\right] \exp\left[-\frac{1}{2}\left(\frac{z}{a}\right)^2\right] \qquad (1)$$

$$\frac{T^*(s,r,z)}{T^*(s,0,0)} = \exp\left[-\frac{1}{2}\left(\frac{r}{\lambda_h b}\right)^2\right] \exp\left[-\frac{1}{2}\left(\frac{z}{\lambda_v a}\right)^2\right] \qquad (2)$$

(21)

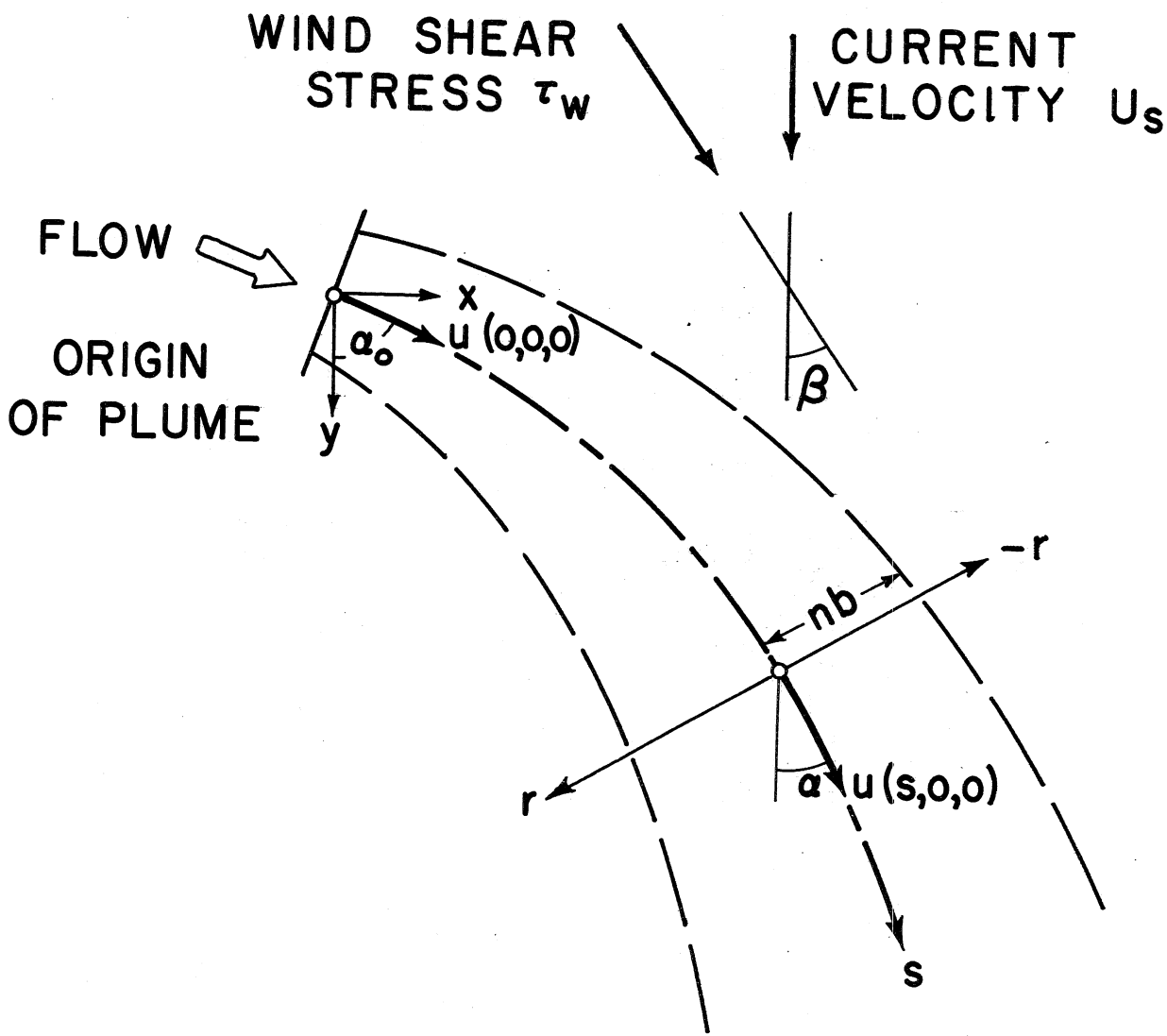

Fig. 1 - Definition Sketch - Plan View of Buoyant Surface Jet

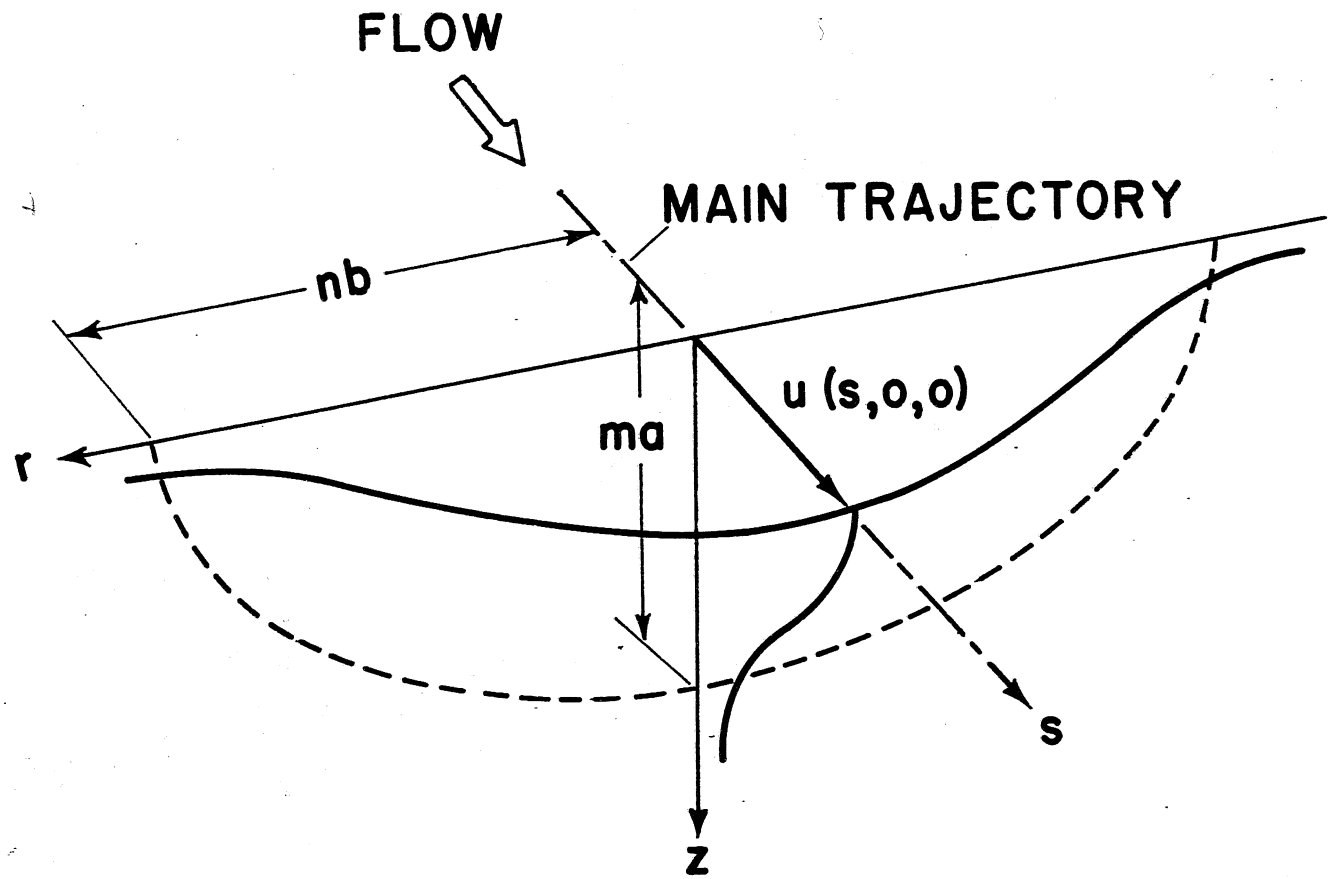

Fig. 2 - Definition Sketch - Cross Section of Buoyant Surface Jet

where $u^*(s,r,z)$ is the velocity at a point with the coordinates (s,r,z) relative to the surrounding fluid; $u^* = u - U_s \cos\alpha$, where u is the absolute local velocity in the plume, U_s is the velocity of a uniform current surrounding the jet, and α is the jet angle relative to the current; the thermal plume is assumed to move imbedded in the current; s is the distance from the beginning of the buoyant jet field which is usually located at or downstream from the actual outlet; r is the normal distance from the main trajectory; z is the depth below the water surface; and $T^*(s,r,z)$ is the water temperature at the same point as u^* relative to the surrounding water. Thus $u^*(s,0,0)$ and $T^*(s,0,0)$ are the relative velocities and temperatures, respectively, on the main trajectory and $a(s)$ and $b(s)$ are standard deviations indicating the lateral or vertical spread of the distributions; $T^* = T - T_\ell$ where T_ℓ is the water temperature in the impoundment.

All velocities in a cross section perpendicular to the main trajectory are assumed to be parallel to the tangent on the main trajectory, and λ_v and λ_h are similarity parameters. In the absence of buoyancy and for fully submerged axisymmetric jets $\lambda_v = \lambda_h = 1.16$ has been used in Ref. [30]. In buoyant surface jets the horizontal spread of momentum is produced in a somewhat different way than the vertical spread. The vertical spread is essentially by turbulent mixing, including the effects of buoyancy; the horizontal spread is by turbulent mixing plus buoyant spread. In a later section an analysis of some experimental data will be given. As will be explained, there is not enough justification at this time for choosing values of λ_h and λ_v different from each other or much different from unity. It is therefore tentatively proposed to use $\lambda_v = \lambda_h = 1.05$.

The local buoyancy force per unit weight will follow a distribution quite similar to that of the temperature. If the temperature range covered by a specific temperature profile is not too wide, the density relationship $\varrho = \varrho(T)$ can be approximated by a straight line and the density deficit distribution is then

$$\frac{\varrho^*(s,r,z)}{\varrho^*(s,0,0)} = \exp\left[-\frac{1}{2}\left(\frac{r}{\lambda_h b}\right)^2\right] \exp\left[-\frac{1}{2}\left(\frac{z}{\lambda_v a}\right)^2\right] \qquad (3)$$

Here $\varrho^* = \varrho_\ell - \varrho$ where ϱ is the actual local density and ϱ_ℓ is the density of the surrounding colder fluid (lake).

The density difference between the heated water in the jet and the cold water in the lake produces a loss in axisymmetry in a plane perpendicular to the main trajectory. In addition, the curvature of the main trajectory of a high-speed turbulent jet due to a cross current should result in a loss of symmetry with respect to a vertical plane (Fig. 3a) as shown in Refs. [34] and [35]. In buoyant and slowly moving surface jets (half-jets) with large radius of curvature of the main trajectory, however, the latter effect should be small. The

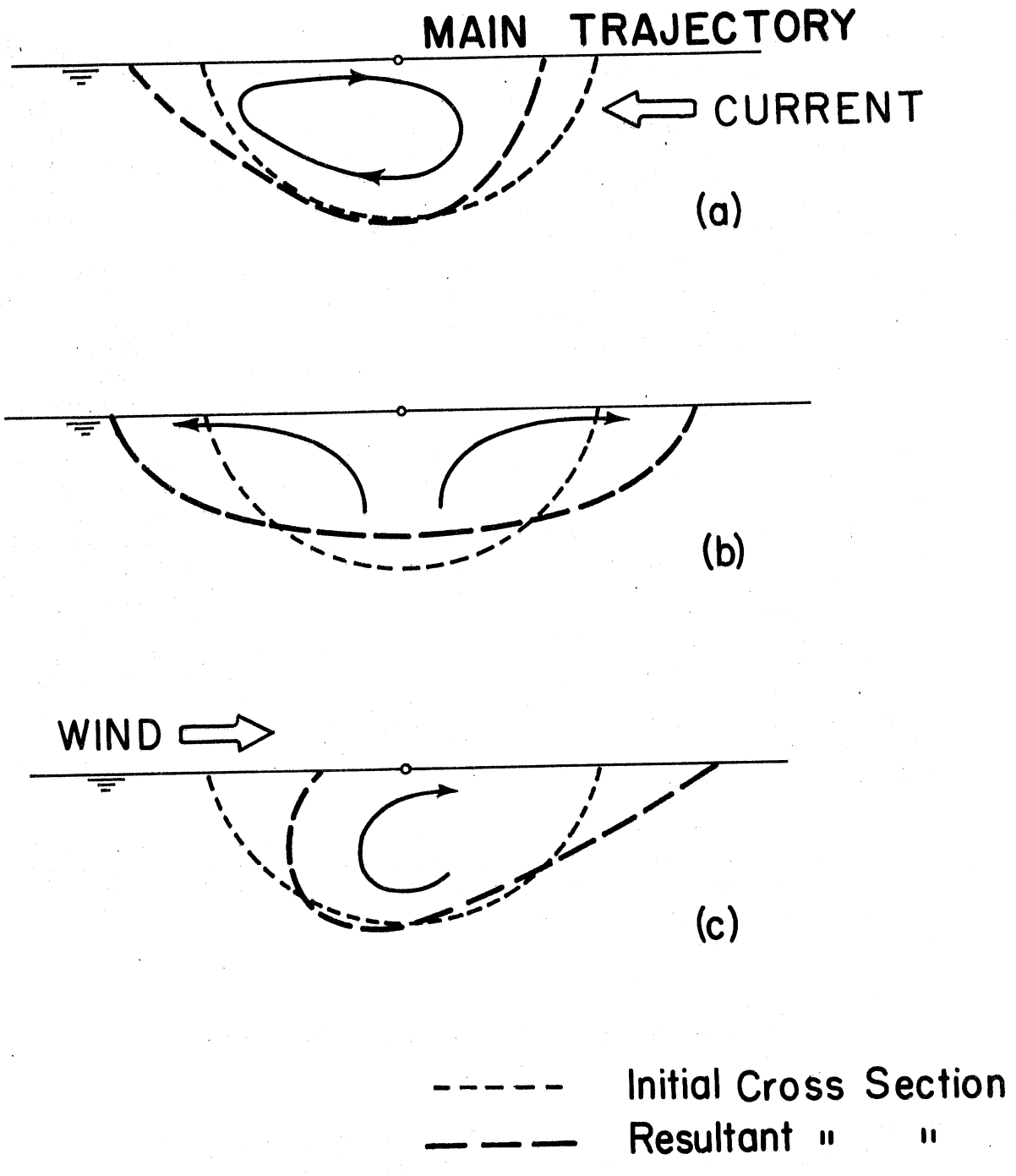

Fig. 3 - Deformation of Cross Section of Plume by (a) current, (b) buoyancy, (c) wind - Schematic

following analysis will therefore be concerned mainly with situations without vortex formation in the wake of the surface jet. This means in part that there is enough turbulence at a small enough scale remaining from the initial momentum of the jet or produced by external currents, as well as enough buoyancy at any cross section, to compensate for the current- or wind-produced destruction of the symmetry of a plume.

Because a thermal plume is also a density stratified flow, it may have features which are well known from open channel flow. In particular it is possible that the thickness of the plume is controlled from downstream rather than upstream. The conditions under which such a control exists in a two-dimensional plume have been discussed in Refs. [15] and [36]. It has been shown [36] that the value of the densimetric Froude number in a given cross section is the controlling dimensionless parameter. If the value of this number is larger than the critical value, a downstream control does not exist. The present model applies to flows for which the densimetric Froude number, as defined later in Eq. (4), remains larger than critical. This is likely to be the case under various natural conditions if there is a current, substantial wind drift, or simply sufficient heat transfer through the water surface. It may not hold true in a lake in which the surface cooling is temporarily very slow or if the wind drift is in direct opposition to the direction of discharge. An internal backwater effect will then become apparent as shown by Fig. 9c of Ref. [36] and by Fig. 12 of Ref. [20]. The internal Froude number can be defined as

$$F = F^* + F_s$$

where

$$F^* = \frac{u^*(s,0,0)}{\left[\frac{\varrho^*(s,0,0)}{\varrho}\, g\, \lambda_v\, a\right]^{1/2}} \quad \text{and} \quad F_s = \frac{U_s \cos\alpha}{\left[\frac{\varrho^*(s,0,0)}{\varrho}\, g\, \lambda_v\, a\right]^{1/2}} \tag{4}$$

To arrive at the basic equations it is necessary to examine the volumetric flux Q, the heat flux H, and the momentum flux M in cross sections perpendicular to the main trajectory of the plume. Since the fluid is incompressible and since the Boussinesq assumption can also be made because temperature-induced density differences are very small, the volumetric flux Q is used instead of the mass flux.

$$Q(s) = \int_{-\infty}^{\infty}\int_{0}^{\infty} u(s,r,z)\, dzdr \tag{5}$$

$$H(s) = \int_{-\infty}^{\infty}\int_{0}^{\infty} u(s,r,z)\ c_p \varrho T^*(s,r,z)\ dzdr \qquad (6)$$

$$M(s) = \int_{-\infty}^{\infty}\int_{0}^{\infty} \varrho u^2(s,r,z)\ dzdr \qquad (7)$$

These fluxes are of course absolute values. The limits of integration of Eqs. (5), (6), and (7) must match the velocity and temperature distributions of Eqs. (1) and (2), which provide for infinite width and depth of the jet. The real jet is limited in width, and therefore the limits of integration should be replaced by $-nb$ and $+nb$ for the r-direction and by zero and ma for the z-direction where n and m are finite numbers. The visual spreading angle of non-buoyant axisymmetric jets is of the order of 14° to 19° according to Refs. [37] and [38]. It is therefore physically meaningful to limit n and m values to $n = m = 3$.

The volumetric flux increases in the flow direction as a consequence of entrainment. The process is very complex. In the initial stage of the plume's development, turbulence is produced mostly by the shearing motion between the heated water jet and the surrounding cold water. In such a flow it has been shown [32] that the rate of entrainment is proportional to the velocity of the main jet relative to its surroundings. Application of the entrainment principle to the buoyant half-jet yields

$$\frac{dQ(s)}{ds} = K\, u^*(s,0,0)\, \frac{(a+b)\pi\sqrt{2}}{2} \qquad (8)$$

The eddies which produce this kind of mixing are on the same geometrical scale as the jet itself. For a neutrally buoyant, fully submerged, axisymmetric turbulent air jet $K = 0.057$ was found to match experimental data [33] best, while a study with liquid jets [38] resulted in $K = 0.059$. $K = 0.082$ is adequate for axisymmetric buoyant plumes with vertical axes [31]. The same value was used in Ref. [33] to match experiments on buoyant plumes with curvilinear main trajectories. $K = 0.089$ has been used for buoyant slot jets [30]. In both two- and three-dimensional situations K was independent of distance from the source, and a comparison of experimentally measured flow rates with the predicted ones was used in support of this hypothesis. In addition, the same amount of entrainment occurred per unit length of jet contour in a given cross section because of the axisymmetry of the flow. Neither of these assumptions is applicable to the horizontal buoyant surface jet, because its entrainment is a function not only of the centerline velocity, but also of the degree of stratification. It is believed that the entrainment principle is still useful, but it must be applied in a

modified form. A variable entrainment coefficient along the contour of the jet must be used. Equation (8) specifies a semi-elliptical contour of the half-jet. Vertical entrainment through the bottom part of the surface jet is inhibited by buoyancy, while horizontal entrainment through the sides of the half-jet is not. Since the real distribution of K values along the contour is unknown, an approximation is used. It is proposed to use a constant horizontal entrainment parameter $K_h = 0.059$. Because density stratification inhibits turbulence, vertical entrainment must be equal to or smaller than the horizontal entrainment, dependent on some stratification parameter. It has been shown [39,40,41] that an overall Richardson number in terms of an overall depth, average velocity, and average density differential is an adequate stratification parameter. Since this number, raised to the power (-2), is equivalent to a densimetric Froude number, the dimensionless parameter F^* as defined in Eq. (4) has been retained as a stratification parameter in this model. Experimental data on the effects of stratification on vertical entrainment are relatively scarce. The field data reported in [41] and the laboratory data reported in [42] and [43] are probably the best known, and various ways of fitting these have been proposed. A short review made in 1969 [44] shows that relationships of the form

$$\left.\begin{aligned} K_v/K_o &= \left(1 + \frac{c_1}{(F^*)^2}\right)^{-a_1} \\ K_v/K_o &= \left(1 - \frac{c_2}{(F^*)^2}\right)^{a_2} \end{aligned}\right\} \qquad (9)$$

$$K_v/K_o = e^{-c_3/(F^*)^2}$$

have been used as best fits with available measurements. Here a_1, a_2, c_1, c_2, and c_3 are positive real numbers and K_o is the eddy exchange coefficient in neutrally buoyant flow. A restriction on Eq. (9) is, of course, that $0 < K_v/K_o < 1.0$. The relationship retained in this study, which fits experimental data from Ref. [42], is, as shown in Fig. 4,

$$\frac{K_v}{K_h} = 1.0 - 1.33 \log \left(\frac{6.32}{F^*}\right) \qquad (10)$$

where K_h is the horizontal entrainment parameter. It is applied in the range $1.12 < F^* < 6.32$ and covers the transition of the entrainment coefficient in the range $0 < K_v/K_h < 1.0$. In Fig. 4 K_v/K_h was plotted on a linear scale because it is believed that the customary logarithmic

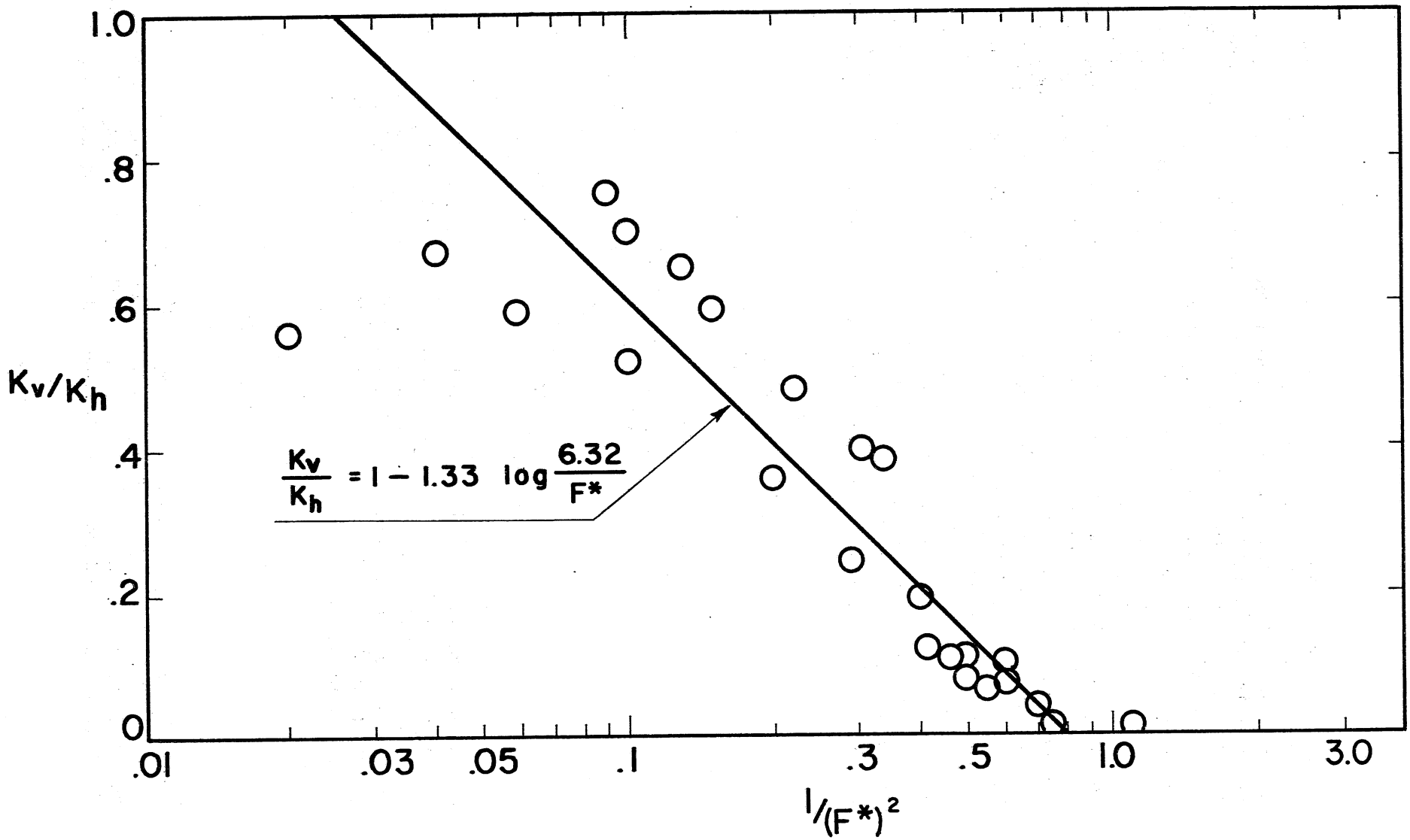

Fig. 4 - Fit of Equation for Vertical Entrainment Coefficient with Experimental Data from Ellison and Turner [42]

distortion of that scale tends to result in too much emphasis on the low values in the fitting process. It is believed that the horizontal entrainment also depends to some extent on the degree of stratification. For lack of experimental data it was not found possible to express this relationship in quantitative form.

If the driving force producing vertical entrainment is not the momentum of the jet, but the shear stress produced by wind blowing over the water surface, Eq. (10) can no longer be applied. It has been shown in Refs. [43] and [45] how an entrainment coefficient can be obtained in that particular situation.

Another change must be made in the horizontal entrainment coefficient to accommodate the turbulence inherent in the ambient current in which the thermal plume is embedded. An entrainment parameter related to the characteristics of the ambient current must then be used. Experiments on jet discharges into co-current streams indicate that entrainment is larger than for jets discharged into stagnant environments, but it appears very difficult at this time to express observations in quantitative form.

Circular jets discharged into a cross current have been found to entrain much more ambient fluid than jets discharged into stagnant fluid. Entrainment coefficients as high as 0.4 and 0.5 have been reported [46]. The increase is caused by a pair of large vortices which form in the cross section of the plume perpendicular to the main trajectory as shown, for example, in Ref. [34]. In a surface jet only one vortex exists, as shown in Fig. 3a. The cross current, which causes the deflection of the main trajectory of the plume, is responsible for the internal vortex-type circulation in the plume. A horizontal entrainment coefficient variable with the radius of curvature of the main trajectory may therefore be used. Based on available experimental and field data, an approximate relationship $K_h = K_h(R)$ may be formulated. When such a relationship is applied to a surface plume, however, there is an additional complication, because buoyancy will oppose the onset of an internal vortex-type circulation pattern. After the internal circulation occurs, the assumed Gaussian distributions of temperature and velocity will be destroyed. This analysis is therefore restricted to situations with sufficient buoyancy or large enough radii of curvature to prevent internal circulation. Tentative bounds are $F^* < 6.3$ and $R/b > 100$, with smaller values of R/b acceptable as F^* decreases.

It is proposed to calculate an average entrainment coefficient K for each cross section from the relationship

$$K = \frac{K_h a + K_v b}{a + b} \tag{11}$$

where $a(s)$ and $b(s)$ are used as measures of the relative depth and width of the plume, respectively.

As the plume moves away from the outlet, the total flow rate increases by turbulent entrainment, and the plume dimensions also increase. It is proposed to use the relationships

$$\left(\frac{db}{ds}\right)_T = c_4 \frac{u^*(s,0,0)}{u^*(s,0,0) + U_s \cos \alpha} \tag{12}$$

and

$$\left(\frac{da}{ds}\right)_T = \left(\frac{K_v}{K_h}\right)^{1/2} \left(\frac{db}{ds}\right)_T \tag{13}$$

to describe the increase in geometrical size of the plume cross section. The first equation implies that the lateral, turbulence-induced spread of the plume is the same as that for non-buoyant jets except that the absolute spreading angle is distorted by the velocity of the surrounding current into which the plume is being injected. The second equation implies that the vertical and horizontal spreading ratio is closely related to the vertical and horizontal mixing ratio. This hypothesis is an extension of non-buoyant jet results to buoyant surface jets. The coefficient c_4 is the spreading angle of a jet in a stagnant reservoir without buoyancy effects. In a three-dimensional jet $c_4 = 0.081$ [37].

The thermal plume will spread laterally not only by turbulent mixing, but also under the effect of buoyancy, as shown in Fig. 3b. In this process some fluid is removed from the center of the plume and moved laterally toward the edges of the plume. An internal circulation pattern with a horizontal peak velocity at some distance from the main trajectory will result (Fig. 3b). Buoyancy may tend to restore the symmetry of the flow lost due to current or wind action. The rate of lateral spread due to buoyancy can be approximated using an equation of the form

$$\left(\frac{db}{dt}\right)_B = c_5 \left[g\, a\, \lambda_v \frac{\varrho^*(s,0,0)}{\varrho} \right]^{1/2} \tag{14}$$

which is analogous to that used in the analysis of unsteady density currents [47]. This equation has been used before to describe the lateral spread [12].

At a distance b from the main trajectory the forward velocity is $u(s,b,0)$. The horizontal buoyancy-induced angle of spread at this point should be

$$\left(\frac{db}{ds}\right)_B = \left(\frac{db}{dt}\right)_B \frac{1}{u(s,b,0)} \tag{15}$$

Hence
$$\left(\frac{db}{ds}\right)_B = \frac{c_5}{u(s,b,0)}\left[g\, a\lambda_v \frac{\rho^*(s,0,0)}{\rho_o}\right]^{1/2} \tag{16}$$

Since
$$u(s,b,0) = c_6\, u(s,0,0) = c_6(u^*(s,0,0) + U_s \cos\alpha) \tag{17}$$

where $c_6 = \exp(-0.5)$ is a coefficient related to the Gaussian velocity distribution, the above equation reduces, using Eq. (4), to

$$\left(\frac{db}{ds}\right)_B = \frac{c_5}{c_6}\frac{1}{F} \tag{18}$$

Conservation of mass in a cross section requires that as the width of the plume increases at the rate given by Eq. (13), the depth decreases; this requirement is satisfied by the relationship

$$\left(\frac{da}{ds}\right)_B = -\frac{a}{b}\left(\frac{db}{ds}\right)_B \tag{19}$$

Equations (18) and (19) represent, respectively, the lateral and the vertical spread due to buoyancy.

The interaction between spread by buoyancy and spread by mixing is complicated. It is proposed to consider the possibility that the effects of turbulence and buoyancy on spreading are additive. It is conceivable that the lateral spreading process also influences the formation of turbulence in the shear zone between the jet fluid and the surrounding fluid, but if this is the case it is impossible to take it into consideration at the present time. The total spread of the jet in the surrounding fluid must be of the order of

$$\frac{db}{ds} = \left(\frac{db}{ds}\right)_B + \left(\frac{db}{ds}\right)_T \tag{20}$$

$$\frac{da}{ds} = \left(\frac{da}{ds}\right)_B + \left(\frac{da}{ds}\right)_T \tag{21}$$

The half-width-to-depth ratio of the plume after a step length ds will have changed from b/a to

$$\delta = \frac{b + db}{a + da} \tag{22}$$

The rate of change of the heat flux is equal to the rate of heat loss to the atmosphere. The unit rate of surface heat transfer can be found [48] from a relationship of the form

$$H_n = K_s[T(s,r,0) - T_E] \tag{23}$$

where the coefficient of surface heat transfer K_s and the equilibrium temperature T_E are essentially functions of the prevailing meteorological conditions: solar radiation, wind velocity, air temperature, and relative humidity. The gradient of the total heat flux in the main direction of the trajectory must be balanced by the heat flux through the water surface:

$$-\frac{dH(s)}{ds} = \int_{-nb}^{nb} H_n \, dr = K_s \int_{-nb}^{nb} [T(s,r,0) - T_E] dr \tag{24}$$

In addition to mixing, spreading, and cooling, the momentum flux must be considered separately with regard to its components in the x- and the y-direction or in the s- and r-directions, all of which are shown in Fig. 1. The rate of change of momentum flux in the s- and r-directions is equal to the force components (forces per unit length) acting on the control volume.

$$\left.\begin{aligned} \frac{dM_s}{ds} &= \Sigma F_s \\ \frac{dM_r}{dr} &= 0 = \Sigma F_r \end{aligned}\right\} \tag{25}$$

External forces which cause changes in momentum flux are produced by wind shear stress at the water surface, dynamic pressures due to the ambient current, and frictional forces which do not result in entrainment. The latter restriction is necessary, as illustrated by the different effects of free and solid boundaries on submerged jets. On a free boundary, frictional forces are translated into entrainment, and no loss in total momentum results from frictional action. A solid boundary does not allow entrainment and will cause a loss in total momentum flux.

A plume without any turbulent entrainment must be laminar in character on all its boundaries. If the resultant shear force in this case is $D_{f\ lam}$, the shear force for the partially mixing plume is approximately

$$D_f = D_{f\ lam} \frac{K_h - K}{K_h} \tag{26a}$$

The lower and upper bounds for D_f are thus zero and $D_{f\ lam}$. The value of $D_{f\ lam}$ can be approximated using Newton's shear law in conjunction with the maximum velocity gradients perpendicular to the contour of the plume to find local shear stresses. Integration of the shear stresses along the contour will result in a force per unit length

$$D_{f\ lam} = -1.965\ \mu\ e^{-1/2} \left(\frac{a}{b} + \frac{b}{a}\right) u^*(s,0,0) \tag{26b}$$

Most often this force will be small compared to other external forces.

The external force resulting from the wind shear stress τ_w on a surface strip of unit length is found from the relationship

$$F_w = 2nb\ \tau_w \tag{27}$$

Numerous empirical relationships have been reviewed for the calculation of wind shear stress from wind velocity data [49,50], and these can be selectively incorporated into the model. A surface stress due to wind transverse to the main trajectory will also tend to stretch the width of the plume. A large-scale eddy with water velocities at the surface in the direction of the wind shear stress will be produced as schematically shown in Fig. 3c. If such a circulation appears, it will tend to destroy the assumed temperature distribution in the model. It is therefore not included in this analysis. It should be mentioned that the wind may blow at any angle β with reference to the x-axis, as is shown in Fig. 1.

Equation (27) does not include wind effects on the cold water, because these are contained in the specifications of the external current into which the heated water is discharged. This is meaningful for two reasons. First, the cold water currents in a body of water receiving thermal effluents frequently depend not only on wind, but also on the shore and bottom topography. In fact, the relationship between currents and wind is quite complex and must be investigated apart from the thermal plume problem. The plume itself is considered to be embedded in the cold water and subject to separate wind action. The second reason is the observation that the cold water current sometimes represents a much larger mass flux than the heated water discharge. The longshore currents in the Great Lakes and the flow in impounded rivers can be cited as examples. These masses of water are less susceptible to motion by wind than the buoyant surface jet which frequently spreads out as a thin layer on top of such a current. A substantial amount of

time is required to reach a steady wind generated current in a large lake.

The current into which a plume discharges produces a dynamic pressure normal to the direction of the main trajectory and also a shear stress parallel to it. If the thermal plume is approximated by a solid body somewhat similar to a bent half-cylinder, the dynamic pressure forces will produce a form drag

$$D_D = C_D \frac{\varrho(U_s \sin \alpha)^2}{2} a \tag{28}$$

perpendicular to the main trajectory and a friction drag

$$D_f = C_f \frac{\varrho(u^*(s,0,0))^2 (b + a)\pi\sqrt{2}}{2} \tag{29}$$

parallel to the main trajectory. The friction forces given in Eqs. (26a) and (29) are of course the same. Equation (26a) may be easier to use than Eq. (29) because of the friction coefficient C_f. The form drag coefficient C_D in Eq. (28) was taken as equal to unity because of the semi-elliptical shape of the plume.

The change in momentum flux must also account for the original momentum of the entrained fluid, meaning $\frac{dQ}{ds} \varrho U_s \cos \alpha$ in the s-direction and $\frac{dQ}{ds} \varrho U_s \sin \alpha$ in the r-direction.

Pressure (buoyancy) forces in the direction of the main trajectory are not included in the analysis. The buoyancy force in any cross section is $g \int_0^{ma} \int_{-nb}^{nb} \varrho^*(s,r,z)\, zdz$ and can be calculated from the density deficit distribution given in Eq. (3). It can be shown that this value is also equal to $0.33\, g\lambda_v f_5\, \varrho^*(s,0,0)\, ab$. The value of this quantity is usually less than one per cent of the momentum flux of the jet. The net longitudinal buoyancy force acting on a control volume in the plume is $0.33\, g\lambda_v f_5 \frac{d[\varrho^*(s,0,0)ab]}{ds}$ which is usually negligible in relation to the momentum flux.

Summarizing, the momentum equations in terms of all external forces are

$$\frac{dM}{ds} = D_f + F_w \cos(\beta - \alpha) + \frac{dQ}{ds} \varrho U_s \cos \alpha \tag{30}$$

$$\frac{dM}{dr} = -\frac{dQ}{ds} \varrho U_s \sin \alpha = -\frac{M}{R} + D_D - F_w \sin(\beta - \alpha) \tag{31}$$

The radius of curvature of the main trajectory is

$$R = \left[\frac{1 + (y')^2}{y''}\right]^{3/2} \tag{32}$$

where $y(x)$ is the equation of the main trajectory in the x-y-plane.

The curvature of the main trajectory is also associated with a change of the flow direction α. Considering a length element ds,

$$d\alpha = \frac{ds}{R} \tag{33}$$

will be a good approximation for the change in angle.

All secondary circulation patterns shown in Fig. 3 tend to destroy the Gaussian velocity and temperature distributions. It can be speculated that the result will often be a more uniform temperature distribution within the plume, but there is no proof of this. Certainly, all the above circulation patterns are superimposed on the main motion of the plume along the main trajectory, and frequently on each other as well. Thus a theoretical argument for the use of symmetrical temperature and velocity profiles such as those used in the preceding section cannot be given. However, experiments in the laboratory and in the field support the assumption.

Solutions of the Basic Equations

The basic equations of the previous sections are solved by an explicit, finite-difference, forward-stepping method. Calculations of the volumetric, heat, and momentum fluxes as defined previously were made using the following formulations:

$$Q_i = u_i a_i b_i f_1 + \frac{\pi}{2} U_s \cos \alpha_i \, ma_i \, nb_i \tag{34}$$

$$H_i = T_i u_i s_i b_i f_2 + T_i U_s \cos \alpha_i \, a_i b_i \, f_4 \tag{35}$$

$$M_i = \rho u_i^2 \, a_i b_i \, f_3 + 2\rho U_s \cos \alpha_i \, u_i \, a_i b_i \, f_1 + \rho \frac{\pi}{2} U_s^2 \cos^2 \alpha_i ma_i nb_i \tag{36}$$

where the subscript i refers to a particular cross section at distance s from the origin of the plume, u_i is equal to the excess-centerline velocity $u^*(s,0,0)$, T_i is equal to the excess-centerline temperature $T^*(s,0,0)$, and the coefficients f_1 through f_4 are constants equivalent to the following definite integral values:

$$f_1 = \frac{1}{a_i b_i} \int_{-nb_i}^{nb_i} \int_{0}^{ma_i} \left\{ \exp\left[-\frac{1}{2} \left(\frac{r}{b_i} \right)^2 \right] \exp\left[-\frac{1}{2} \left(\frac{z}{a_i} \right)^2 \right] \right\} dr dz$$

$$= \pi \, \mathrm{erfn}\left(\frac{n}{\sqrt{2}} \right) \mathrm{erfn}\left(\frac{m}{\sqrt{2}} \right) \tag{37}$$

$$f_2 = \frac{1}{a_i b_i} \int_{-nb_i}^{nb_i} \int_{0}^{ma_i} \left\{ \exp\left[-\frac{1}{2}\left(\frac{r}{b_i}\right)^2\right] \exp\left[-\frac{1}{2}\left(\frac{z}{a_i}\right)^2\right] \exp\left[-\frac{1}{2}\left(\frac{r}{\lambda_h b_i}\right)^2\right] \right.$$

$$\left. \exp\left[-\frac{1}{2}\left(\frac{z}{\lambda_v a_i}\right)^2\right] \right\} dr\,dz = f_1 \frac{\lambda_v \lambda_h}{\lambda_v \lambda_h + 1} \tag{38}$$

$$f_3 = \frac{1}{a_i b_i} \int_{-nb_i}^{nb_i} \int_{0}^{ma_i} \left\{ \exp\left[-\frac{1}{2}\left(\frac{r}{b_i}\right)^2\right] \exp\left[-\frac{1}{2}\left(\frac{z}{a_i}\right)^2\right] \right\}^2 dr\,dz$$

$$= \frac{\pi}{2} \operatorname{erfn}(n) \operatorname{erfn}(m) \tag{39}$$

$$f_4 = \frac{1}{a_i b_i} \int_{-nb_i}^{nb_i} \int_{0}^{ma_i} \left\{ \exp\left[-\frac{1}{2}\left(\frac{r}{\lambda_h b_i}\right)^2\right] \exp\left[-\frac{1}{2}\left(\frac{z}{\lambda_v a_i}\right)^2\right] \right\} dr\,dz$$

$$= f_1 \lambda_v \lambda_h \tag{40}$$

Values of f_1 through f_4 can also be calculated if other than Gaussian velocity and temperature distributions are used.

Basic input parameters include the initial flow rate Q_o, the initial depth a_o, the initial momentum flux M_o, the outlet temperature T_o, the lake temperature T_ℓ, the current velocity U_s, and the outlet angle α_o with respect to the current direction. If there is wind, its direction β and the shear stress on the water surface τ_w which it produces are specified. Since τ_w must be calculated from wind speed, it is possible to include such calculations in the program. The wind speed W at a specified altitude (e.g., 30 ft) is then an input variable.

Prediction of surface heat loss requires specification of the equilibrium temperature T_E and the surface heat transfer coefficient K_s. These can be calculated from semi-empirical relationships [51]. If the actual calculations are again transferred into the program, the necessary input values must include solar radiation H_s, dew point temperature T_D, and wind speed W.

The step length d_s and the number of steps must be chosen. Values approximately equivalent to the outlet depths were chosen for the step length. The number of steps depends, of course, on the size of the flow field to be investigated.

The set of equations can be solved numerically in a meaningful manner and at little cost in computer time by extrapolating forward from one cross section to another starting at the outlet. The process is the same as that used in backwater profile computations in supercritical channel flows. The procedure is justified by the fact that a heated water surface jet as described herein is an internally supercritical (or at least critical) three-dimensional flow. The heated water surface jet may lose this property at some distance downstream from the outlet. The centerline densimetric Froude number defined in Eq. (4) can be used as an indicator. Anticipating results to be shown later, it appears that the critical densimetric Froude number value is in the vicinity of 3.0. The analysis of the thermal plume using a heated jet type model and the procedure described herein should not be carried on if the densimetric Froude number values are less than critical. The physical significance of this statement is relatively simple: The flow should not be considered a jet flow if its momentum has become small compared to the buoyant forces. The magnitude and direction of external forces thus have great influence on the size of the area in which the analytical jet-type flow model can be applied. By definition, the area is considered equivalent to the nearfield. Onshore wind or currents may reduce the nearfield considerably, while longshore currents and offshore winds may stretch it.

Effects of the farfield or downstream controls on heated water surface jets have been reported for two-dimensional flows [15,36,52] and will be further investigated in Part II of this report.

Details of the numerical computations can be gathered from the computer program given in Appendix A. The following explanations will be helpful: The initial conditions as described above are used to compute an initial plume width b_o and centerline velocity u_o such that the initial flow rate and the initial momentum flux are as specified. Equations (34) and (36) are used for that purpose. Then the equations given earlier are solved in a specific order. First the entrainment is found from Eq. (8) with the aid of Eqs. (10) and (11). Then $Q_{i+1} = Q_i + dQ_i$. The heat loss dH_i is found from Eq. (24) in the form

$$-dH_i = [T_i b_i f_5 + 2(T_\ell - T_E) n b_i] \frac{K_s ds}{c_p \varrho} \tag{41}$$

$$\text{where} \quad f_5 = \frac{1}{b_i} \int_{-nb_i}^{nb_i} \exp\left[-\frac{1}{2}\left(\frac{r}{\lambda_h b_i}\right)^2\right] dr = \lambda_h \sqrt{2\pi}\, \text{erfn}\left(\frac{n}{\sqrt{2}}\right) \tag{42}$$

Then $H_{i+1} = H_i + dH_i$. Equation (30) is then used to evaluate the change in momentum flux in the direction of the main trajectory and Eq. (31) to find the radius of curvature of the main trajectory R_i. Then $M_{i+1} = M_i + dM_i$ and with the radius of curvature from Eq. (31), the change in the trajectory angle $d\alpha_i$ can be calculated using Eq. (33).

$$d\alpha_i = R_i \, ds \tag{43}$$

Then $\alpha_{i+1} = \alpha_i + d\alpha_i$.

The plume characteristics in the (i+1)-th cross section--in particular the standard deviations a_{i+1} and b_{i+1}, the centerline velocity u_{i+1}, and the centerline temperature excess T_{i+1}--can be found from the previously calculated fluxes Q_{i+1}, M_{i+1}, and H_{i+1} in conjunction with the spread characteristics of Eqs. (20), (21), and (22). Simultaneous solution of Eqs. (34) and (36) for the (i+1)-th values instead of the i-th gives u_{i+1} and the area $(a_{i+1}\, b_{i+1})$, and the individual values of the (i+1)-th standard deviations are then found using Eq. (22). Prior to this, Eqs. (12) through (21) must be solved for each individual step. The centerline temperature T_{i+1} can then be found directly from Eq. (35). After completion of all these calculations, the orientation of the main trajectory and the velocity and temperature distributions in the (i+1)-th cross section are known. If the calculations are repeated for N steps, the characteristics of a whole plume can be found. The described process is simple and explicit, and changes in step lengths have little effect on the results if the step length remains of the order of the initial depth.

The limitations of the model described lie, of course, in the assumptions made initially: similarity of all profiles, specific lateral spreading patterns regardless of wind and current conditions, and absence of solid boundaries. The coefficients used are derived from a rather small number of experiments.

To facilitate interpretation of the output, the numerical program was extended by a contour plotting program which is a modified version of program CONTOUR from the University of Michigan. As a result, an output consisting of isotherm patterns can be obtained; Fig. 31 is an example. The point of discharge is at the center bottom of the picture, and there is no wind or current. The plot shows surface temperatures. Near the outlet the contour interpolation is slightly erroneous because of the large grid sizes and the interpolation procedure in the contour plotting package.

To determine the accuracy of the method, predicted temperatures were compared with measurements in the field and under laboratory conditions. Results and comparisons with laboratory data will be given in the following section.

Non-Dimensional Analysis and Results

The procedure described in the previous section will produce results for an individual plume under individual ambient conditions. However, dimensionless quantitative information on, for example, temperature decay, spread, and flow velocities in a plume in terms of all the relevant parameters influencing the behavior of the thermal plume is also desirable. Such information would greatly aid in making generalized predictions of the character of the plume for different field conditions. Attempts to provide such general information have failed owing to the large number of factors affecting the plume characteristics as well as the interaction and mutual interference among these parameters. If the initial plume characteristics $u_o = u(0,0,0)$ and $a_o = a(0)$ and the initial water temperature excess $T_o - T_\ell = T(0,0,0) - T_\ell$ are chosen as reference values, the independent variables can be written as

$$\frac{b_o}{a_o},\quad F_o,\quad \frac{U_s}{u_o},\quad \frac{W}{u_o},\quad \frac{T_E - T_\ell}{T_o - T_\ell},\quad \frac{K_s(T_o - T_E)}{u_o \rho c_p},\quad \alpha_o,\quad \beta$$

in which F_o is the initial densimetric Froude number. The dependent variables are

$$\frac{u}{u_o},\quad \frac{T - T_\ell}{T_o - T_\ell},\quad \frac{a}{a_o},\quad \frac{b}{b_o},\quad \frac{Q}{Q_o},\quad \frac{H}{H_o},\quad \frac{\alpha}{\alpha_o},\quad \frac{y}{a_o},\quad \frac{x}{a_o}$$

where the subscript zero again refers to the initial cross section at $(s = 0)$. It has not been found possible to produce dimensionless results for the dependent variables in terms of all the independent parameters. However, it was found that the initial behavior of most of the heated water surface jets investigated is controlled mainly by the hydrodynamic and turbulent convective processes. For purposes of illustration it is therefore justifiable and useful to eliminate those independent variables which refer to heat transfer through the water surface by setting $T_\ell = T_E$ and $K_s = 0$. The results will then refer to the mixing zone near the point of discharge only. The remaining independent variables then are

$$\frac{b_o}{a_o},\quad F_o,\quad \frac{U_s}{u_o} \text{ and } \frac{W}{u_o},\quad \alpha_o,\quad \beta$$

The effects of several combinations of these dimensionless parameters on dependent variables were investigated in two groups: plumes in wind without cross currents $(U_s = 0)$ and plumes in cross currents without wind $(W = 0)$. The wind or current was assumed to be at right

angles to the discharge ($\alpha_o = \pi/2$ or $\beta = 0$). The results of those investigations are shown in Figs. 5 through 20.

Figures 5 through 20 are largely self-explanatory. The first four figures refer to a low Froude number discharge ($F_o = 3.75$) into wind. The deflection of the main trajectory as shown in Fig. 5 is more substantial for the semicircular jet ($b_o/a_o = 1$) than for a wide semi-elliptical one ($b_o/a_o = 4$). The reason is that the circular discharge has a smaller initial flow rate and initial momentum than the wider one. There is substantial dilution of the discharge (Fig. 6), resulting in a significant temperature drop (Fig. 7) despite significant stratification. The second set of four figures refers to a higher Froude number discharge ($F_o = 15$). The deflection of the main trajectory is larger than before for identical W/u_o ratios (Fig. 9). The reason is the larger amount of entrainment of the faster jet, which is associated with larger plume dimensions, including surface areas exposed to wind. There is a substantial difference in the dilution of the circular ($b_o/a_o = 1$) and the wide elliptical ($b_o/a_o = 4$) discharge. The centerline temperature decay by turbulent mixing with ambient lake water is overwhelming. Figure 12 shows very nicely the initial jet regime followed by a stratified flow process. It can also be noted that wind will tend to sustain turbulent entrainment (Fig. 10) and further growth of the plume's thickness (Fig. 12). The third and fourth sets of figures refer to heated surface jet discharges at right angles into cross-currents at a low densimetric Froude number ($F_o = 3.75$) and a high densimetric Froude number ($F_o = 15.0$), respectively.

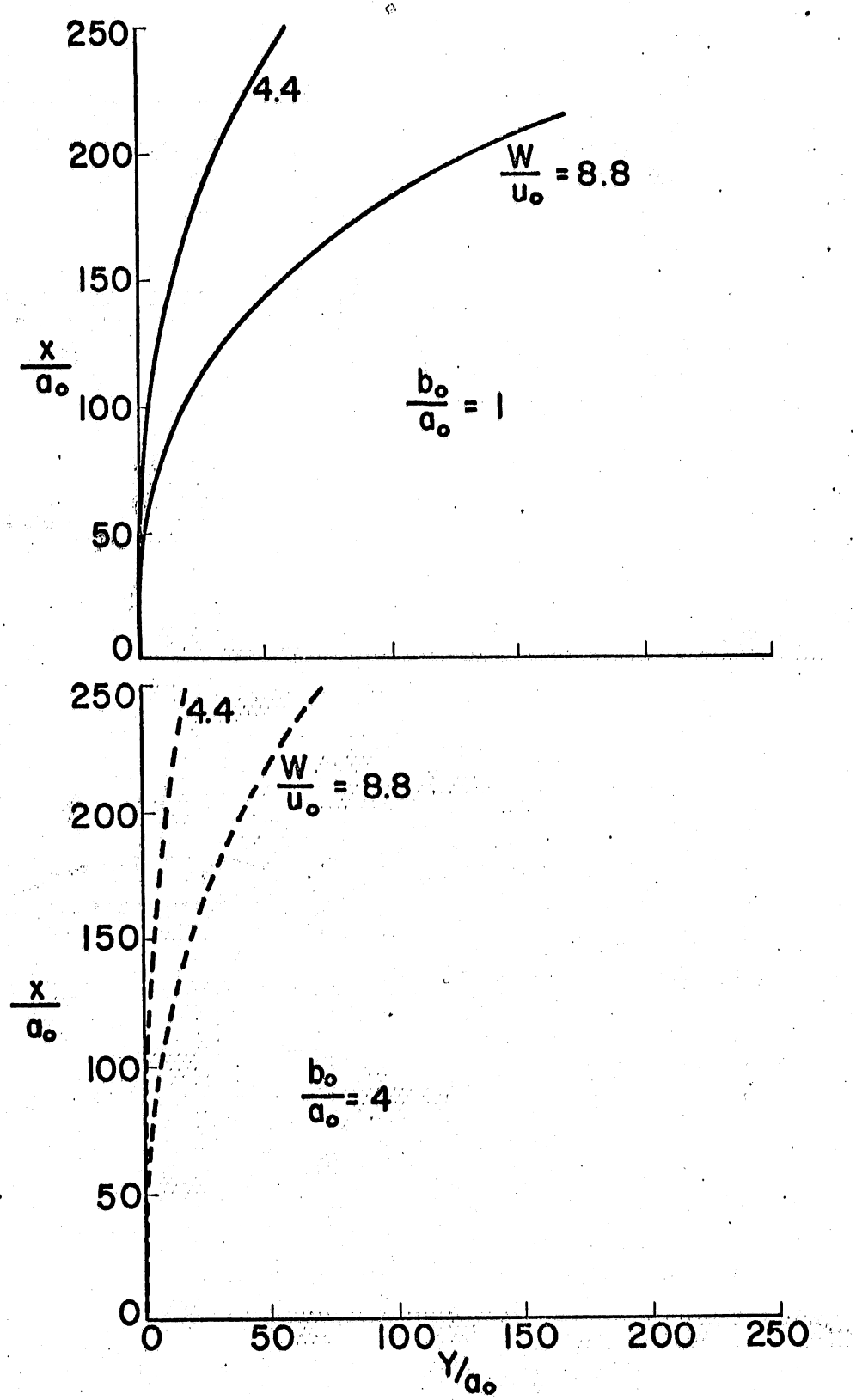

Fig. 5 - Plume Trajectory in Cross-wind Perpendicular to Discharge. $\alpha_o = 90^o$, $\beta = 0$, $F_o = 3.75$, $U_s = 0$, $K_s = 0$

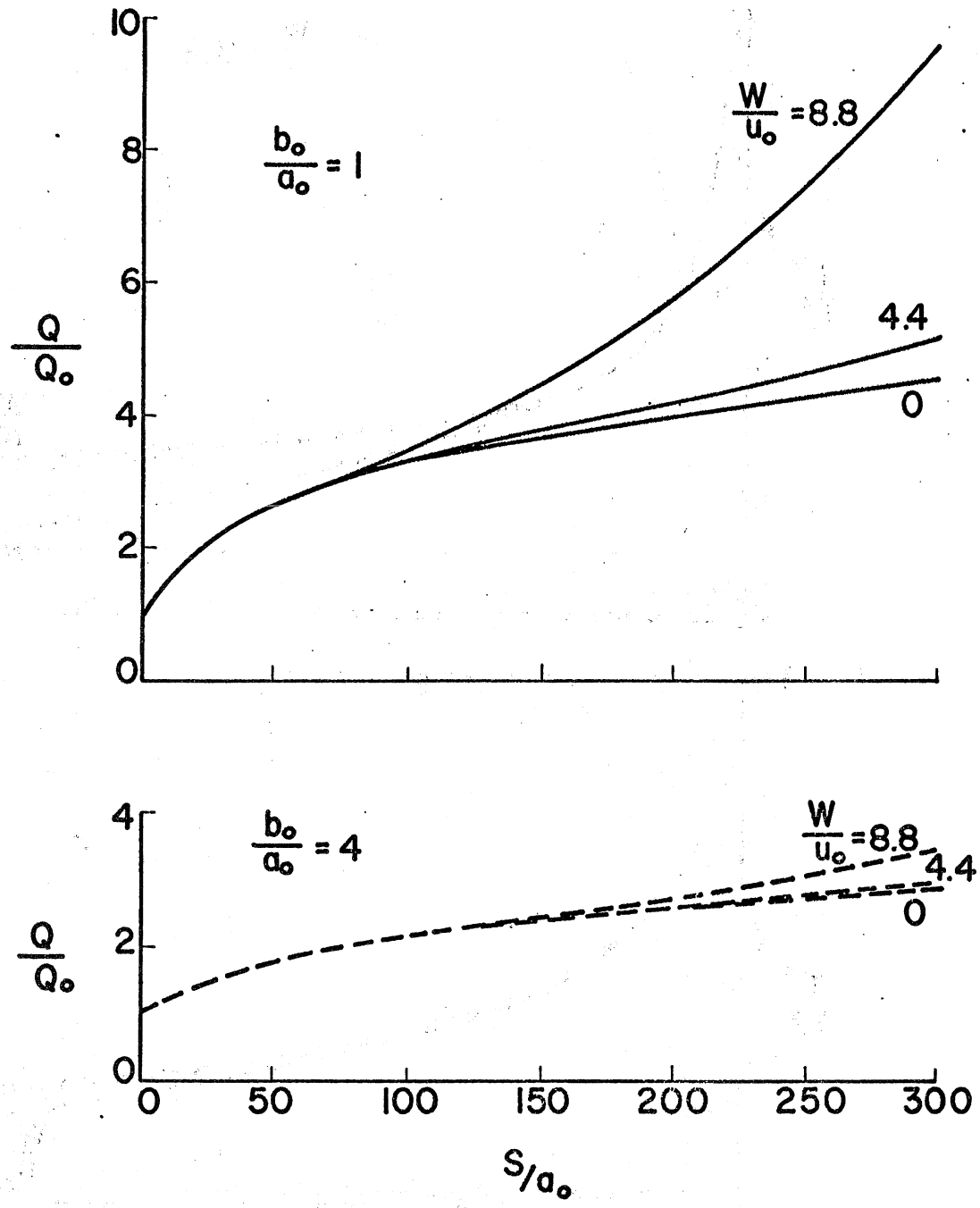

Fig. 6 - Total Volumetric Flow Rate versus Distance of Travel. Plume in Cross-wind perpendicular to Discharge. $\alpha_o = 90^o$, $\beta = 0$, $F_o = 3.75$, $U_s = 0$, $K_s = 0$

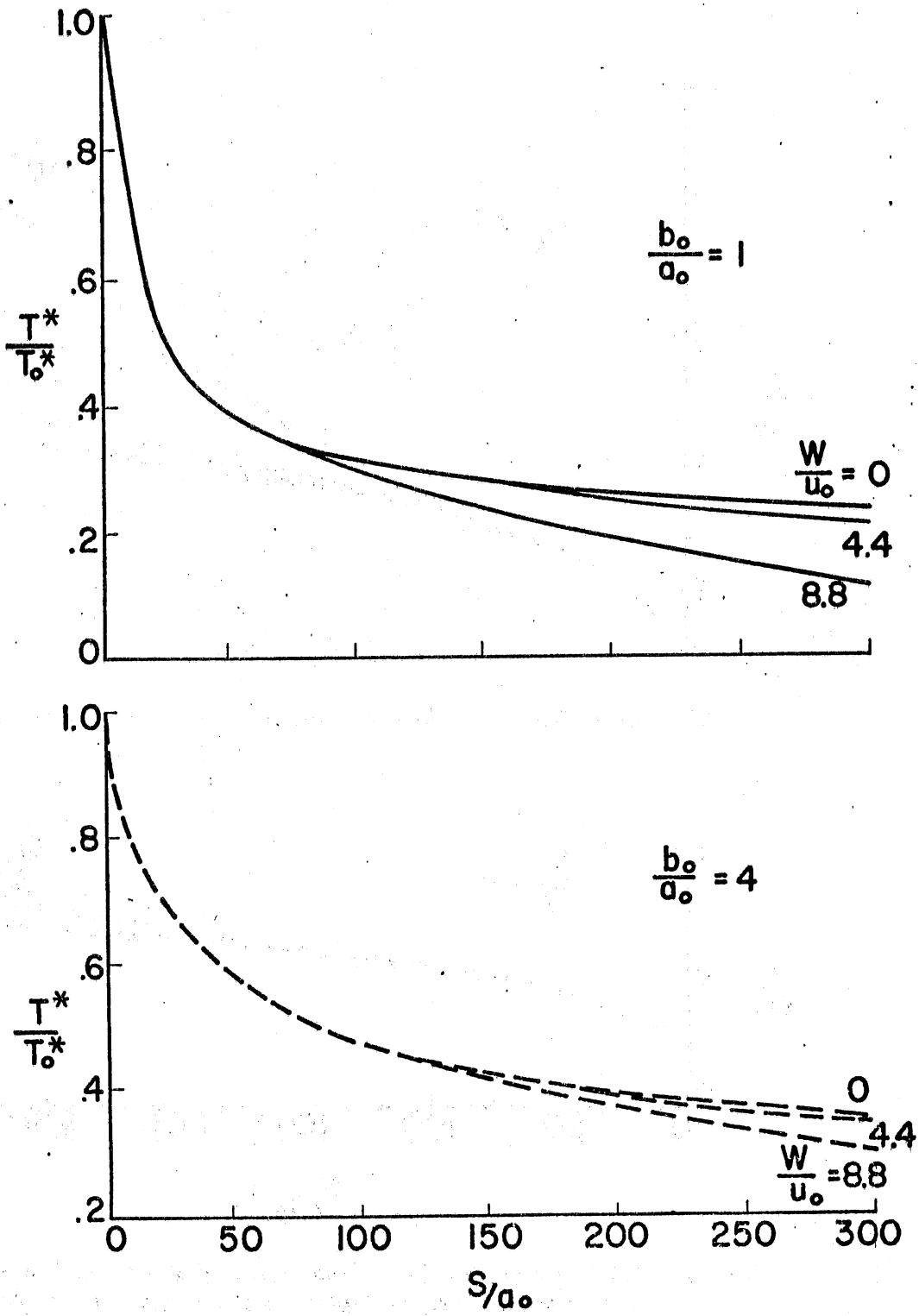

Fig. 7 - Excess Temperature above Ambient along Main Trajectory. Plume in Cross-wind Perpendicular to Discharge. $\alpha_o = 90^o$, $\beta = 0$, $F_o = 3.75$, $U_s = 0$, $K_s = 0$

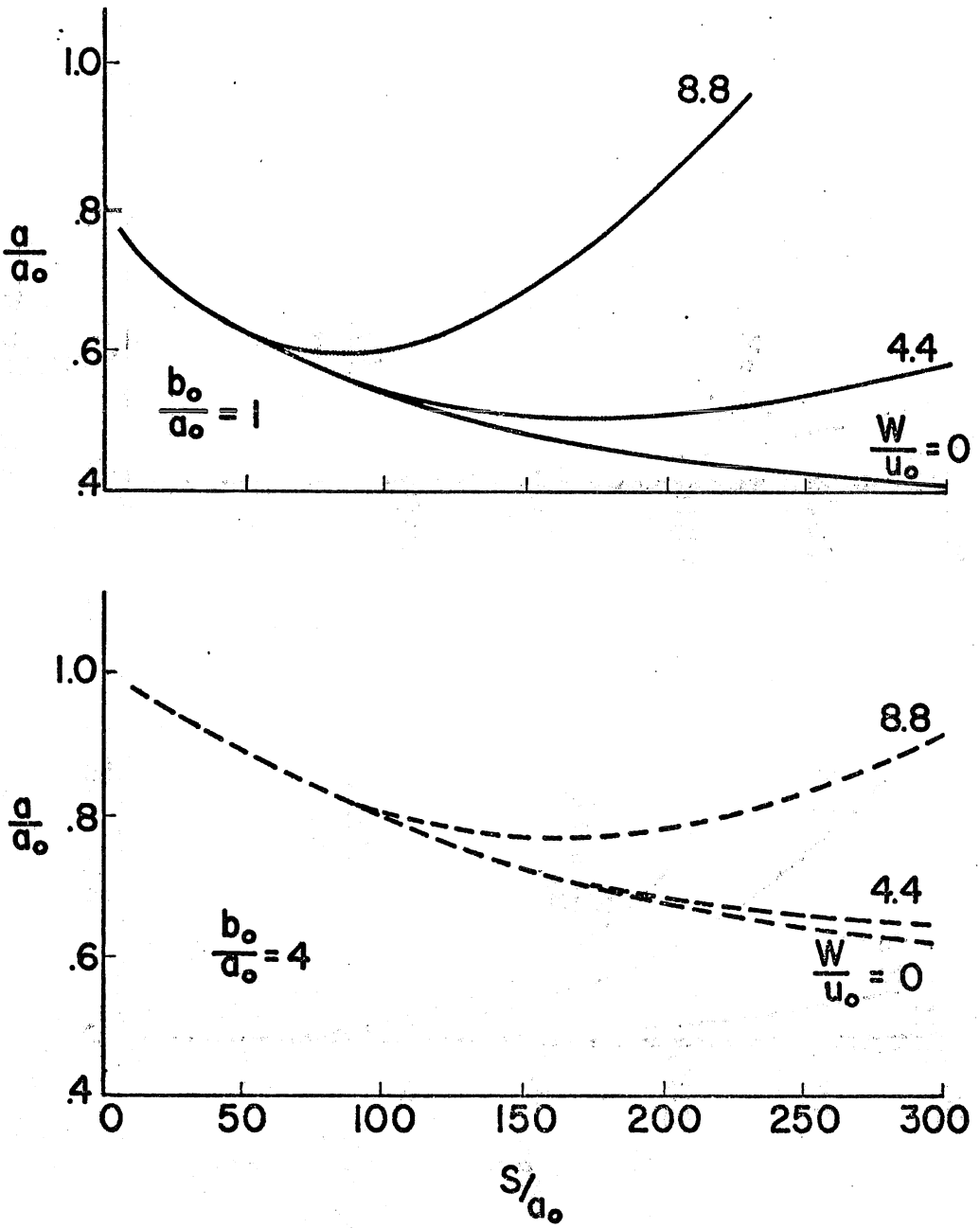

Fig. 8 - Depth of Thermocline below Water Surface along Main Trajectory. Plume in Cross-wind Perpendicular to Discharge. $\alpha_o = 90^o$, $\beta = 0$, $F_o = 3.75$, $U_s = 0$, $K_s = 0$

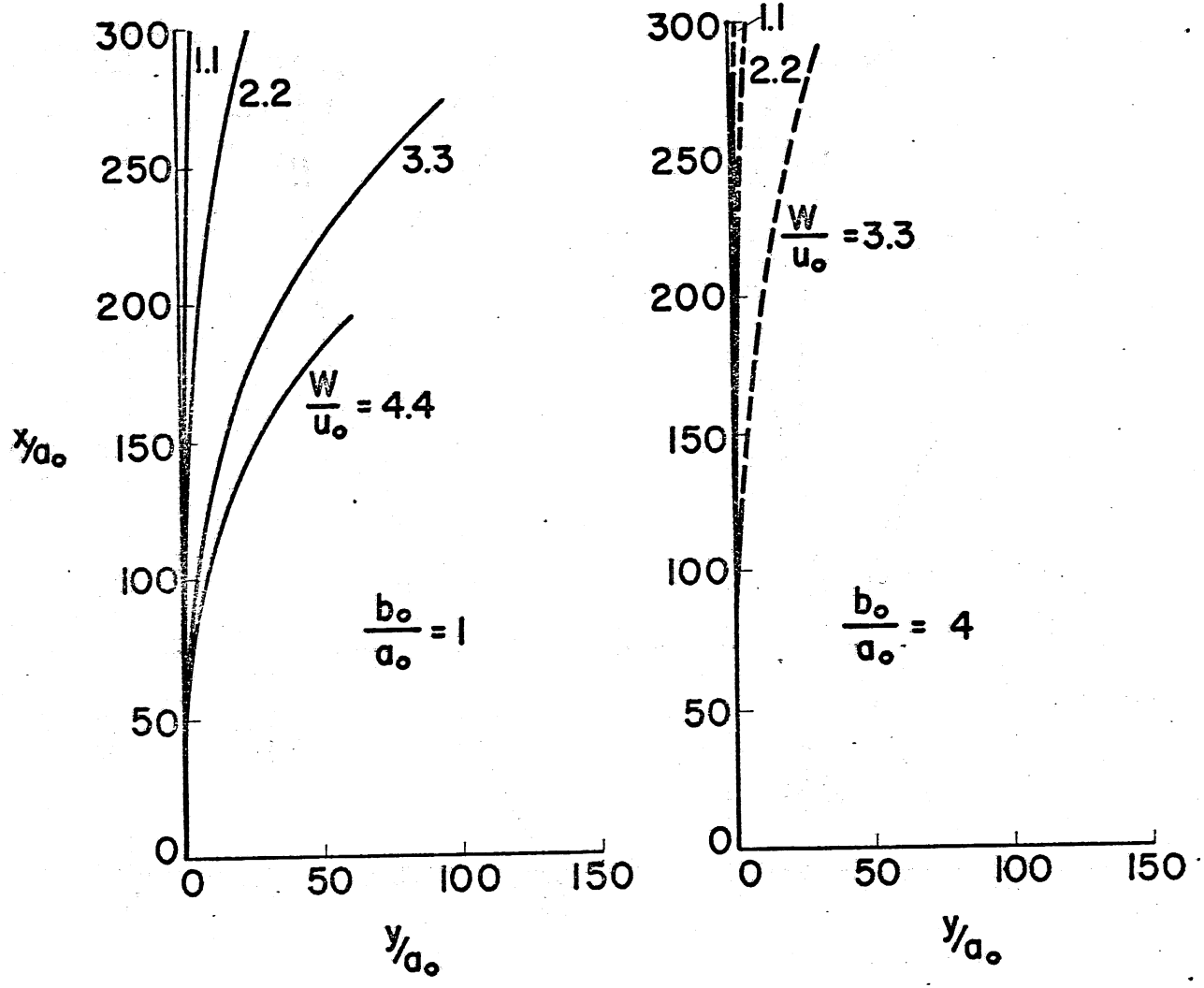

Fig. 9 - Plume Trajectory in Cross-wind Perpendicular to Discharge.
$\alpha_o = 90^o$, $\beta = 0$, $F_o = 15.0$, $U_s = 0$, $K_s = 0$

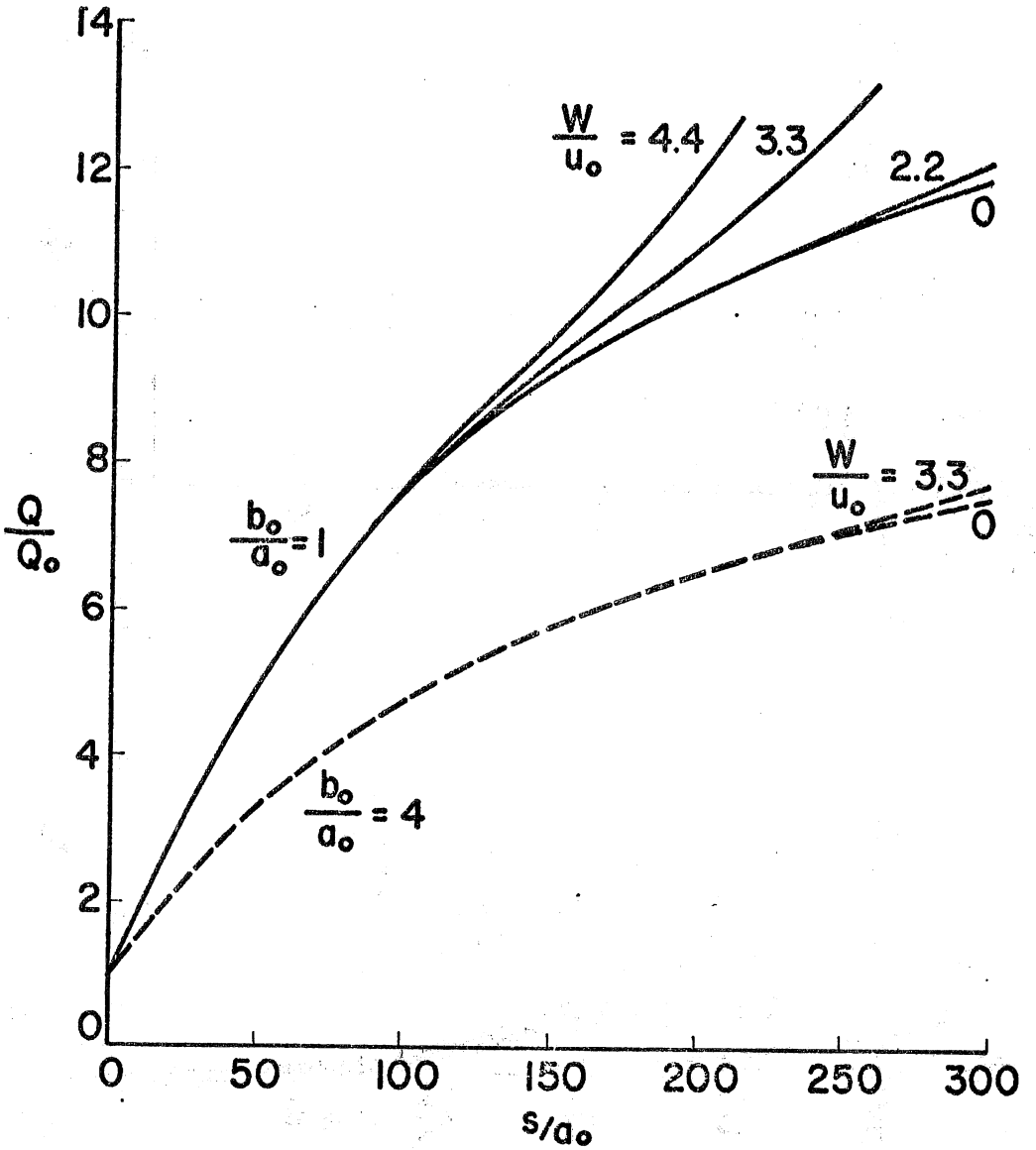

Fig. 10 - Total Volumetric Flow Rate versus Distance of Travel. Plume in Cross-wind Perpendicular to Discharge. $\alpha_o = 90^o$, $\beta = 0$, $F_o = 15.0$, $U_s = 0$, $K_s = 0$

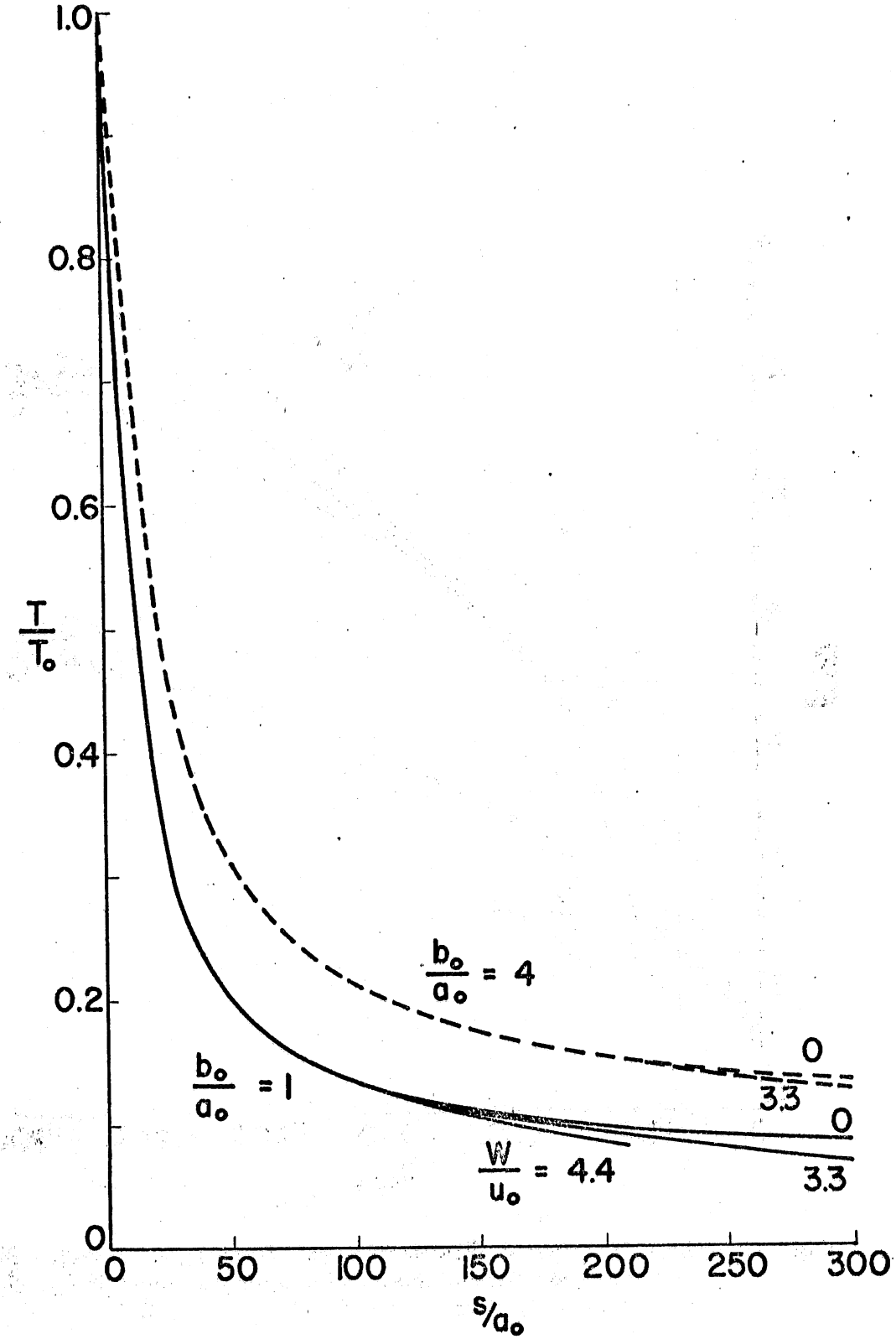

Fig. 11 - Excess Temperature above Ambient along Main Trajectory. Plume in Cross-wind perpendicular to Discharge. $\alpha_o = 90^o$, $\beta = 0$, $F_o = 15.0$, $U_s = 0$, $K_s = 0$

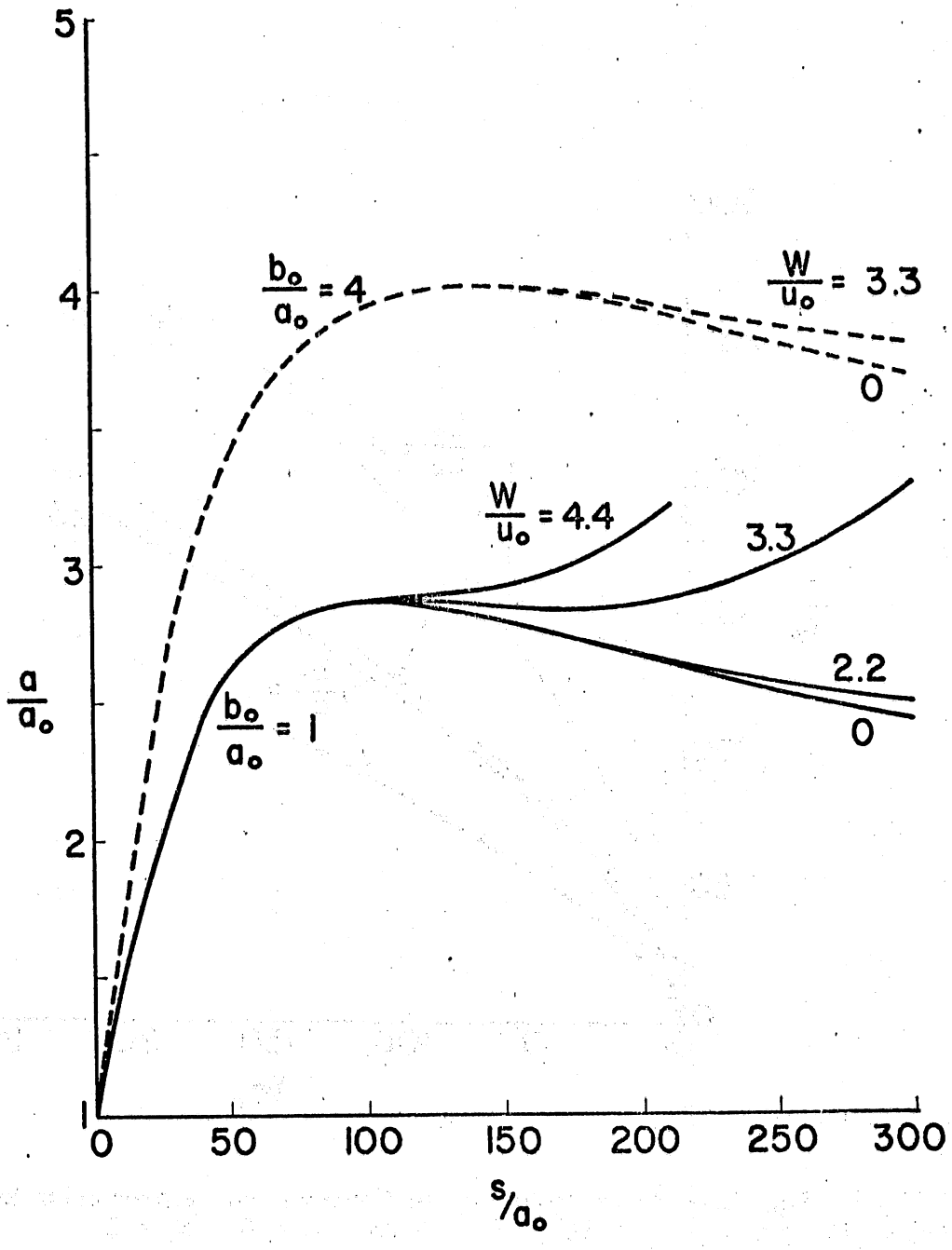

Fig. 12 - Depth of Thermocline below Water Surface along Main Trajectory. Plume in Cross-wind perpendicular to Discharge. $\alpha_o = 90^o$, $\beta = 0$, $F_o = 15.0$, $U_s = 0$, $K_s = 0$

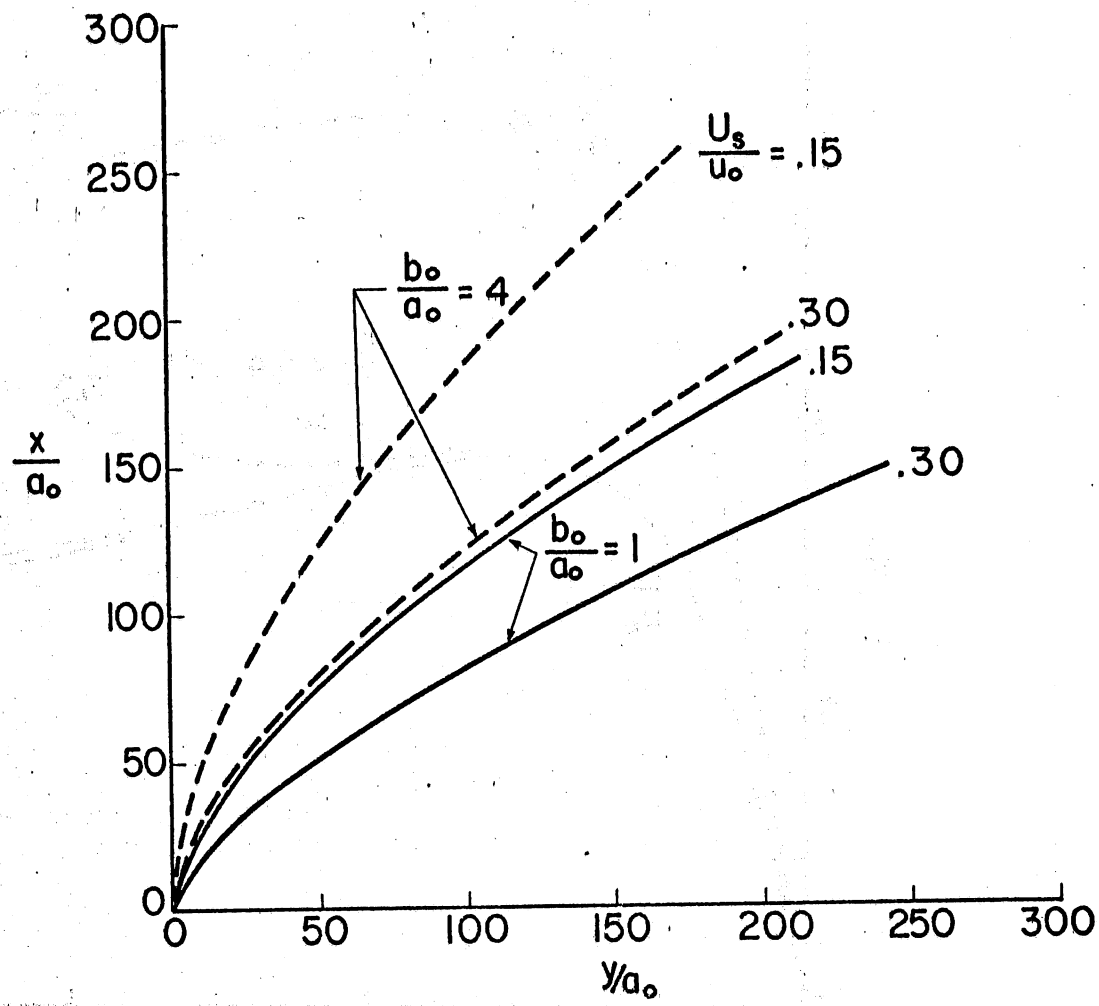

Fig. 13 - Plume Trajectory in Cross-current Perpendicular to Discharge.
$\alpha_o = 90^o$, $F_o = 3.75$, $W = 0$, $K_s = 0$

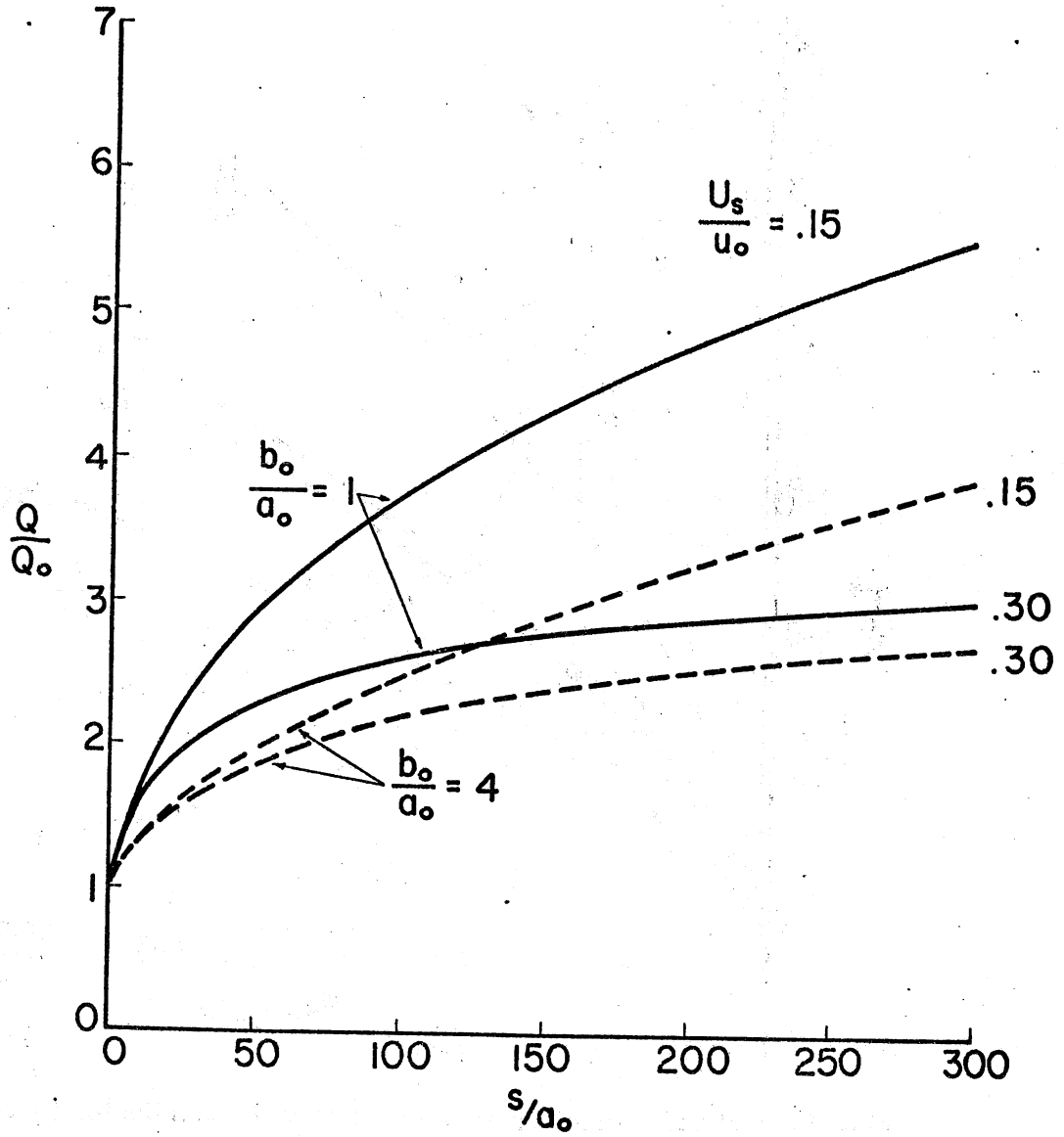

Fig. 14 - Total Volumetric Flow Rate versus Distance of Travel. Plume in Cross-current Perpendicular to Discharge. $\alpha_o = 90^o$, $F_o = 3.75$, $W = 0$, $K_s = 0$

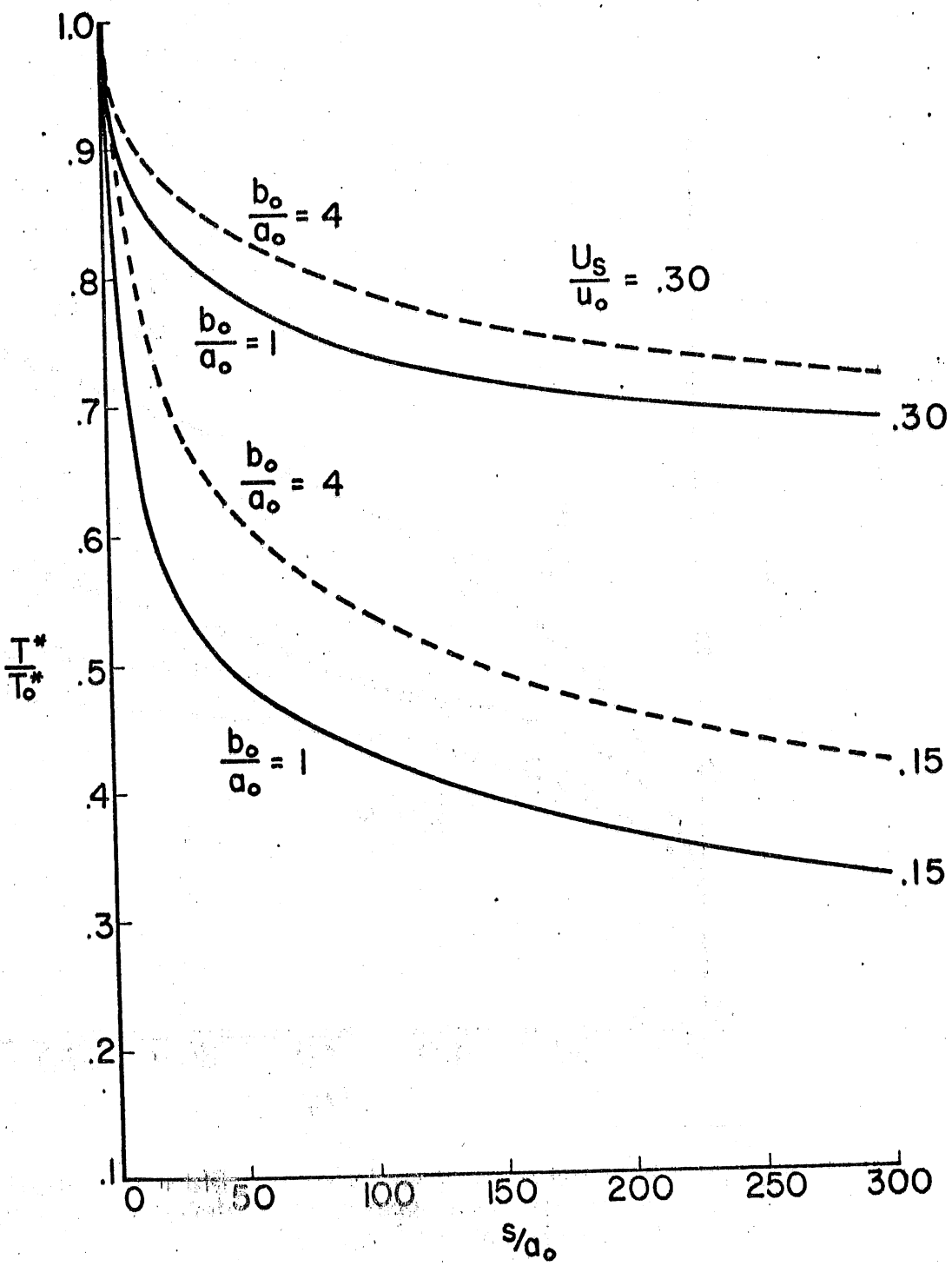

Fig. 15 - Excess Temperature above Ambient along Main Trajectory. Plume in Cross-current perpendicular to Discharge. $\alpha_o = 90^o$, $F_o = 3.75$, $W = 0$, $K_s = 0$

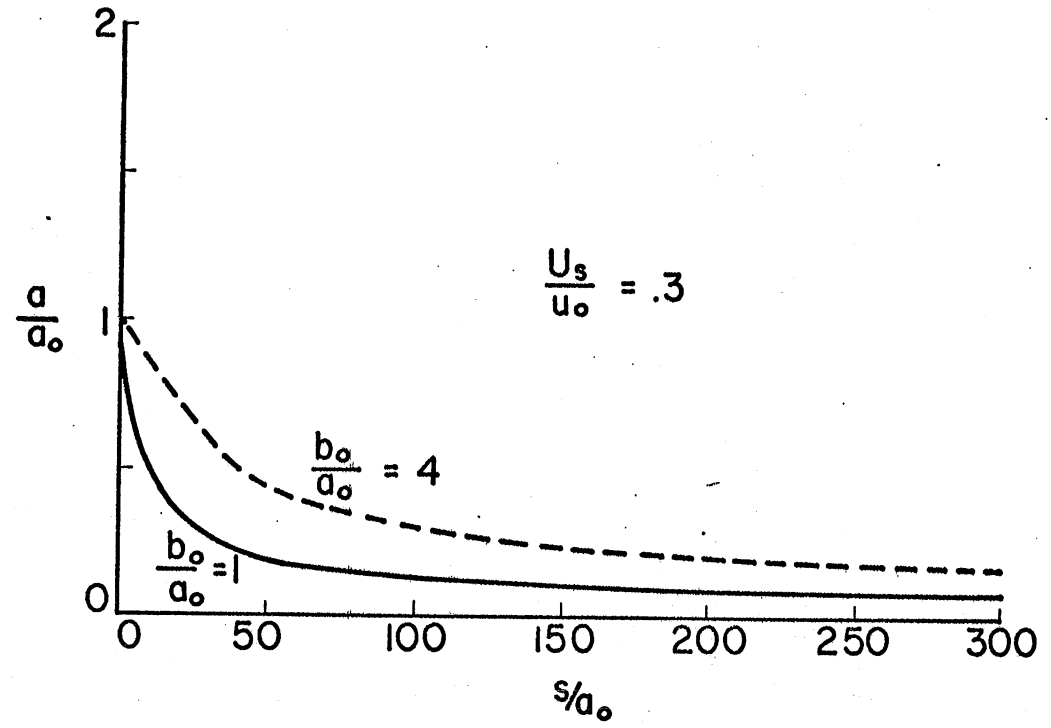

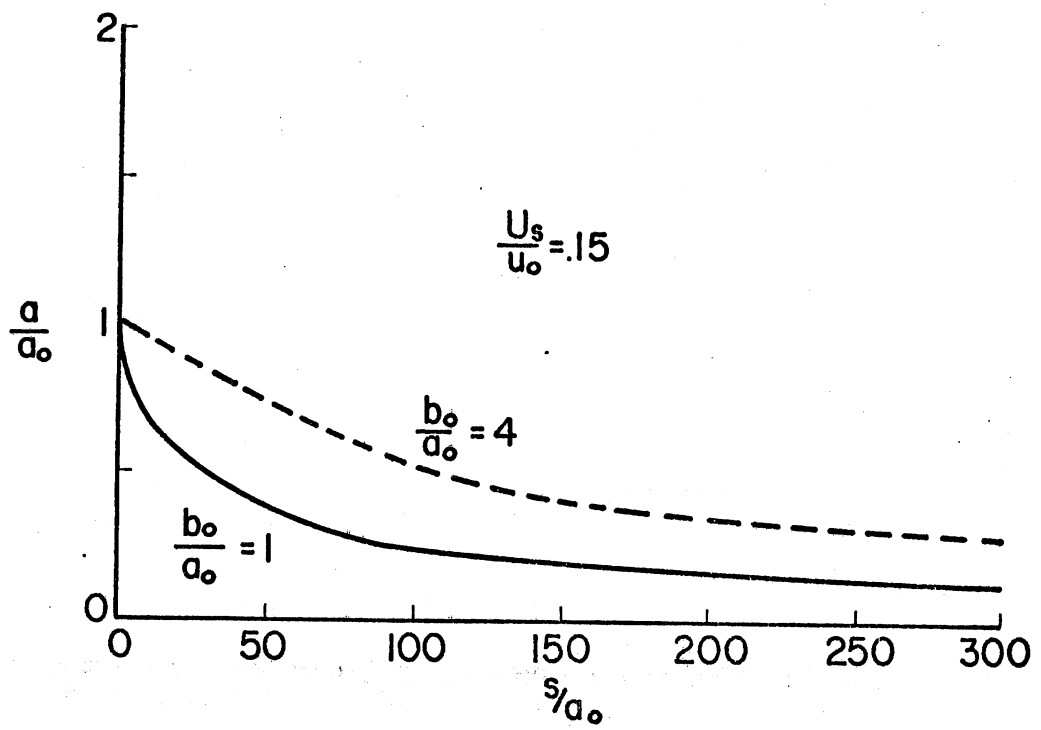

Fig. 16 - Depth of Thermocline below Water Surface along Main Trajectory. Plume in Cross-current perpendicular to Discharge. $\alpha_o = 90^o$, $F_o = 3.75$, $W = 0$, $K_s = 0$

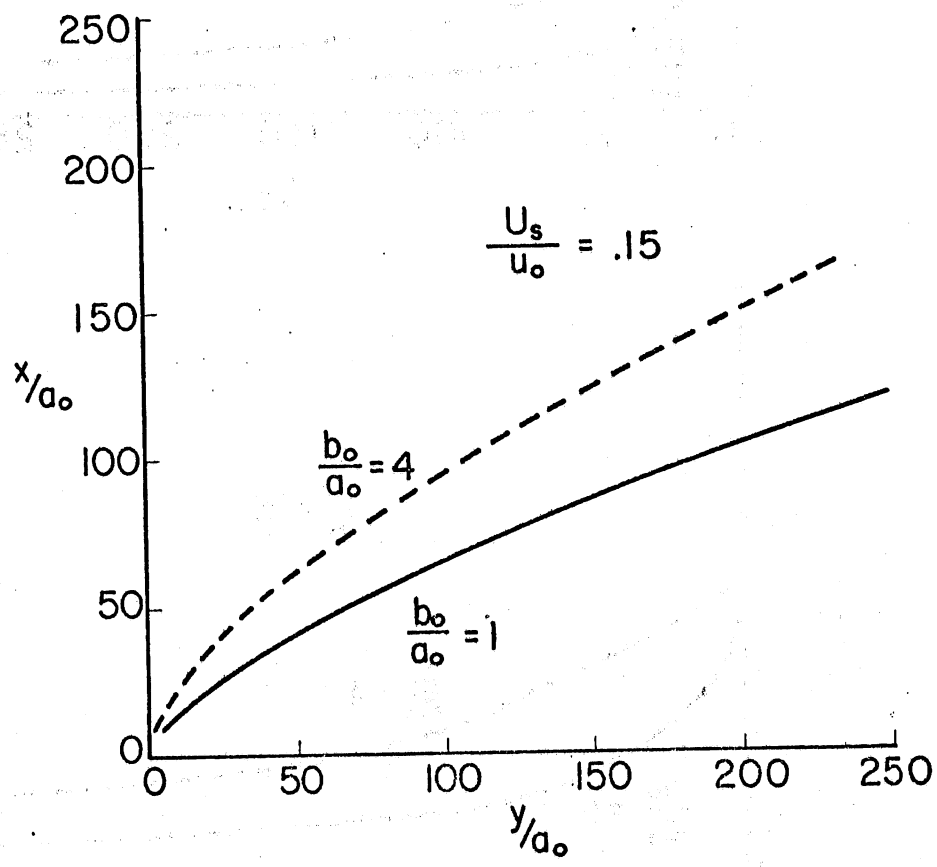

Fig. 17 - Plume Trajectory in Cross-current perpendicular to Discharge. $\alpha_o = 90^o$, $F_o = 15.0$, $W = 0$, $K_s = 0$

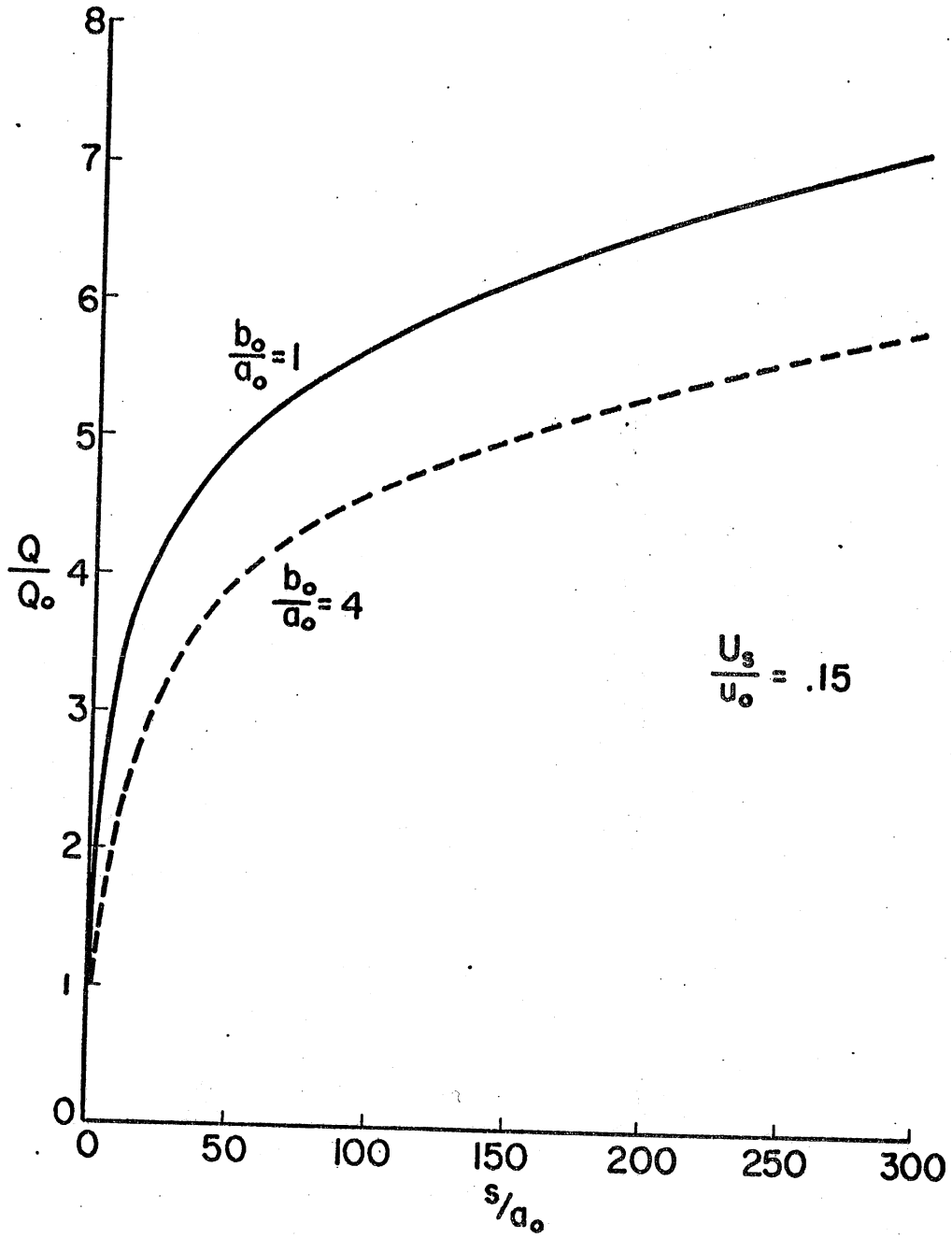

Fig. 18 - Total Volumetric Flow Rate versus Distance of Travel. Plume in Cross-current Perpendicular to Discharge. $\alpha_o = 90°$, $F_o = 15.0$, $W = 0$, $K_s = 0$

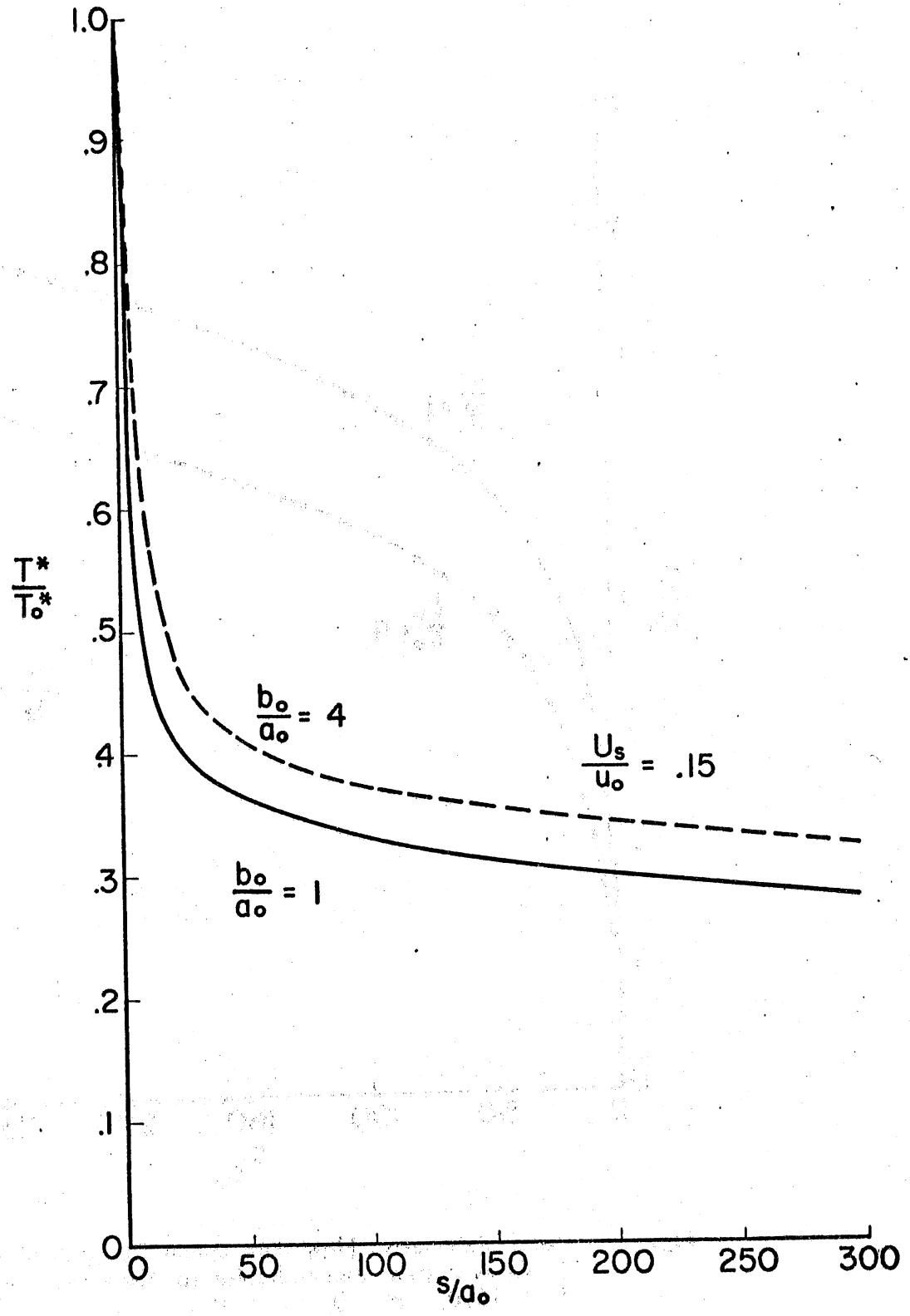

Fig. 19 - Excess Temperature above Ambient along Main Trajectory. Plume in Cross-current perpendicular to Discharge. $\alpha_o = 90^o$, $F_o = 15.0$, $W = 0$, $K_s = 0$

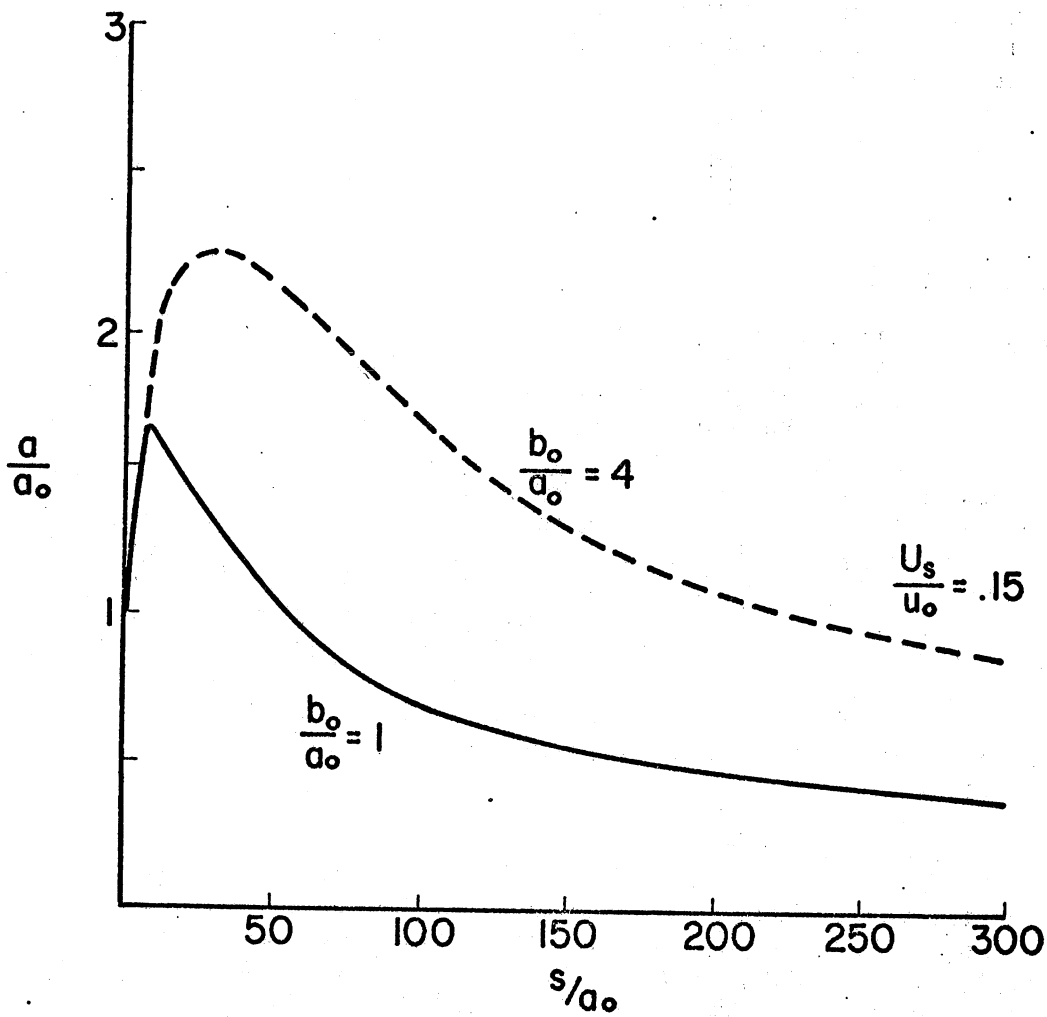

Fig. 20 - Depth of Thermocline below Water Surface along Main Trajectory. Plume in Cross-wind Perpendicular to Discharge. $\alpha_o = 90^o$, $F_o = 15.0$, $W = 0$, $K_s = 0$

SECTION VI

EXPERIMENTAL STUDY

Apparatus and Data Acquisition

The experimental apparatus consisted of a large rectangular tank 17 ft wide, 40 ft long, and 2 ft deep. Hot water was discharged from a channel 6 inches wide and approximately 1.6 inches deep at right angles into the tank, which was filled with cold water. Point measurements of temperature and velocity were taken in the vicinity of the outlet with the aid of a combined temperature-velocity probe described in Ref. [22]. To assure steady-state conditions, cold water was fed into the tank constantly at very low velocity. The excess flow drained over a weir at the downstream end of the tank. Cross-currents and wind were absent in the experiments. More information on the experimental apparatus is given in Ref. [22].

Data Preparation

The experimental data obtained by the procedures outlined in Ref. [22] consisted of velocity and temperature measurements at variable depth z at a given location (x,y) in the tank. Figure 21 will serve as a definition sketch. Velocity components in the x-direction (u-component) and in the y-direction (v-component) were measured. Usually fifteen to thirty measurements per profile were available. Temperature and velocity were usually not measured at the same depth z because of the particular configuration of the tethered sphere probe used. Therefore 51 equidistant data points at 0.01 ft vertical spacing were obtained by interpolation for each vertical profile. Temperature profiles were approximated using a third order polynomial between any three given measurements, and the interpolation was carried out numerically. For the velocity profiles a graphical interpolation was preferred because the data had more scatter and smoother velocity distributions were desirable.

Table 1 summarizes the conditions for which experimental data were available. "FLUSH" signifies that the discharge channel terminated in the wall of the tank, while "PROJ." means that the outlet channel projected 4.8 ft into the tank. Q_o is the heated water discharge rate, d_o is the depth of the outlet channel, T_o is the outlet water temperature, T_ℓ is the cold water temperature in the tank (lake), T_a is the air temperature, and Re_o is the outlet Reynolds number defined as

$$Re_o = \frac{U_o d_o}{\nu_o} = \frac{Q_o}{w_o \nu_o} \tag{44}$$

Table 1 - SUMMARY

EXP. NO.	OUTLET TYPE	OUTLET Q_o (cfs)	OUTLET d_o (ft)	OUTLET T_o (^oF)	TANK T_ℓ (^oF)	AIR T_a (^oF)	Re_o (-)	F_o (-)
215	FLUSH	.00645	.162	91.0	70.0	78	1,590	.62
207	FLUSH	.0131	.165	76.5	51.5	78	2,700	1.38
216	FLUSH	.0376	.162	92.0	73.0	81	9,370	3.73
214	PROJ.	.00645	.155	87.0	68.0	80	1,520	.72
211	PROJ.	.0141	.159	84.0	60.0	76	3,190	1.43
217	PROJ.	.0376	.155	92.5	73.5	81	9,400	3.98

OF EXPERIMENTS

$T_o - T_a$ (^oF)	$T_o - T_\ell$ (^oF)	$\frac{T_o - T_a}{T_o - T_\ell}$ (-)	H_o ($ft^3 {}^oF/sec$)	C_o ($^oF\ ft^2$)	D_o (ft)
13	21	.619	.135	1.70	.40
-1.5	25	-.060	.328	2.06	.40
11	19	.578	.715	1.54	.40
7	19	.369	.123	1.47	.40
8	24	.333	.339	1.91	.40
11.5	19	.605	.715	1.47	.40

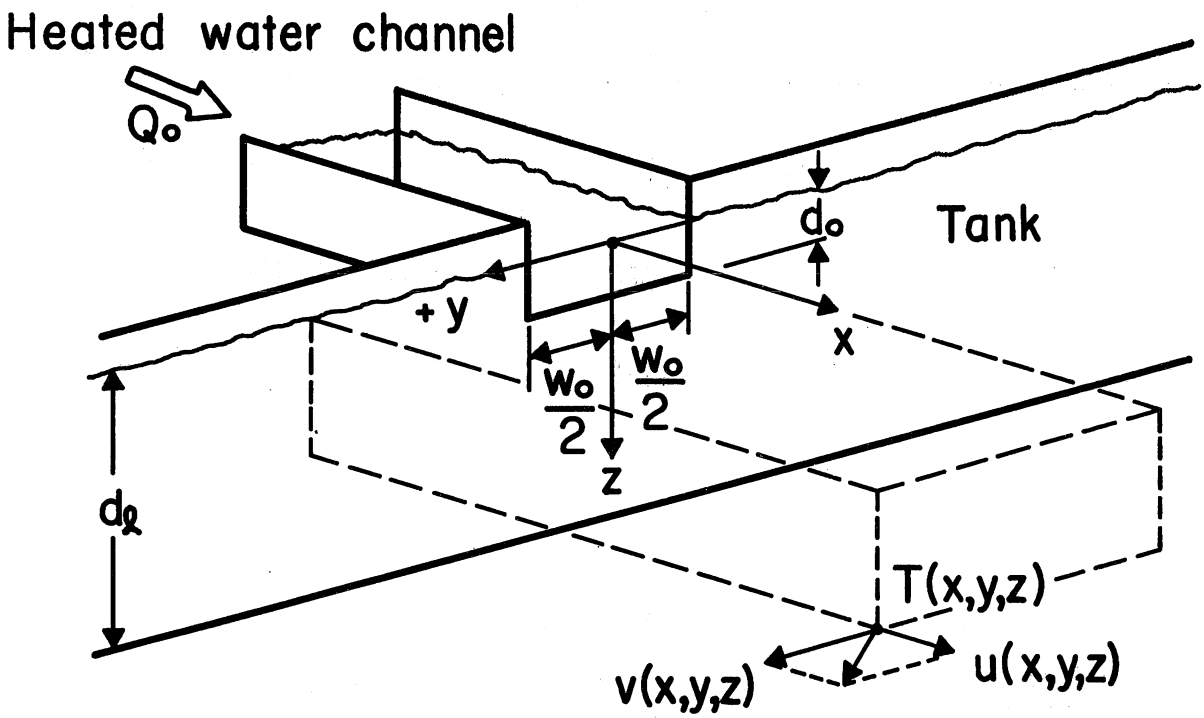

Fig. 21 - Definition Sketch - Surface Discharge into Experimental Tank

where U_o is the average discharge velocity, $w_o = 0.5$ ft is the width of the outlet channel, and ν_o is the kinematic viscosity at the outlet. F_o' is the outlet densimetric Froude number, defined as

$$F_o = U_o(g'd_o)^{-1/2} = Q_o(g'w_o d_o^3)^{-1/2} \tag{45}$$

where $g' = \frac{\Delta\varrho_o}{\varrho} g$ is a reduced acceleration of gravity. The outlet heat discharge (heat flux) into the tank is

$$H_o = \varrho c_p Q_o(T_o - T_\ell) \tag{46}$$

and the relative heat content in the outlet cross section is

$$C_o = \varrho c_p d_o w_o(T_o - T_\ell) \tag{47}$$

D_o is the hydraulic diameter of the outlet cross section defined as

$$D_o = 4d_o w_o(2d_o + w_o)^{-1} \tag{48}$$

Data Processing

Distribution Functions

Each temperature or velocity profile measured in a vertical section was graphed using a scaleplot subroutine (SCLPLT) from the CDC 6600 system library of the University of Minnesota Computer Center. The graphs obtained were of course nearly identical to those obtained with the raw data and reported in Refs. [22] and [53]. Mere inspection of the output showed that the measured profiles were similar to each other and to normal distribution functions only in first approximation. As stated in Ref. [53], there appears to be no unique function which rigorously describes all distributions in a plume. A sample of measured velocities in Fig. 22 may illustrate this point.

The standard deviations identified as a and λa in Eqs. (1) and (2), respectively, were calculated for each temperature and velocity profile. The standard deviation for the velocity profiles was found from the relationship

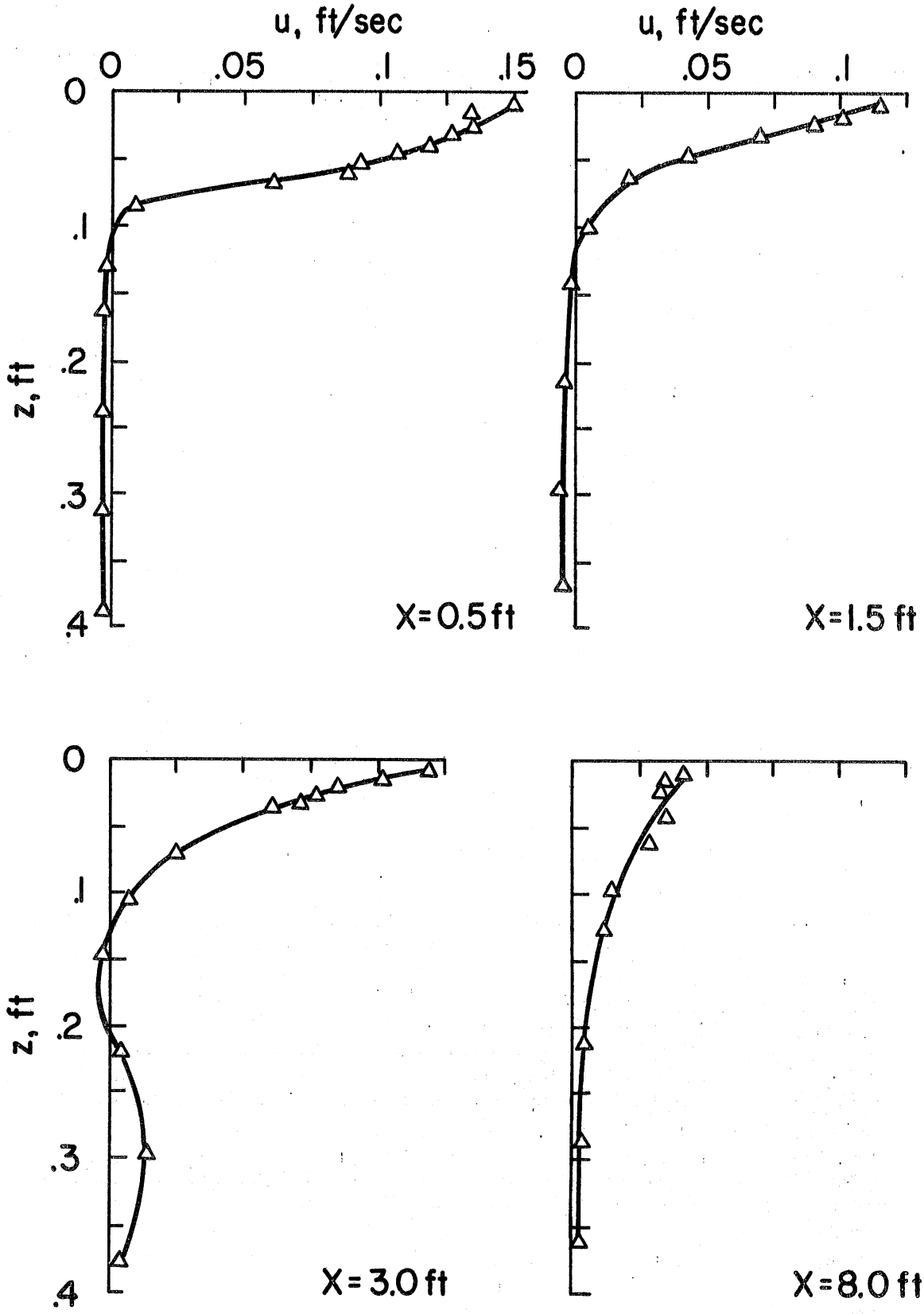

Fig. 22 - Variation of Velocity Component u with Depth at Various Distances from the Outlet along Centerline of tank. Exp. 215

$$a_u = a = \left[\frac{\sum_{j=1}^{N_p} u_j z_j^2}{\sum_{j=1}^{N_p} u_j} \right]^{1/2} \tag{49}$$

where u_j is the velocity component in the x-direction at a point and N_p is the number of positive measurements in a profile. A vertical profile consisted of no more than $N_p = 51$ points. Similarly, the standard deviation for temperature profiles was calculated from

$$a_T = \lambda_v a = \left[\frac{\sum_{j=1}^{N_p} (T_j - T_\ell)\, z_j^2}{\sum_{j=1}^{N_p} (T_j - T_\ell)} \right]^{1/2} \tag{50}$$

The calculated values of a_T and a_u showed dependence on location. Figure 23 gives values for all six experiments as a function of distance from the outlet. Predictions made with the aid of the analytical model are shown as solid lines. There is a substantial amount of scatter in the experimental data, particularly those derived from velocity measurements. The analytical model predicted the measured standard deviations, especially those for temperatures, reasonably well.

The vertical distortion parameter $\lambda_v = a_T/a_u$ was assumed to be calculable from the standard deviations for temperature and velocity. It was found to vary considerably from one location to another. This is shown in Fig. 24. Values of λ_v less than unity mean that the temperature profile reached smaller depths than the velocity profile, a situation which characterizes fast momentum transfer and slow heat transfer, as would be typical for a very stably stratified shear flow. Values of λ_v larger than unity indicate that the temperature profile covered a larger depth than the velocity profile, a situation which could be produced by the accumulation of warm water in the experimental tank before it flowed over the weir at the downstream end of the tank. It is known that this condition existed in the downstream portion of the tank for those experiments using the largest flow rates. Heat conduction could also be responsible for the temperature distributions' reaching larger depths than the velocity distributions. Considering the residence times of the heated water in the upstream portion of the

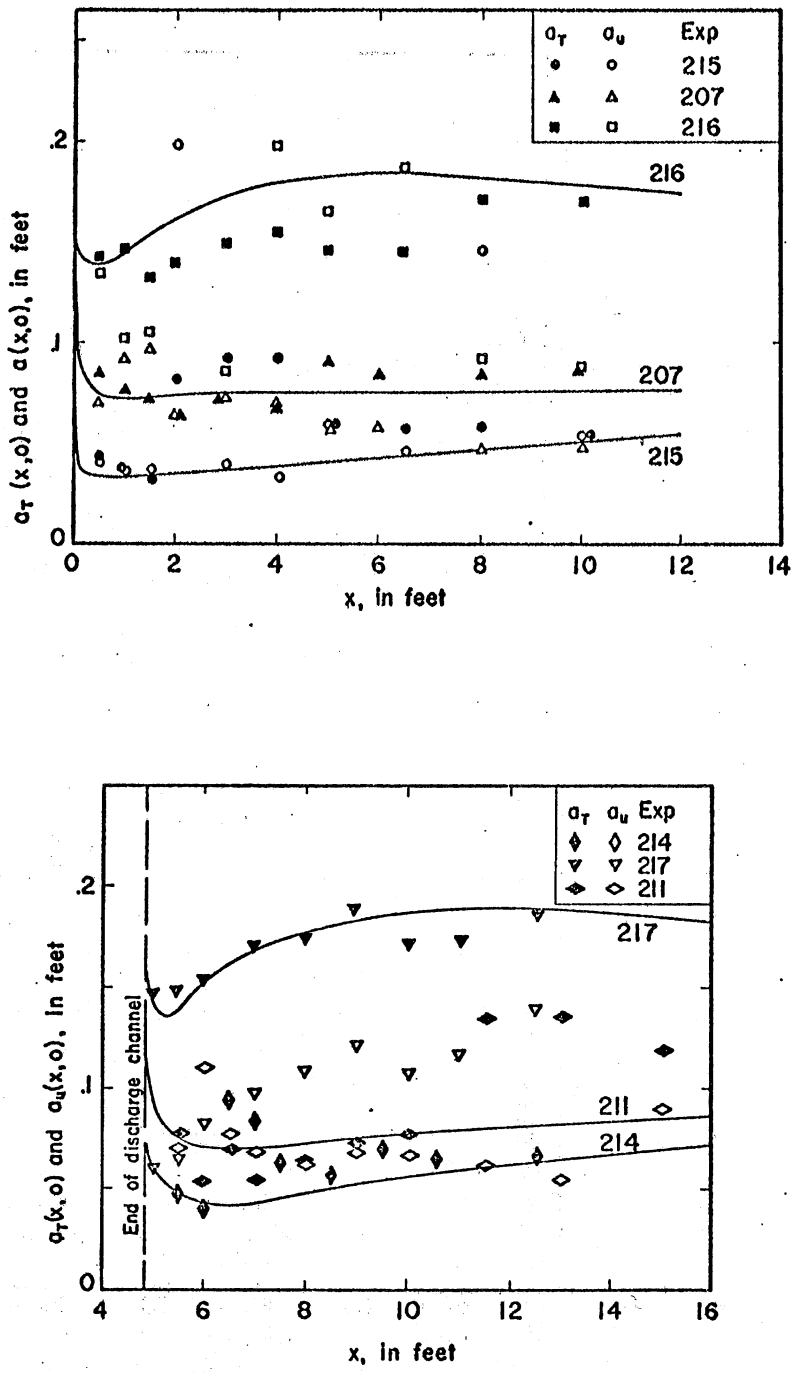

Fig. 23 - Standard Deviations a_U and a_T of Velocity Component u and Temperature T respectively as derived from Velocity and Temperature Profiles measured at Selected Locations along Main Trajectory of the Heated Water Surface Jet. Comparison with Predictions of Analytical Model (solid lines)

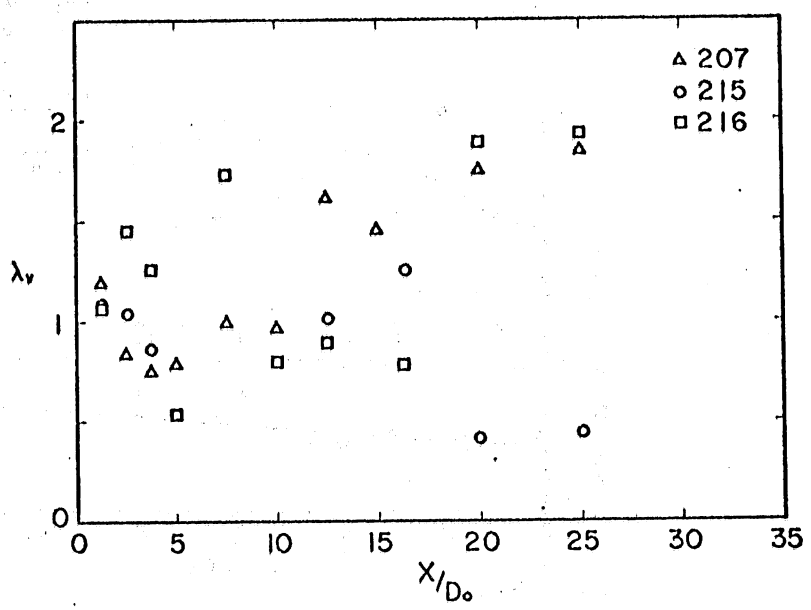

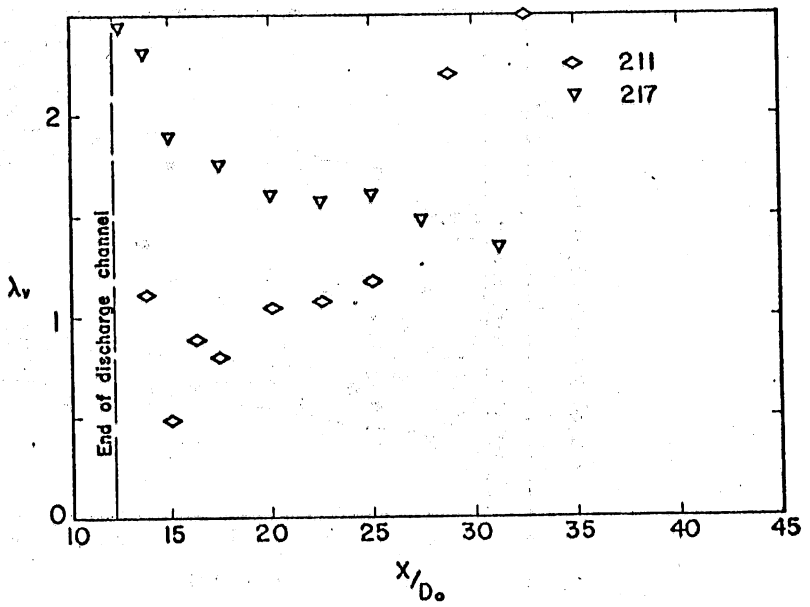

Fig. 24 - Similarity Parameter λ_v versus Distance along Main Trajectory from Discharge Point

tank, however, this is only a remote possibility. While the above mechanisms can be cited to explain whatever trend can be detected in the data, much of the scatter in Fig. 24 is due to experimentation, particularly the difficulties encountered in measuring small velocities in a thin layer of heated water.

The way in which the similarity parameter λ_v varied in cross sections perpendicular to the main trajectory was also examined. The results presented in Fig. 25 show that there is a slight tendency for λ_v values to increase toward the edges of the jet. This is the result of an existing temperature stratification in the tank outside the heated water jet, as illustrated by Fig. 31f. It may also be noted that λ_v is usually in the range $1 < \lambda_v < 2$. For the above reasons it was not really possible to accurately assess the value of λ_v, but it appears justified to use a value of λ_v close to 1 for a heated jet into a non-stratified environment.

To determine how well the measured temperature and velocity profiles agreed with assumed Gaussian distributions, a standard error was calculated for each vertical profile. The error is defined for a velocity profile as

$$\epsilon_u(x,y) = \left[\frac{1}{N_p}\sum_{j=1}^{N_p}\left(u_e(x,y,z_j) - u_{th}(x,y,z_j)\right)^2\right]^{1/2} \tag{51}$$

where u_e and u_{th} refer to experimental (measured) and theoretical (calculated) velocities, respectively. The theoretical value u_{th} was calculated from Eq. (1), in which x and y were substituted for s and r, respectively, because of the absence of wind and cross-currents, and $a_u(x,y)$ was used as the standard deviation. Thus

$$u_{th}(x,y,z_j) = u_e(x,y,0)\ \exp\left[-\frac{1}{2}\left(\frac{z_j}{a_u(x,y)}\right)^2\right] \tag{52}$$

For easier interpretation a dimensionless standard error $\epsilon_u^*(x,y)$ was actually calculated

$$\epsilon_u^*(x,y) = \frac{\epsilon_u(x,y)}{u_e(x,y,0)} \tag{53}$$

The results given in Fig. 26 show no specific effect of distance. Standard errors average out to nearly 0.1. This is a good result considering that the standard error computation has nothing to do with a best fit, but is rather an evaluation of the shape of the velocity distribution in which the measured surface value is used as a reference.

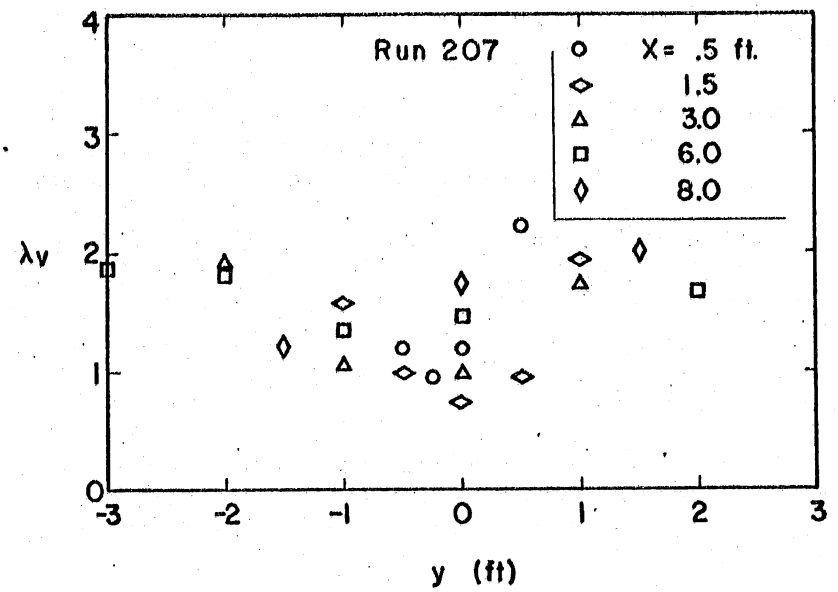

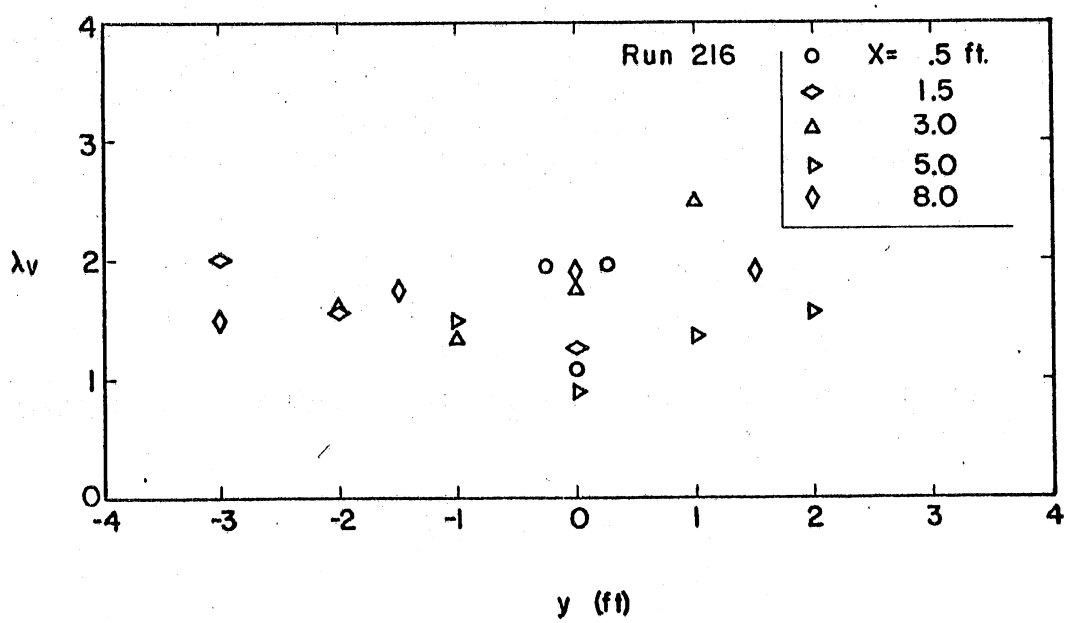

Fig. 25 - Similarity Parameter λ_v versus Distance from Main Trajectory

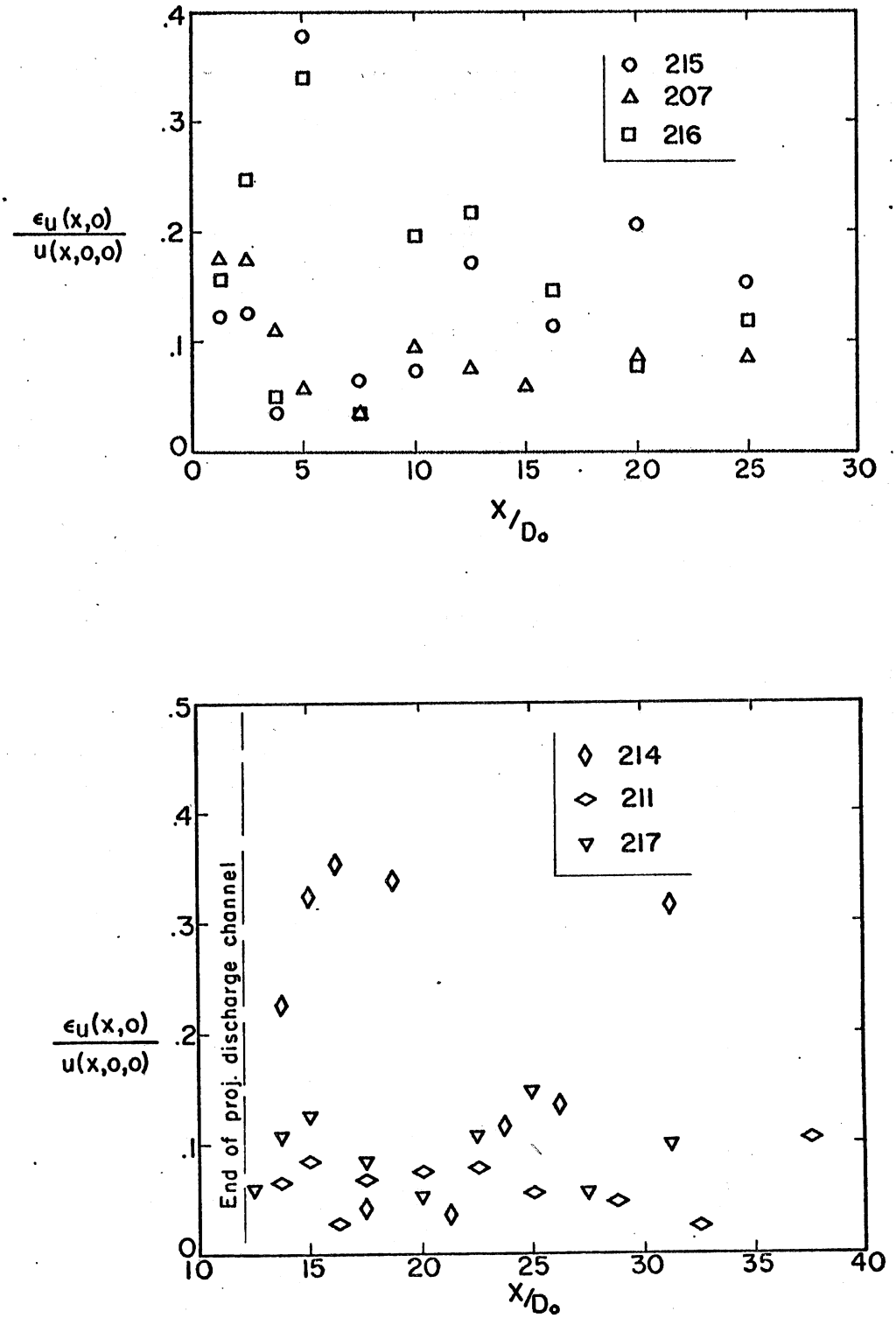

Fig. 26 - Standard Error between Normal Distribution Functions and Experimental Velocity Profiles Measured along Main Trajectory

Standard errors were also calculated for the temperature data or, more precisely, the excess temperature $T^*(x,y,z_j)$ above the cold water temperature. The final equation used is

$$\frac{\epsilon_T(x,y)}{T_e^*(x,y,0)} = \left[\frac{1}{N_p}\sum_{j=1}^{N_p}\left[\frac{T_e^*(x,y,z_j)}{T_e^*(x,y,0)} - \exp\left[-\left(\frac{1}{2}\,\frac{z_j}{a_T(x,y)}\right)^2\right]\right]^2\right]^{1/2} \tag{54}$$

where $T_e^* = T_e - T_\ell$. The results were plotted in Fig. 27. They are quite consistent with those in Fig. 26. The results for the temperature data seem to suggest certain trends with distance (plotted in dimensionless form with the hydraulic diameter $D_o = 0.4$ ft as a reference length), but there are not really enough data to warrant analysis of this detail.

The previous discussions centered around vertical distributions of temperature and velocity components in the x-direction. The analytical model described also specifies the horizontal distributions as Gaussian. There were not enough data in any horizontal section to really check this hypothesis. No more than seven measurements were taken in a horizontal cross section at a constant depth. The raw data reported in Ref. [53] suggest that normal distribution functions should be descriptive of what was observed. No further analysis is possible. It was noted that the widths of the velocity and excess temperature distributions were very similar, suggesting that the horizontal similarity parameter λ_h must also have a value close to 1.

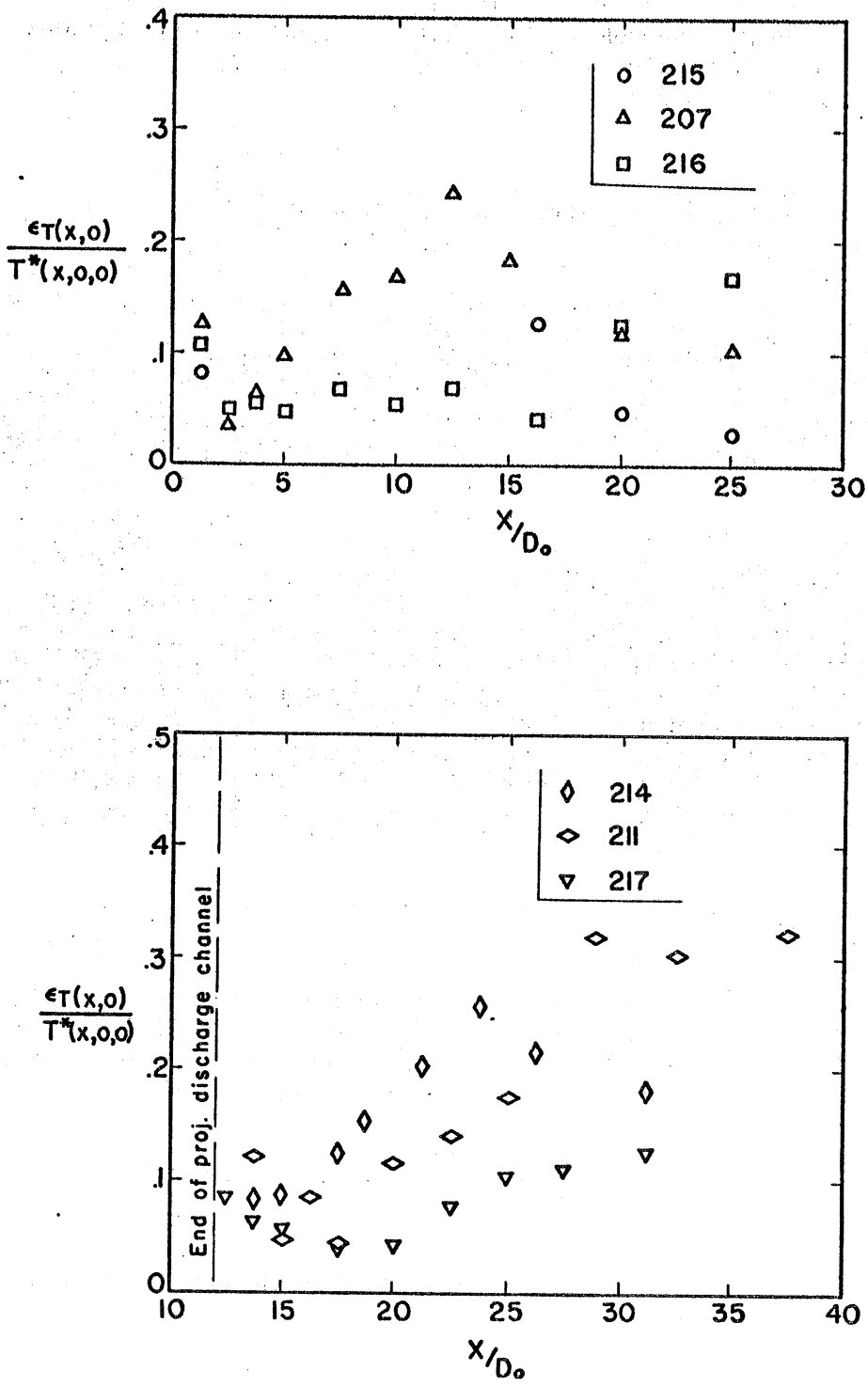

Fig. 27 - Standard Error between Normal Distribution Functions and Experimental Temperature Profile measured along Main Trajectory

Spread

A second major objective was to obtain information on the horizontal and vertical spread of the plume after discharge. Spread was evaluated in several different ways using

a) Velocity
b) Spread of isotherm patterns
c) Spread of velocity distributions
d) Visual spread

Spread Velocities -- The velocity component v perpendicular to the main trajectory is probably the most direct measure of lateral spread. In the analytical model it was assumed to be related to a densimetric Froude number for the centerline section. Plots of lateral (spread) velocity components v are given in Fig. 28 as an example. Apparently surface lateral spread velocities reach a maximum at a distance approximately one-third of the total width of the plume from the main trajectory. In the analytical model this point would be represented by $y = b$, where b is the standard deviation defined in Eq. (1). The lateral spread velocity changes with depth. It reverses direction at some distance from the water surface. Outward spread velocities (away from the main trajectory) are found near the water surface and inward flow at some depth below. Figure 29 shows examples of measurements. The reversal in flow direction occurs at a depth approximately equal to the thermocline or standard deviation a in Eq. (1). The inward flow appears to provide the necessary fluid for entrainment and also for the replacement of warm water when lateral spread reduces the depth of the thermocline. The observation of an inward flow thus supports the displacement (spread) equation (19) in the analytical model.

Equation (18) suggests that the buoyancy-induced surface lateral spread velocity at a distance $y = b$ from the main trajectory is related to the centerline densimetric Froude number. The spread velocities v reported in Figs. 28 and 29 are totals produced by turbulence and buoyancy. According to Eq. (21) the two effects are additive. In Ref. [37] it has been shown that the centerline velocity u in a fully developed non-buoyant, axisymmetric jet varies according to

$$\frac{u(x,0,0)}{u(0,0,0)} \frac{x}{D_o} = 6.2 \qquad (x > 6.2\ D_o) \tag{55}$$

using the notations of this paper. The lateral spread velocity was found [37] to have a maximum of

$$\frac{v(x,b,0)}{u(0,0,0)} \frac{x}{D_o} = 0.35 \tag{56}$$

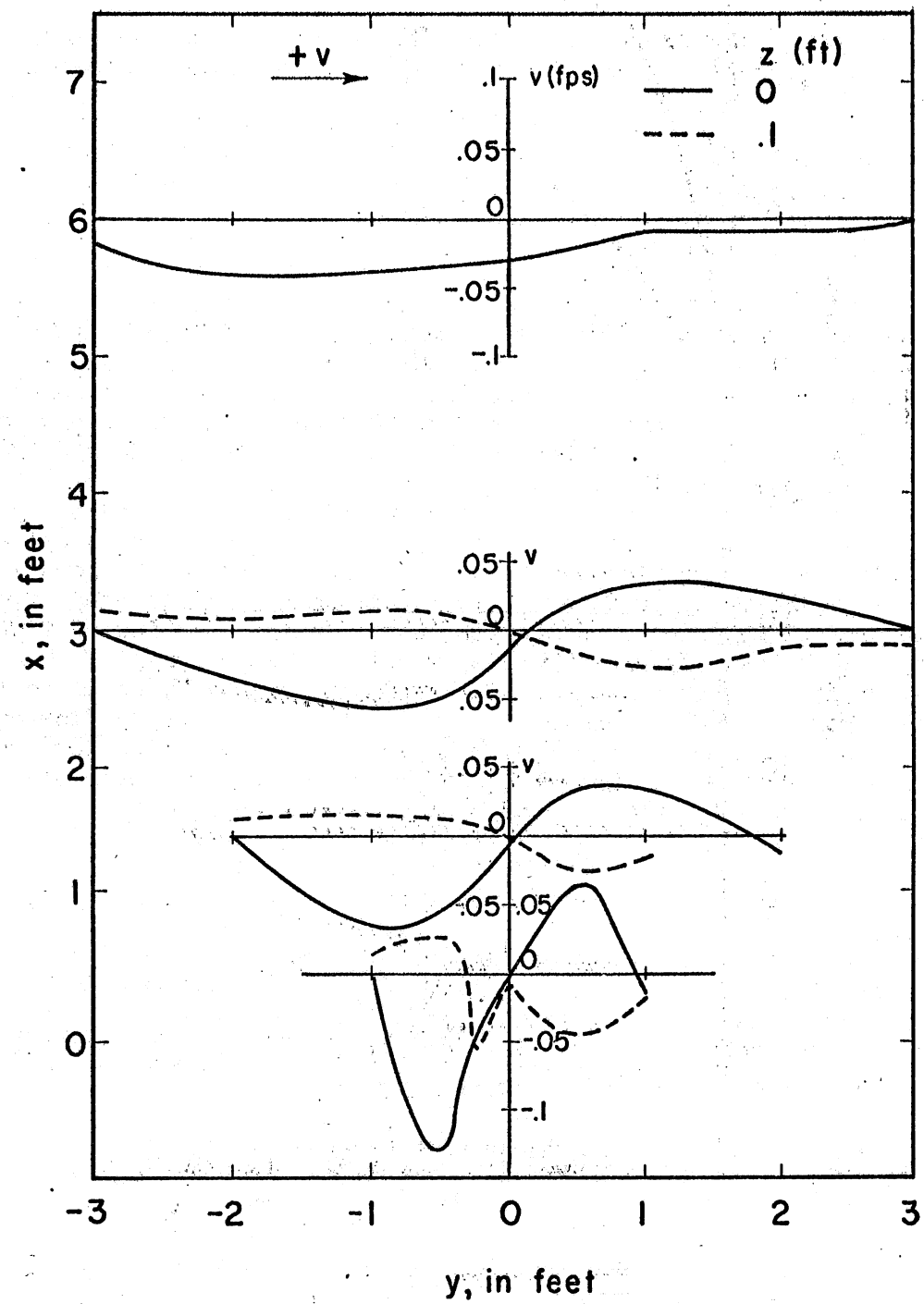

Fig. 28 - Lateral Spread Velocities v at Two Depths (z = 0 and z = 0.1 ft) for Exp. 207

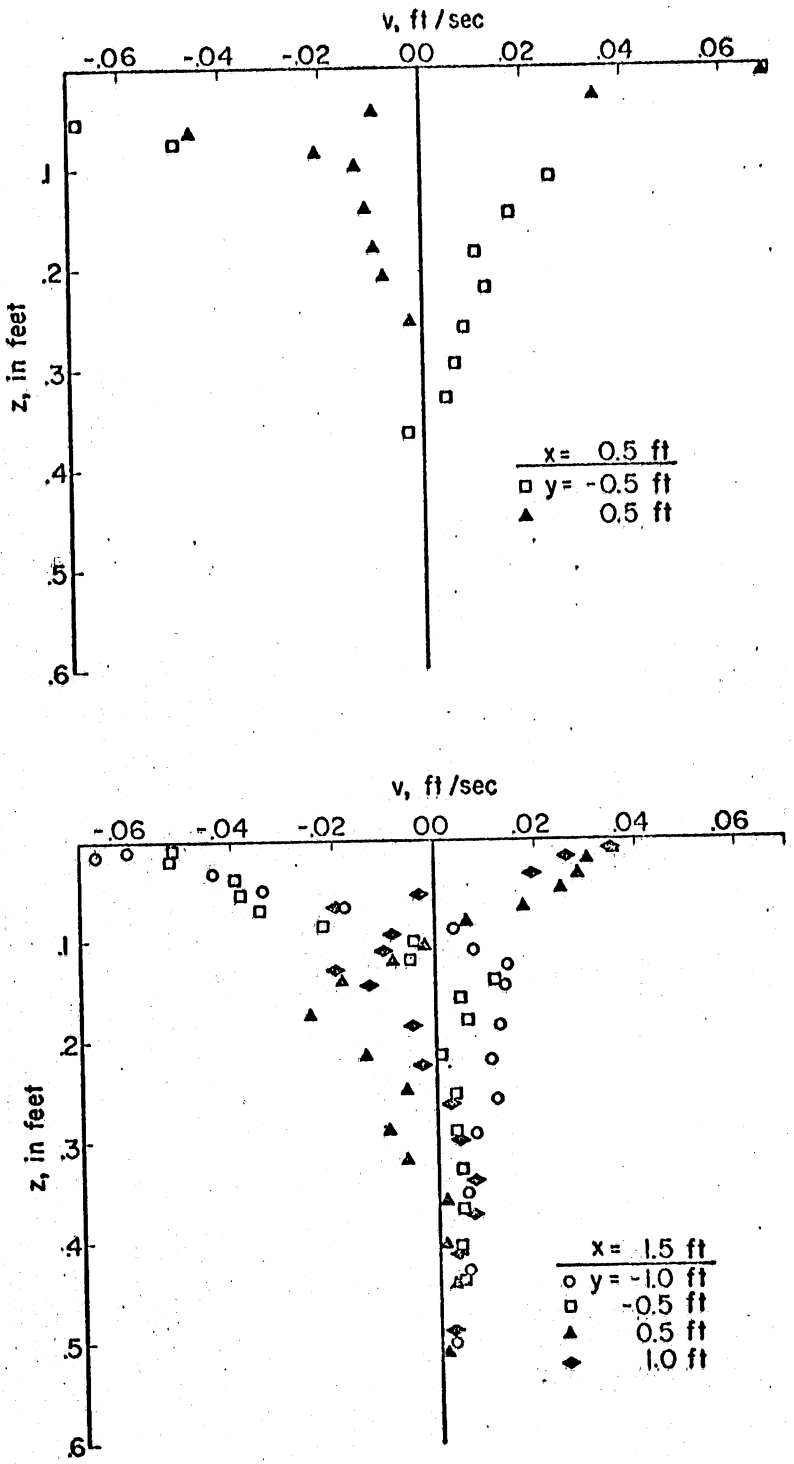

Fig. 29 - Variation of Velocity Component v with Depth at Various Distances from the Outlet and the Main Trajectory. Exp. 207

Thus the turbulence-induced spread in dimensionless form has a value of

$$\frac{(db/dt)_T}{u(x,0,0)} = \frac{v(x,b,0)}{u(x,0,0)} = \frac{0.35}{6.2} = 0.0565 \tag{57}$$

The buoyancy-induced spread according to Eqs. (14) and (4) is

$$\left(\frac{db}{dt}\right)_B = c_5 \frac{u(x,0,0)}{F^*} \tag{58}$$

which in the absence of both a cross current and wind is also equal to

$$\frac{(db/dt)_B}{u(x,0,0)} = \frac{c_5}{F} \tag{59}$$

To evaluate the coefficient c_5, measured maximum spread velocities (Fig. 28) were reduced to dimensionless form and a value of 0.0565 subtracted. The resulting values were plotted in Fig. 30 versus $1/F$. The results suggest that $c_5 \approx 0.5$.

Spread of Isotherm Patterns -- Another, more descriptive way to illustrate the spread of the heated water surface jet is to graph isotherms in various sections. Isotherm patterns in vertical planes along the main trajectory and perpendicular to it have been given in Refs. [22] and [53]. The results indicated in Ref. [53] are also reflected in the data of Fig. 23 of this report. The standard deviations of temperature profiles (and velocity profiles) as plotted in Fig. 23 can be used as measures of vertical spread. It is quite apparent that temperature induced buoyancy caused the heated water to spread on the surface of the tank without significant penetration into it.

To obtain a picture of the horizontal spread of the surface jet a different kind of graph was used. Figure 31 gives examples. Program CONTOUR was used to do the plotting. The outlet is at the bottom center of each map and the flow is from the bottom to the top of the map. Coordinates are given in feet with reference to the upstream end of the tank (bottom of picture) and the centerline of the tank, respectively. Alternate contours are printed. The numbers inside the map are dimensionless excess temperatures of the form $T^*(x,y,z)/T^*(0,0,0)$ multiplied by a factor of 10. Examination of the maps reveals a number of features. First, in each run a "typical" plume temperature distribution is formed around the outlet. The depth d_T at which the pattern disappears has been plotted versus the densimetric outlet Froude number in Fig. 32. The results can be approximated by the relationship

$$\frac{d_T}{do} = \sqrt{\frac{F_o}{2}} \tag{60}$$

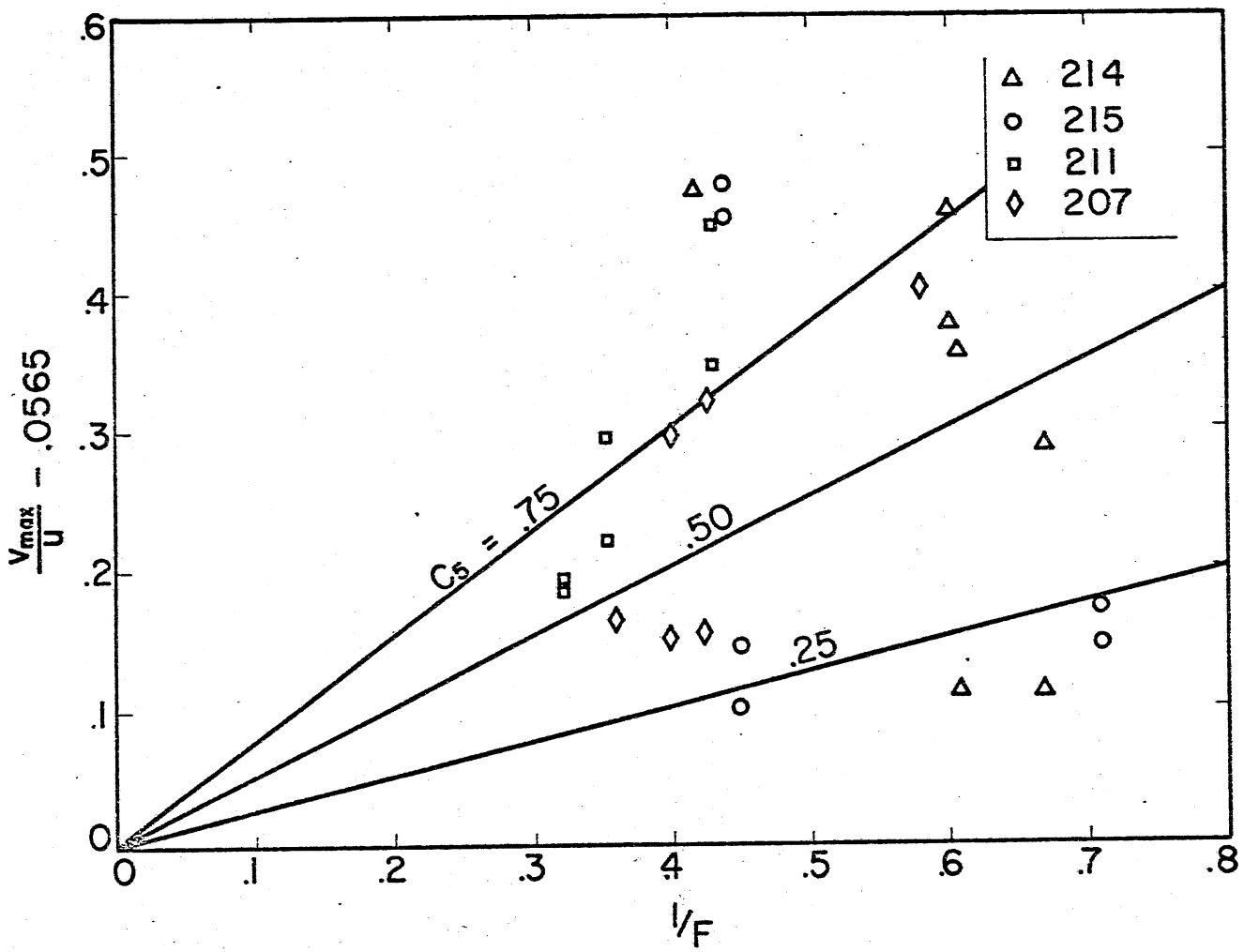

Fig. 30 - Maximum Spread Velocities versus Centerline Densimetric Froude Numbers for Individual Cross Sections Perpendicular to the Main Trajectory

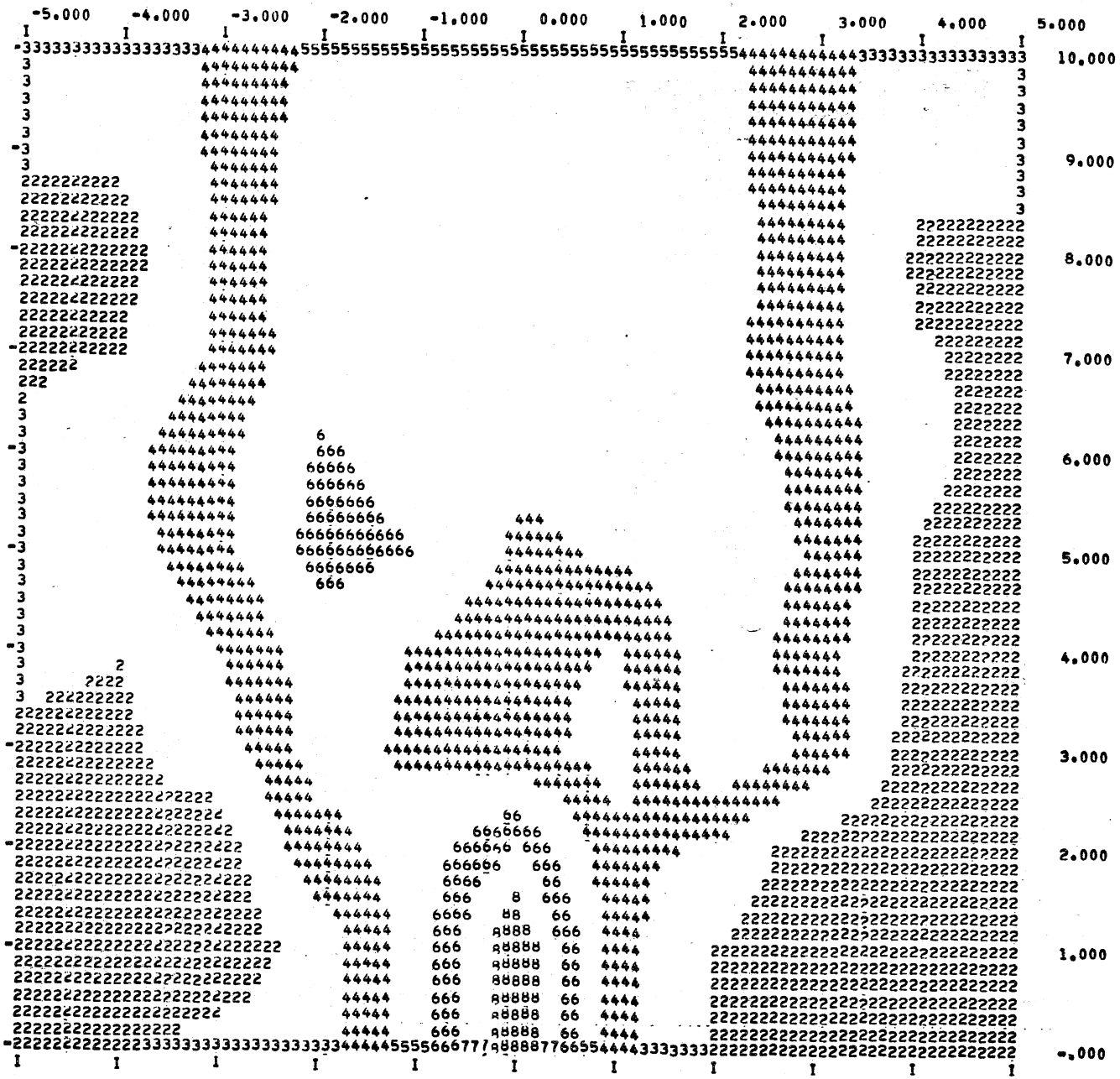

Fig. 31a - Isotherms for Run 215 (Horizontal section for depth z = 0.01 ft)

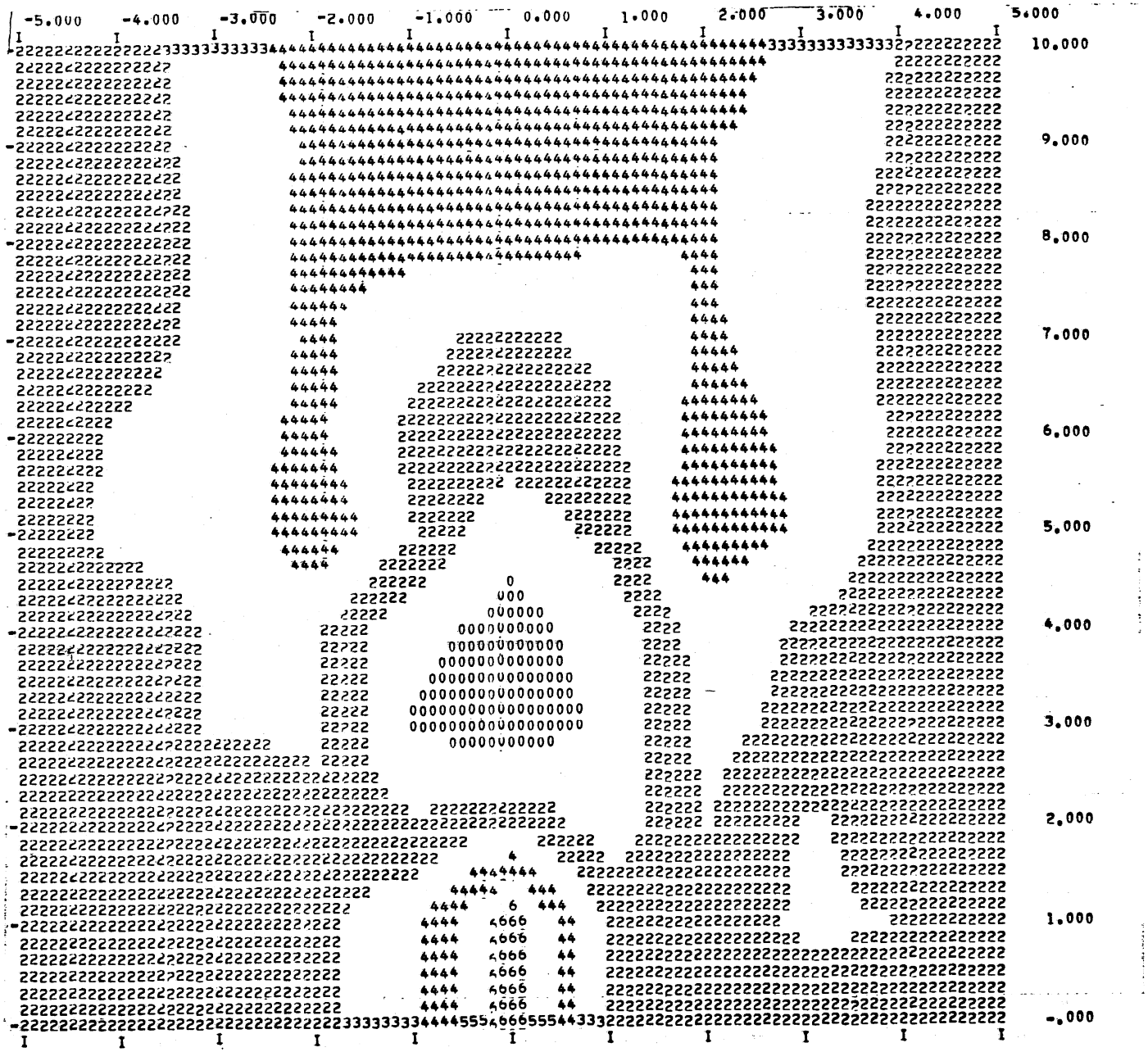

Fig. 31b - Isotherms for Run 215 (Horizontal section for depth z = 0.03 ft)

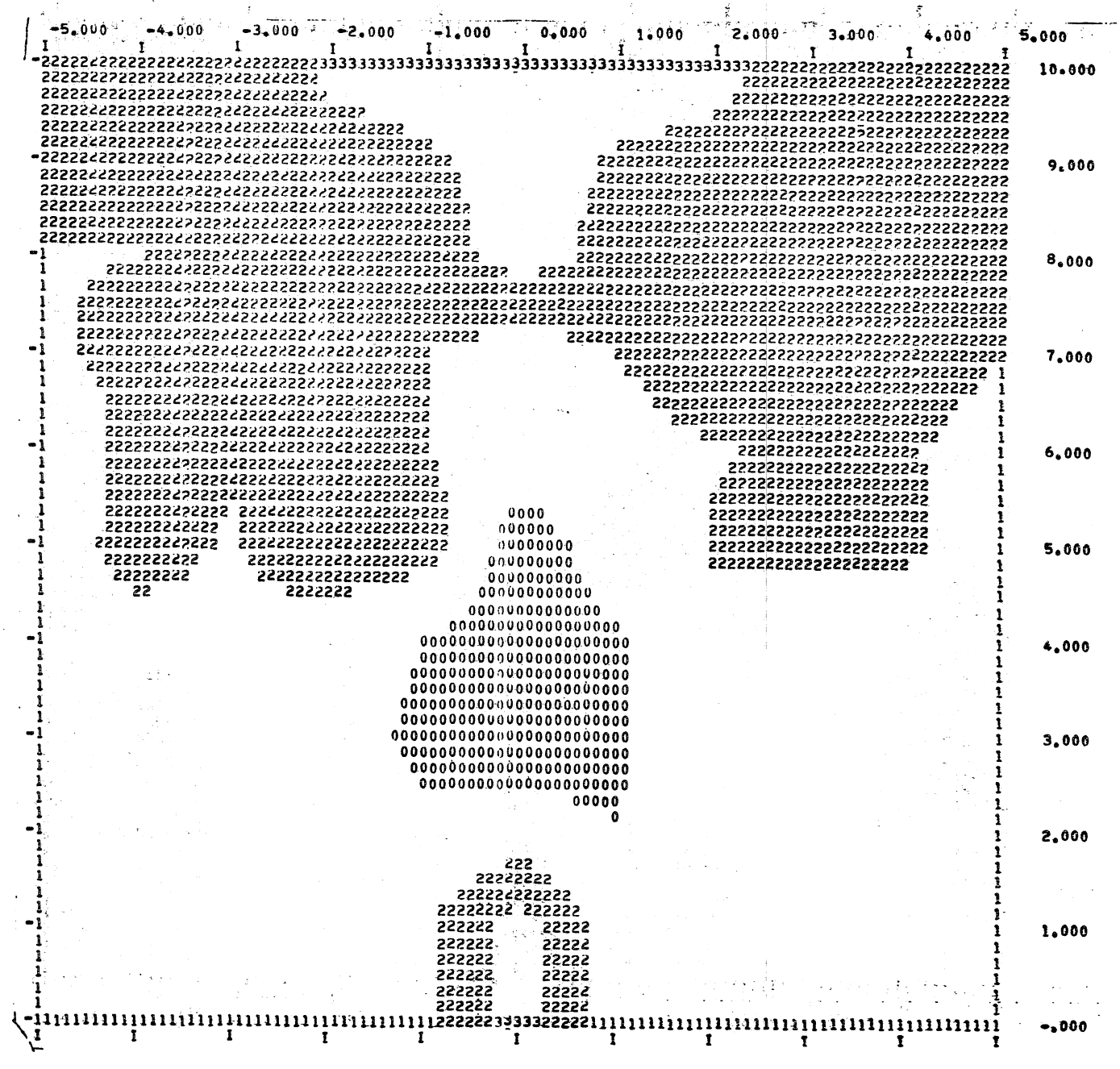

Fig. 31c - Isotherms for Run 215 (Horizontal section for depth z = 0.05 ft)

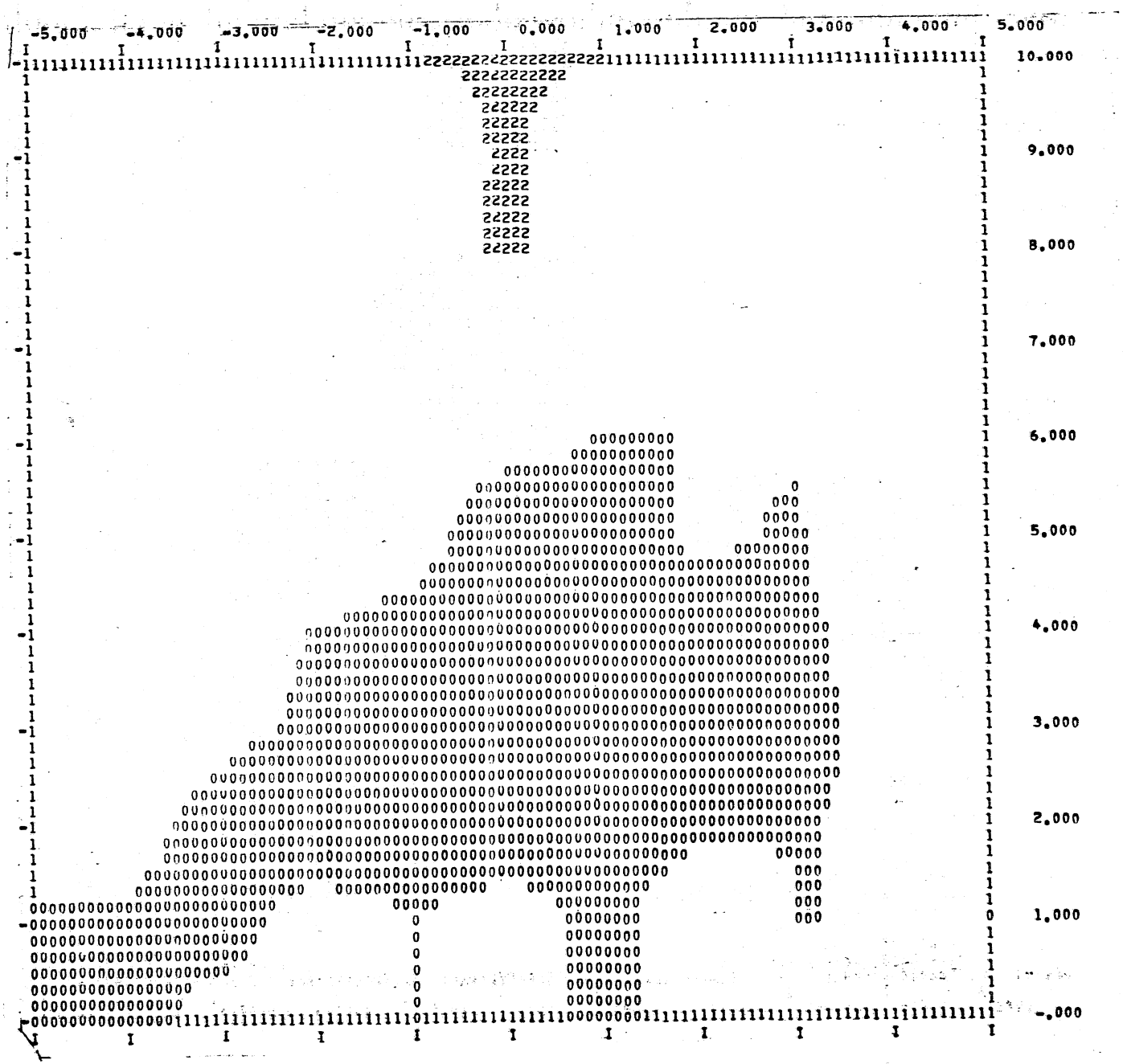

Fig. 31d -
Isotherms for Run 215
(Horizontal section
for depth z = 0.07 ft)

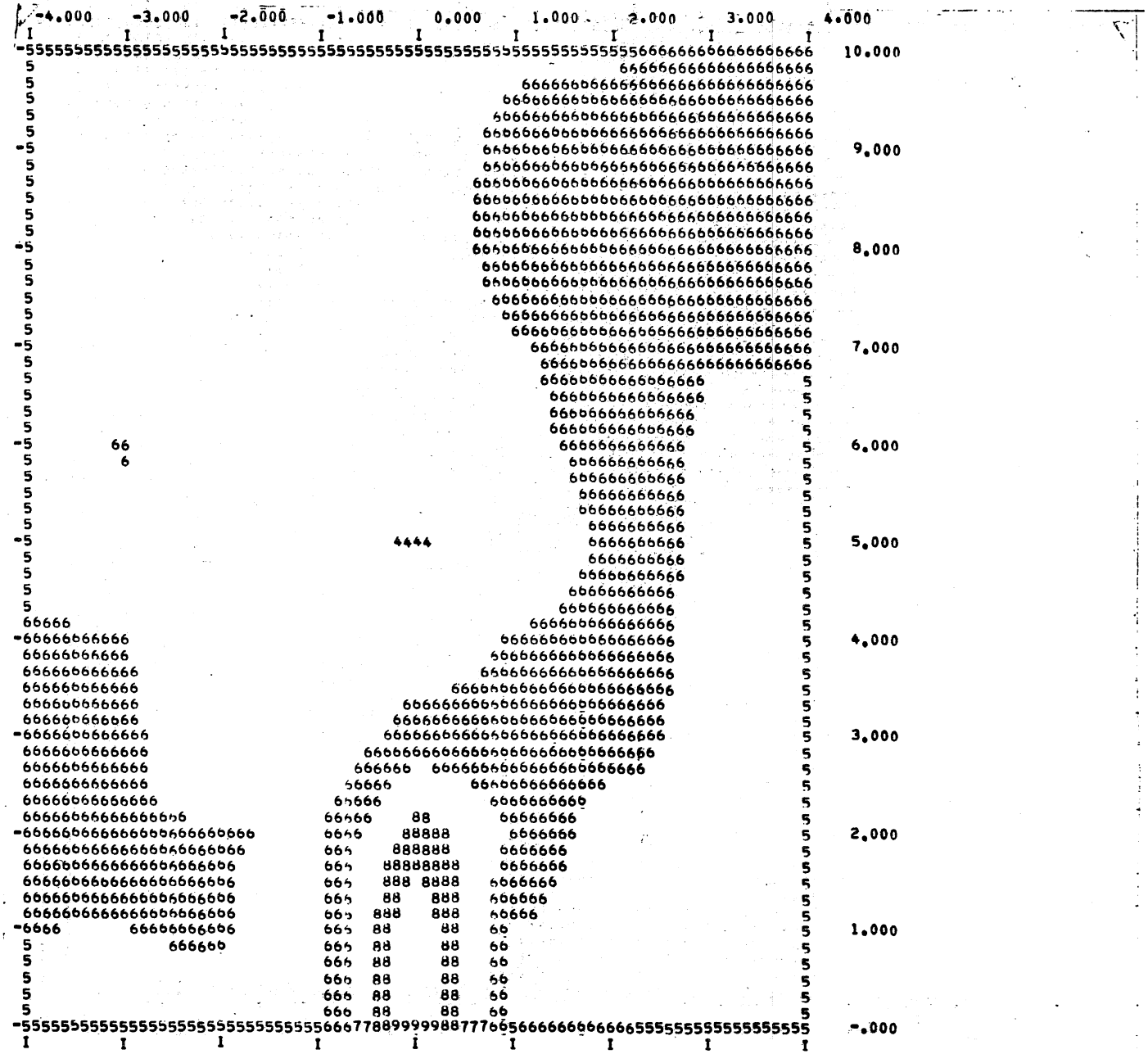

Fig. 31e -
Isotherms for Run 207
(Horizontal section
for depth z = 0.01 ft)

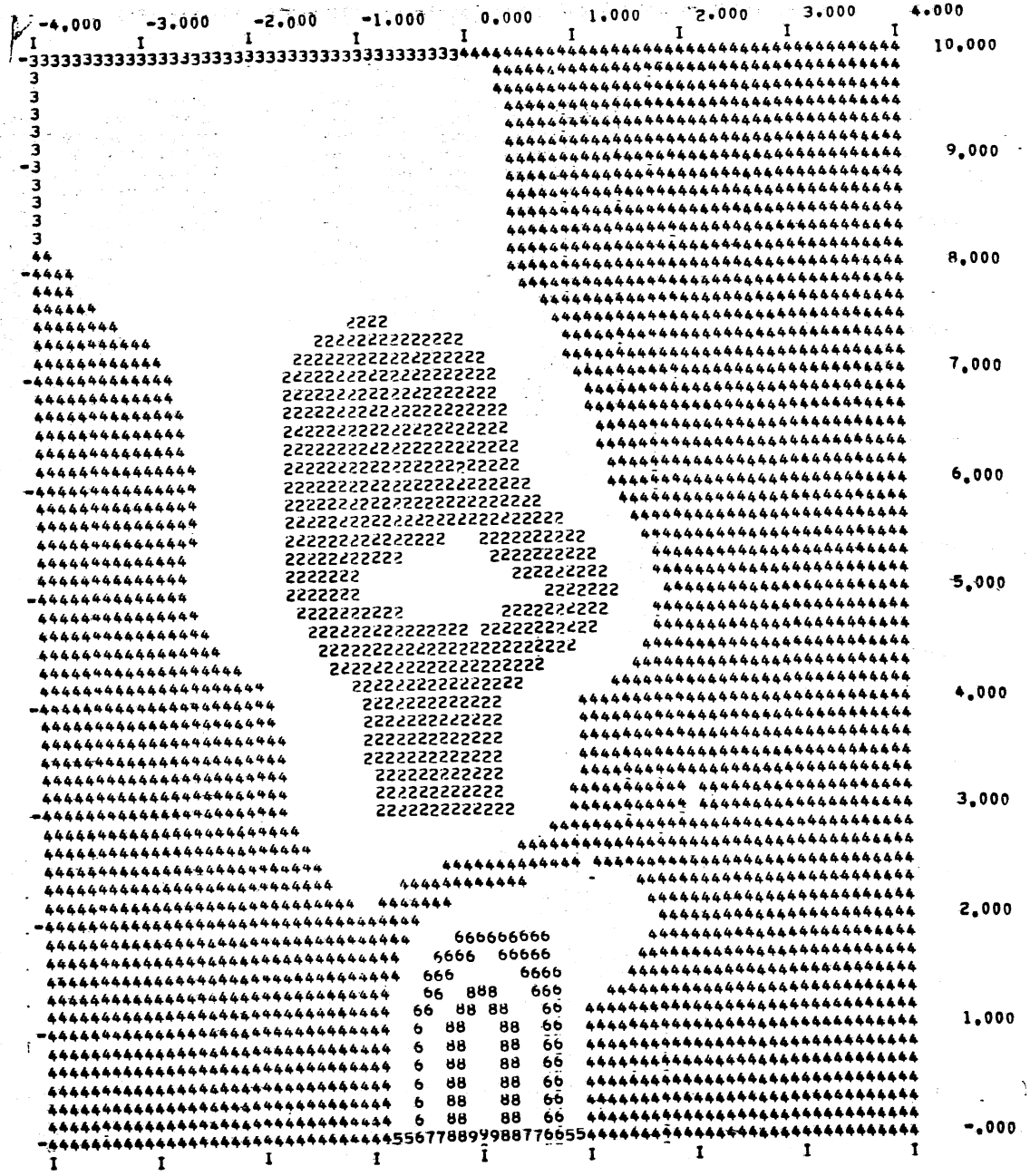

Fig. 31f - Isotherms for Run 207 (Horizontal section for depth z = 0.05 ft)

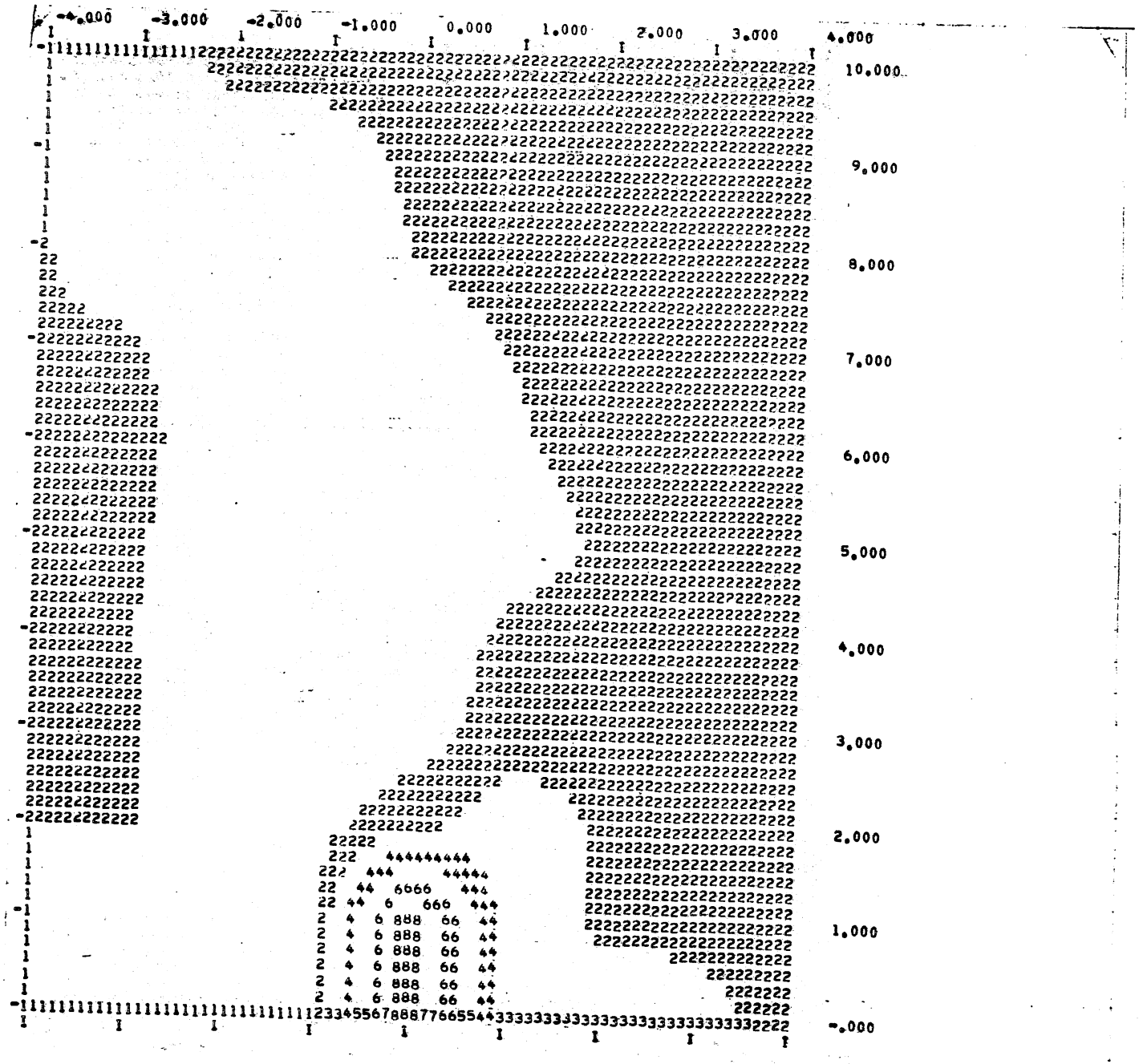

Fig. 31g - Isotherms for Run 207 (Horizontal section for depth z = 0.10 ft)

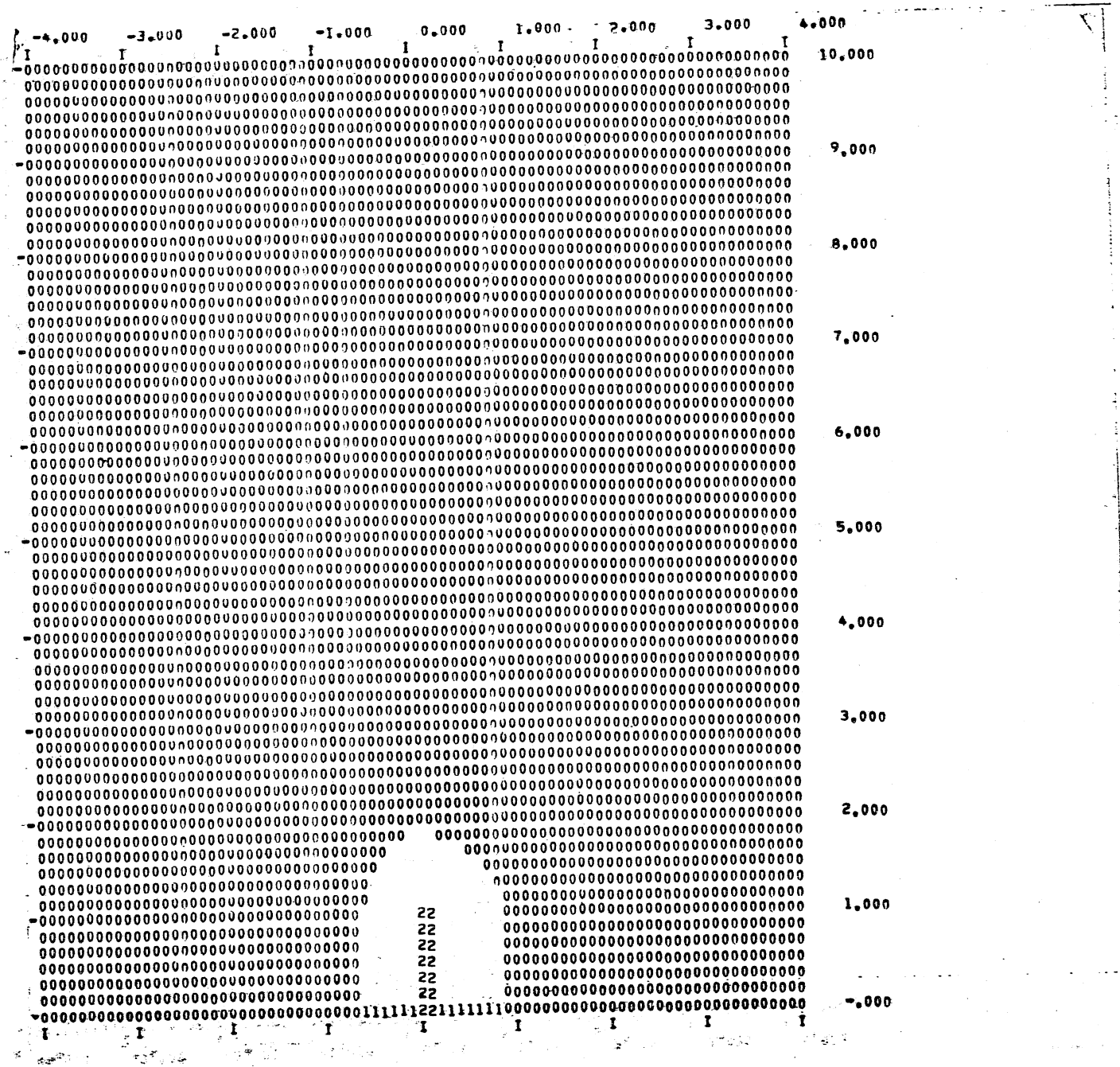

Fig. 31h - Isotherms for Run 207 (Horizontal section for depth z = 0.16 ft)

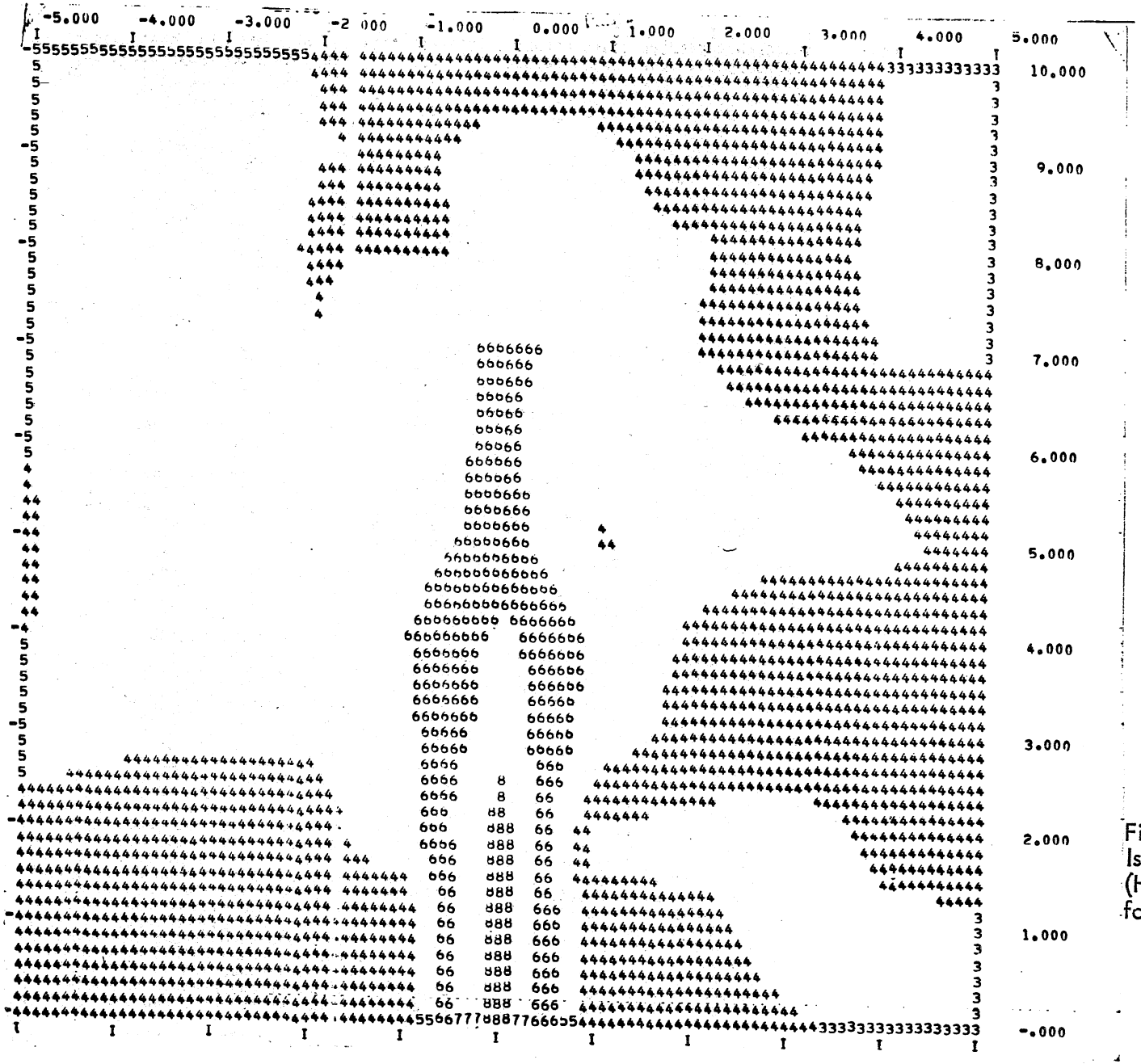

Fig. 31i - Isotherms for Run 216 (Horizontal section for depth z = 0.01 ft)

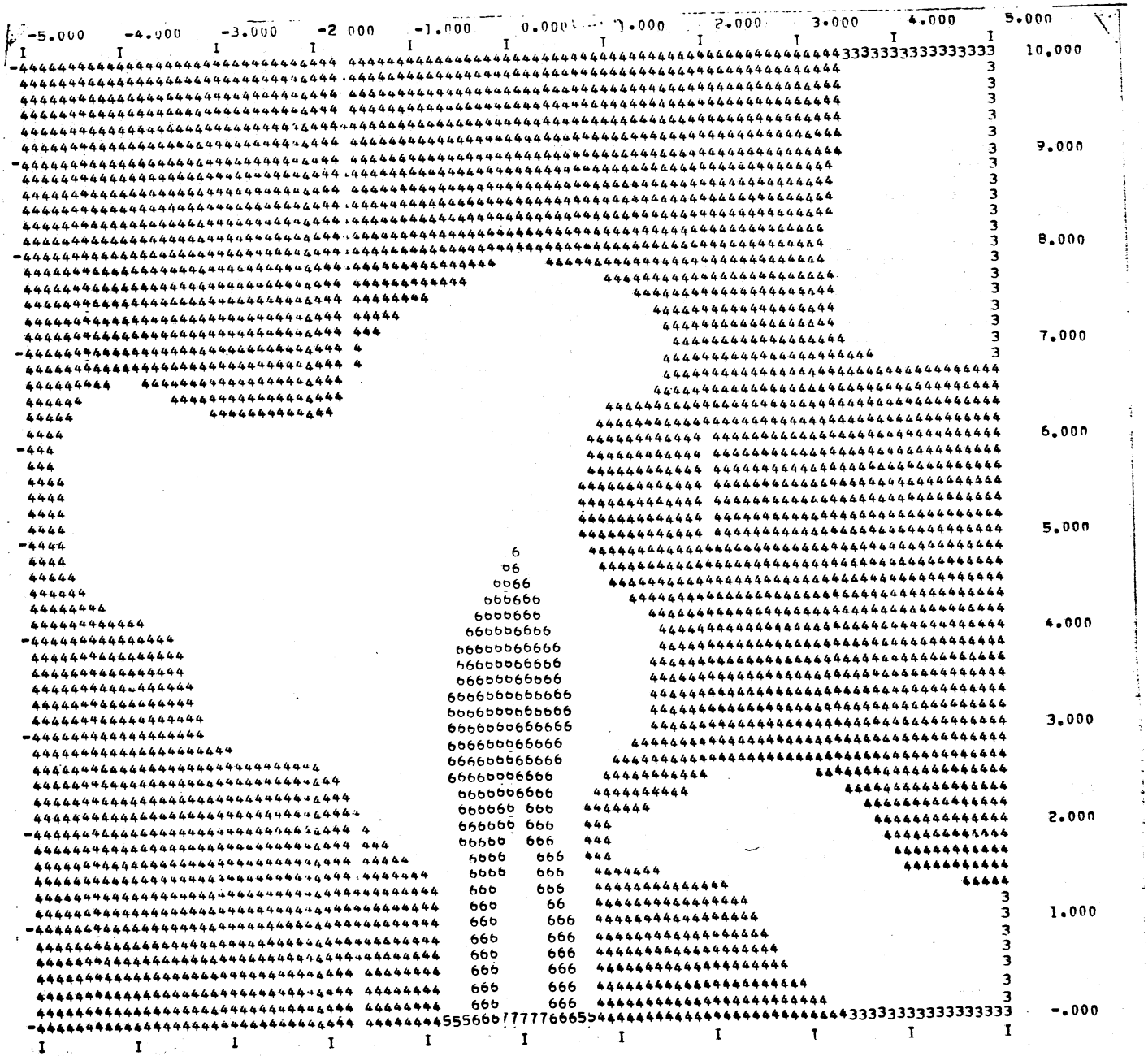

Fig. 31j -
Isotherms for Run 216
(Horizontal section
for depth z = 0.05 ft)

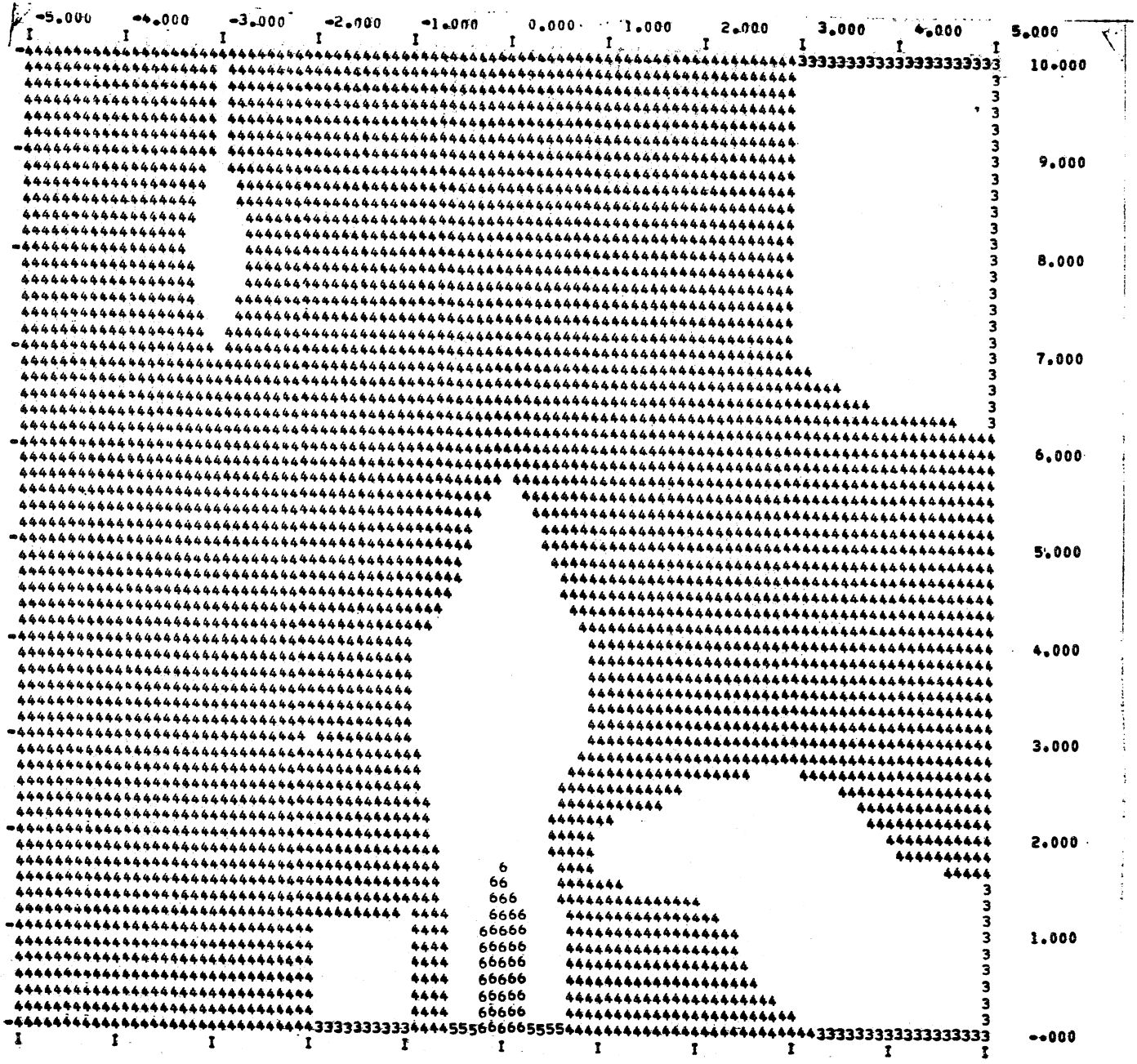

Fig. 31k - Isotherms for Run 216 (Horizontal section for depth z = 0.10 ft)

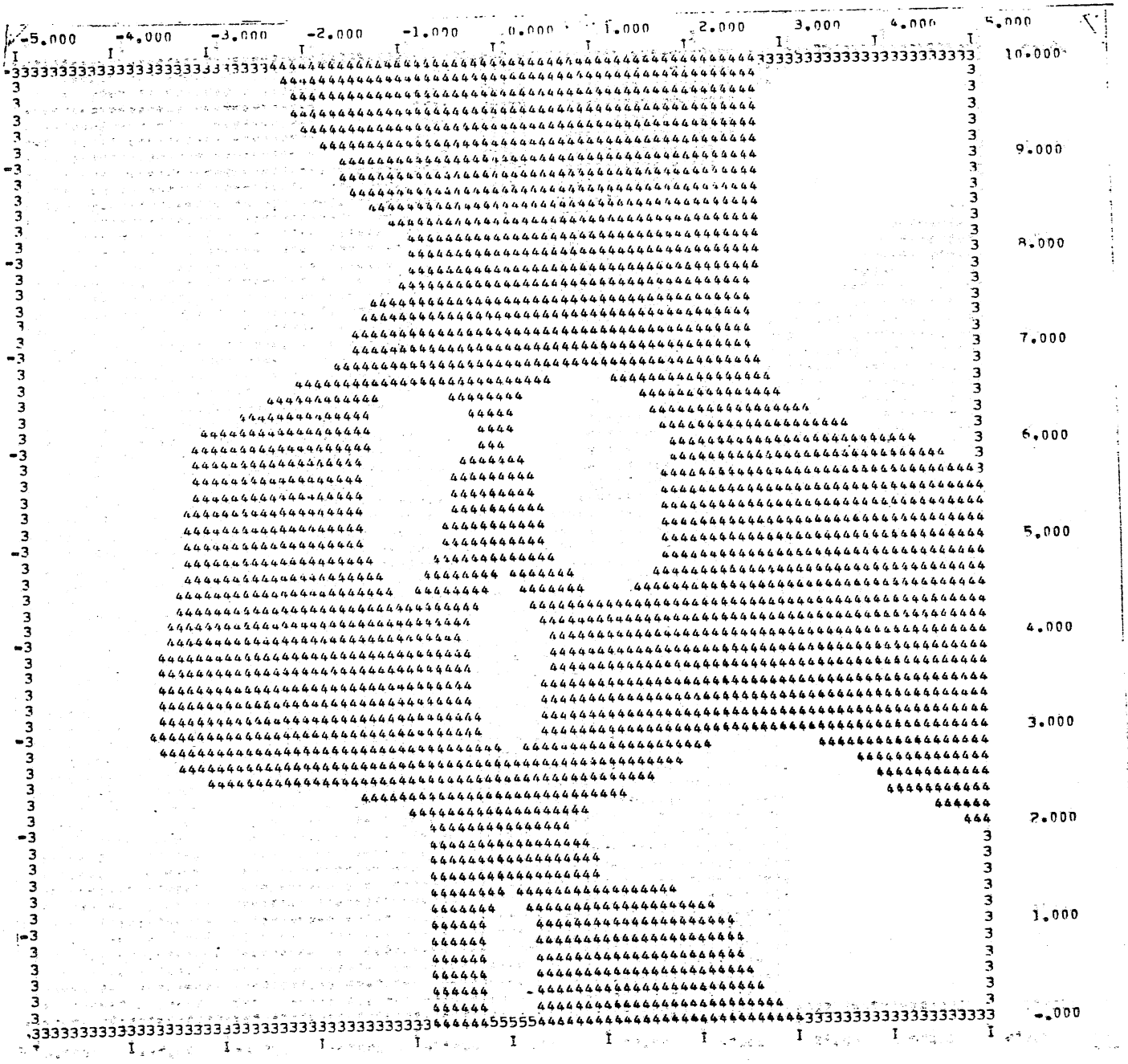

Fig. 31ℓ - Isotherms for Run 216 (Horizontal section for depth z = 0.14 ft)

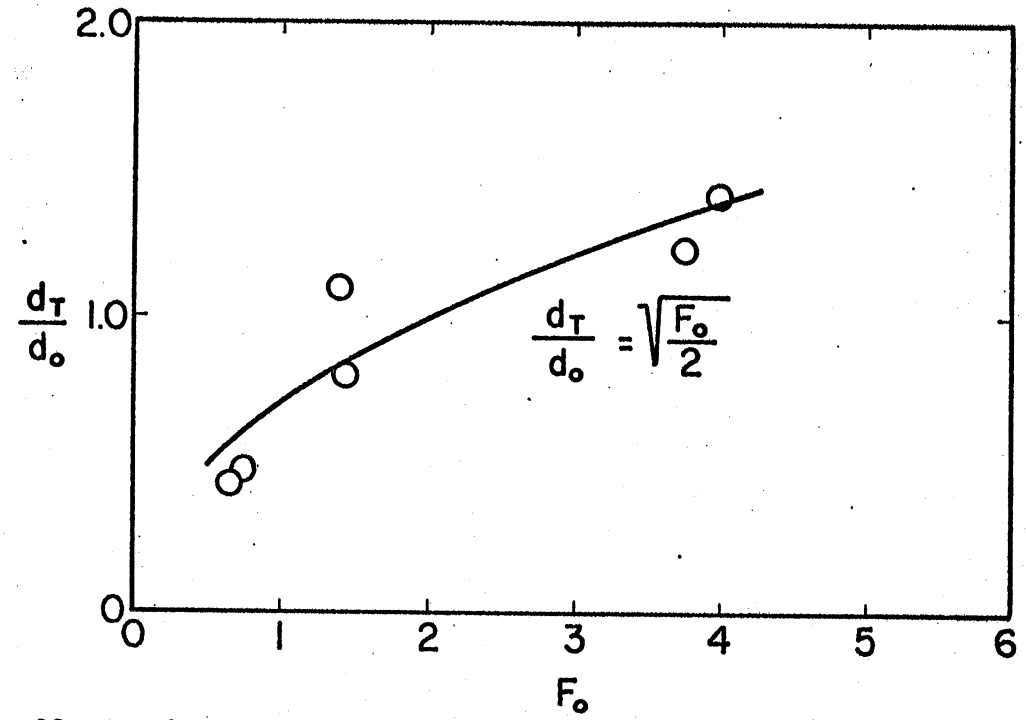

Fig. 32 - Depth of Penetration d_T of Heated Water Surface Jet as derived from Isotherm Patterns

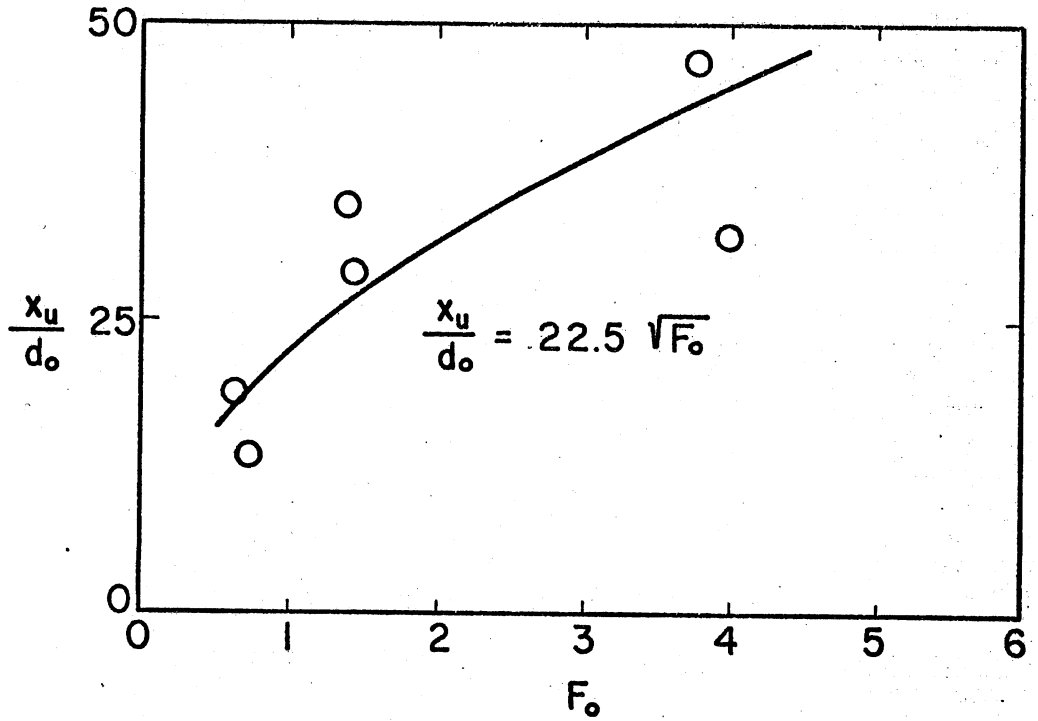

Fig. 34 - Length x_T of Identifiable Jet Type Flow as derived from Velocity-Concentration Patterns

with $0.7 < F_o < 4.0$. The depth d_m can be considered a measure of the depth to which the outlet (jet) flow penetrates into the ambient water.

The second observation pertains to the temperatures in the water surrounding the surface jet pattern. The ambient surface temperatures are not those of the cold water, but have some intermediate value. The heated water is discharged into a tank with an unintended existing (weak) temperature stratification which has been produced by flow conditions established through the boundaries of the tank and by the heat loss from the tank surface to the atmosphere. The tank had an overflow weir placed at the downstream end and vertical walls on either side. In the absence of any currents in a prototype a similar situation can exist.

A third observation regards the shape of the plume as shown by the isotherm patterns. The near surface patterns ($z = 0.01$ ft) generally consist of a very nearly uniform flow over a short distance (one foot) beyond the outlet followed by a gradual lateral expansion. The angle of lateral spread can be seen to depend somewhat on the outlet densimetric Froude number.

A fourth observation regards the randomness in the temperature distribution patterns. From a theoretical point of view all temperature distributions should be symmetrical with reference to the centerline of the tank. But except for a small area near the outlet, measurements do not show such perfect symmetry, because the tank is not a perfectly quiescent pool. The low-velocity inflow of cold water at the bottom of the tank, the free surface flow over the weir at the end of the tank, and the pair of very large and very slow eddies forming frequently on either side of the outlet all contributed to some very slow and barely detectable flow patterns on which the heated water jet flow and the free shear turbulence associated with it were superimposed. Near the outlet the jet mechanism was dominant, but at larger distance from the outlet more randomness in the patterns became clearly apparent. This investigation dealt only with the buoyant jet-type flow mechanism near the outlet and did not cover anything beyond. Motion of the ambient fluid exists in any bounded experimental tank with throughflow. The relevance of measurements very far downstream from the outlet must therefore be questioned.

Prototype plumes also break up into complex velocity and temperature patterns, usually by passive diffusion in currents. Wind frequently contributes to the disappearance of the typical plume patterns.

Spread of Iso-Velocity Concentrations -- Rather than temperature measurements, velocity measurements could be used to obtain maps similar to those of Fig. 31. Velocity components in the x-direction (u-component) were used for that purpose. Local measurements were reduced to dimensionless velocity concentrations using the average discharge velocity as a reference value. Thus velocity concentrations are defined as $u(x,y,z)/U_o$, where $U_o = Q_o/(w_o d_o)$. Figure 33 shows

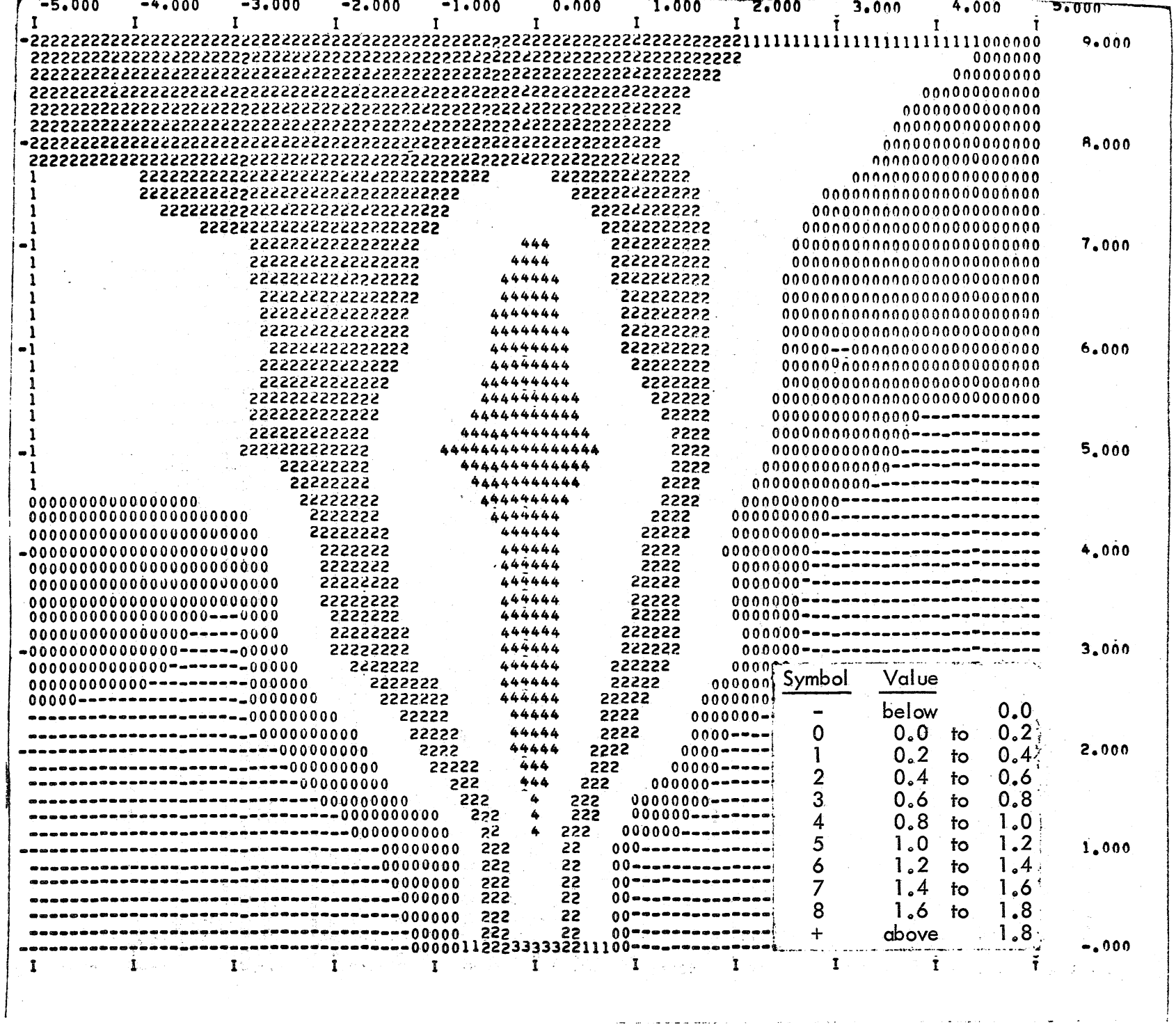

Fig. 33a - Iso-velocity concentrations of u-component for Run 207 (horizontal section for depth z = 0.01 ft)

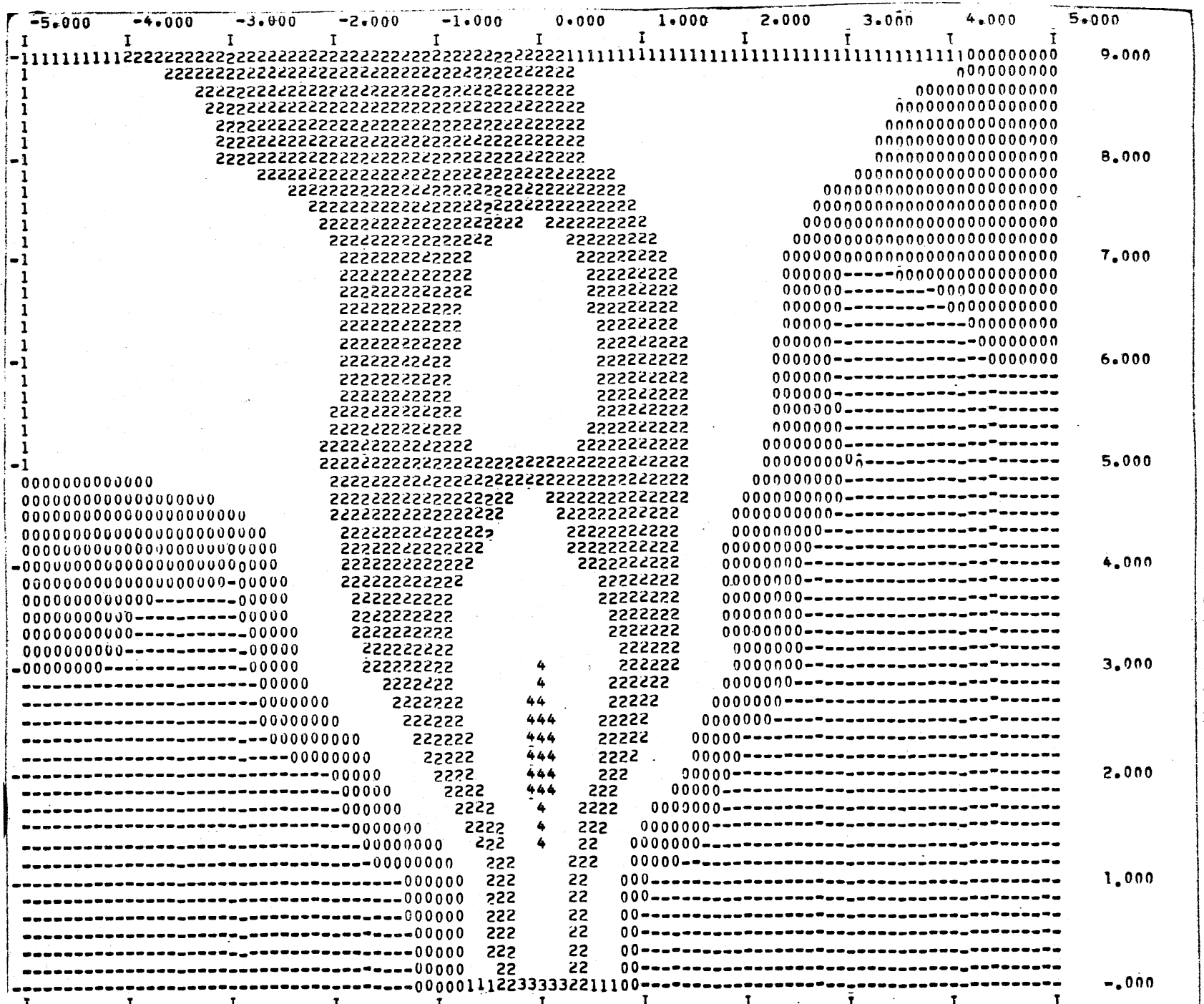

Fig. 33b - Iso-velocity concentrations of u-component for Run 207 (horizontal section for depth z = 0.03 ft)

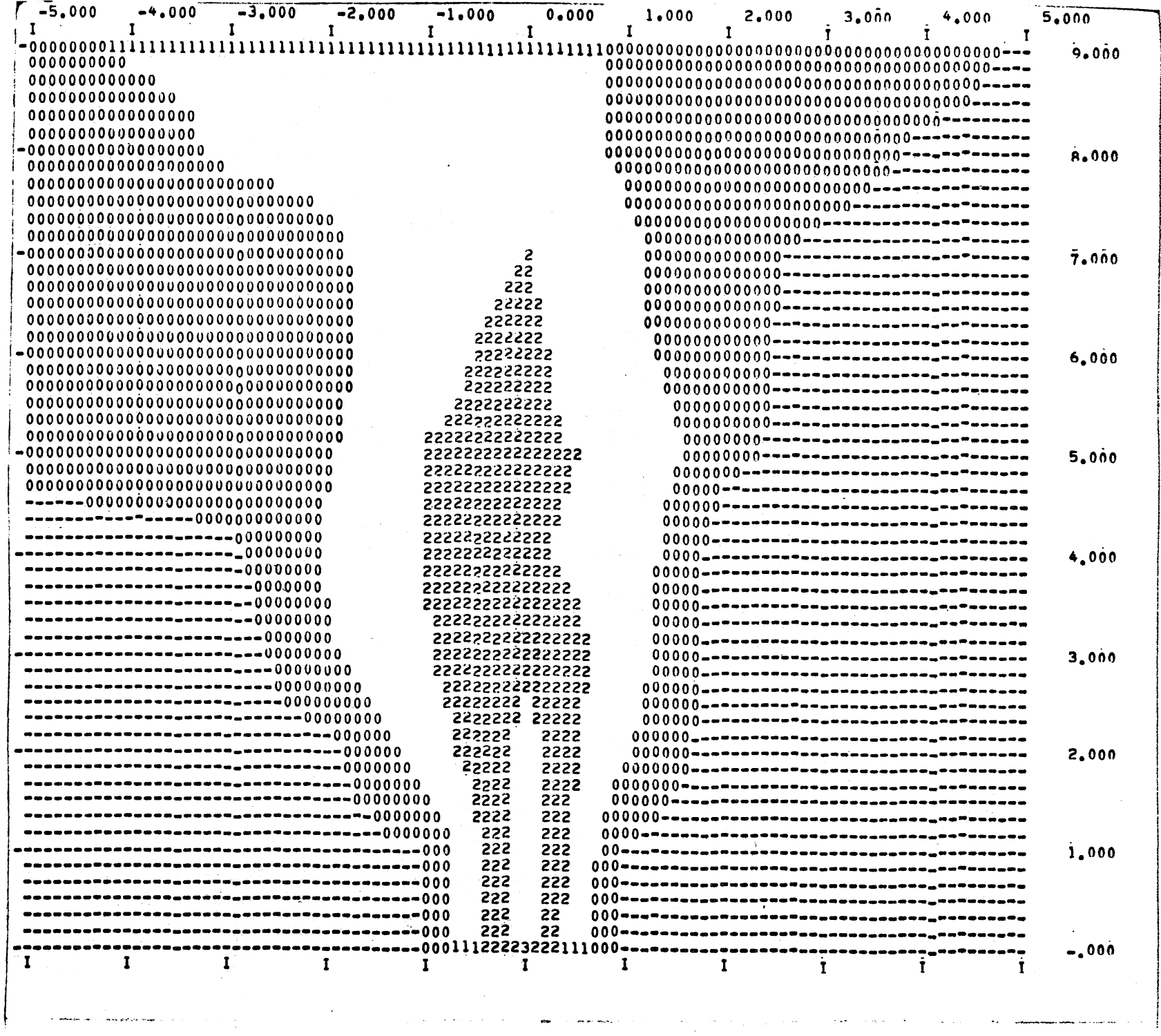

Fig. 33c - Iso-velocity concentrations of u-component for Run 207 (horizontal section for depth z = 0.07 ft)

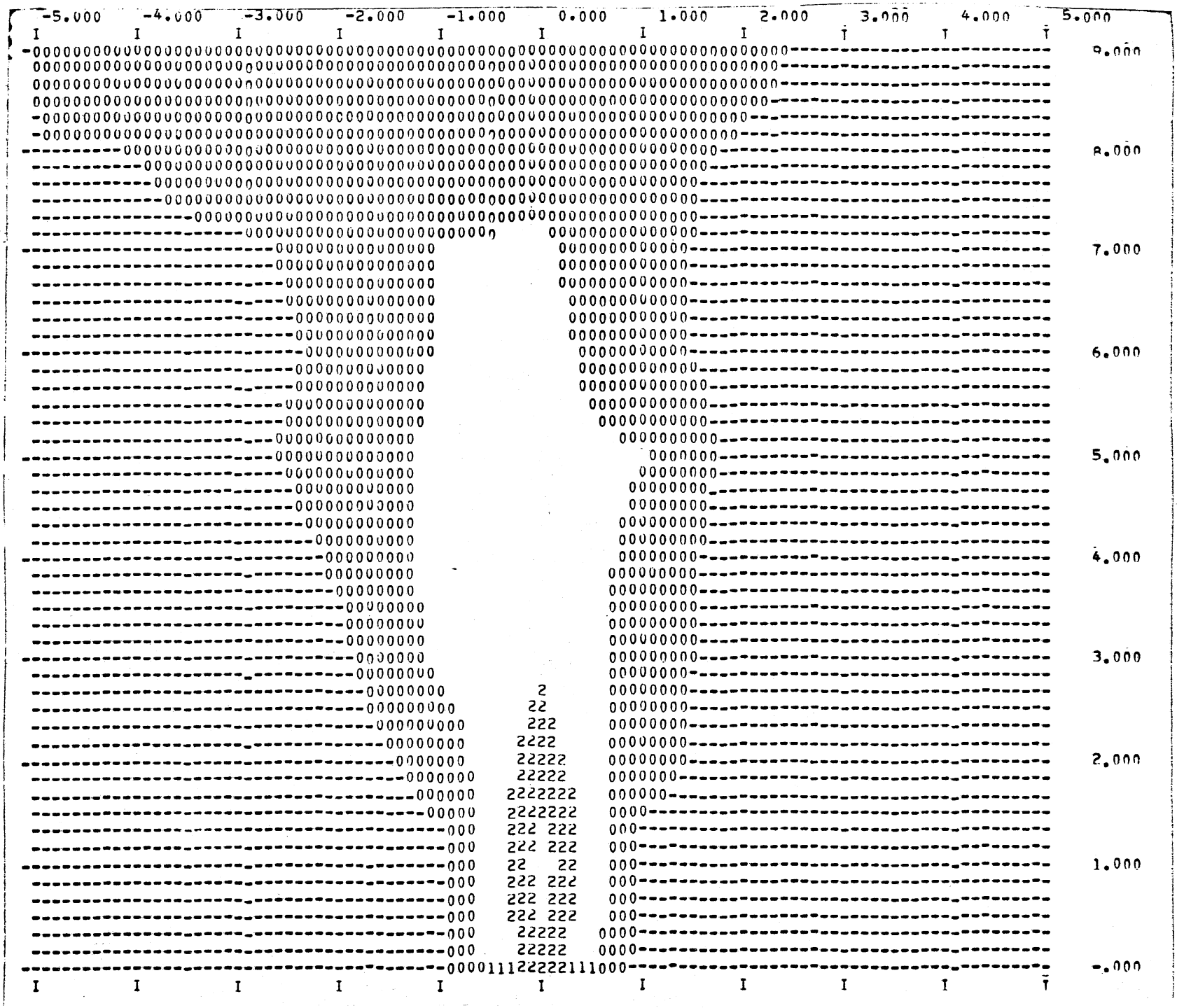

Fig. 33d - Iso-velocity concentrations of u-component for Run 207 (horizontal section for depth z = 0.10 ft)

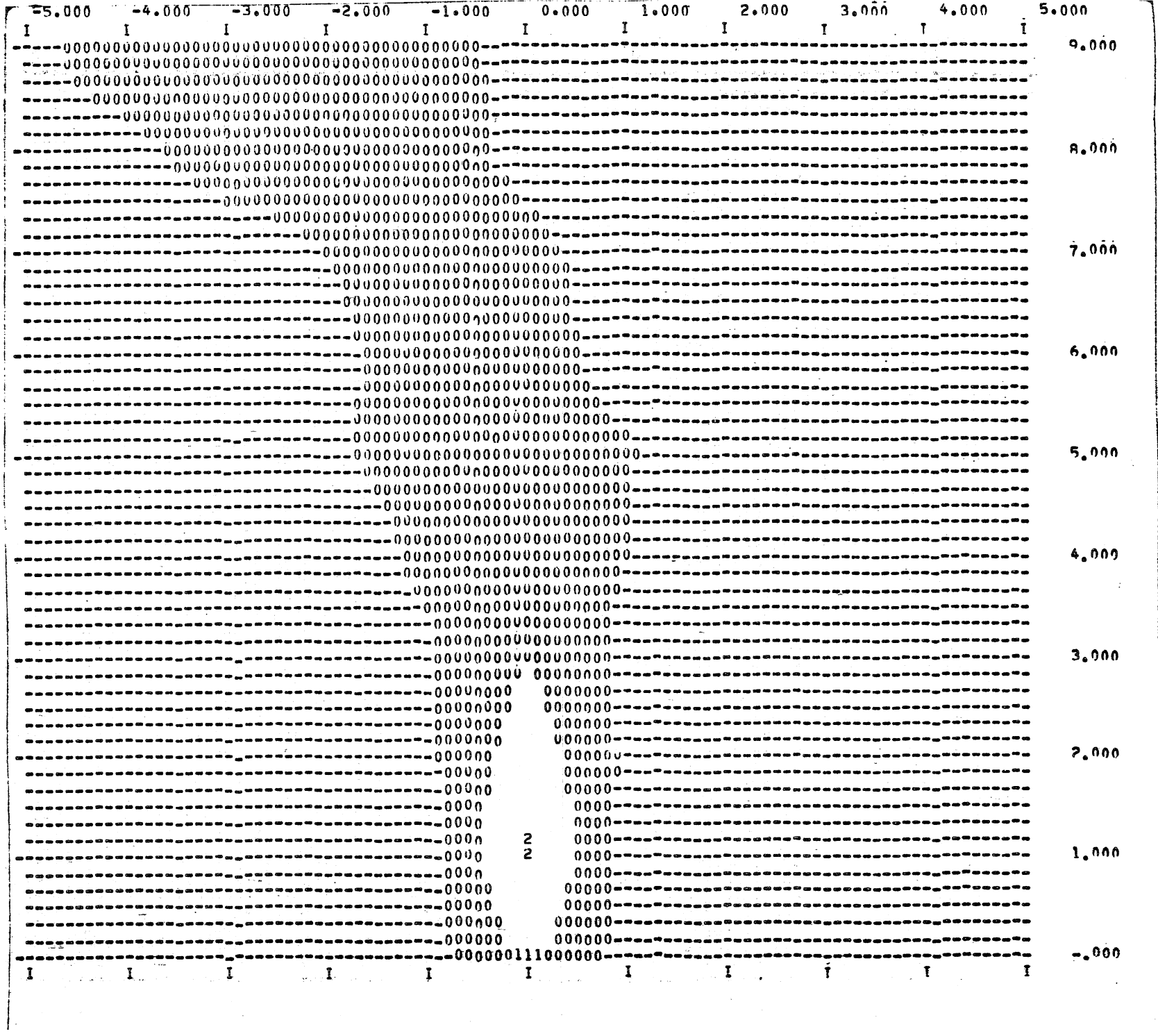

Fig. 33e - Iso-velocity concentrations of u-component for Run 207 (horizontal section for depth z = 0.14 ft)

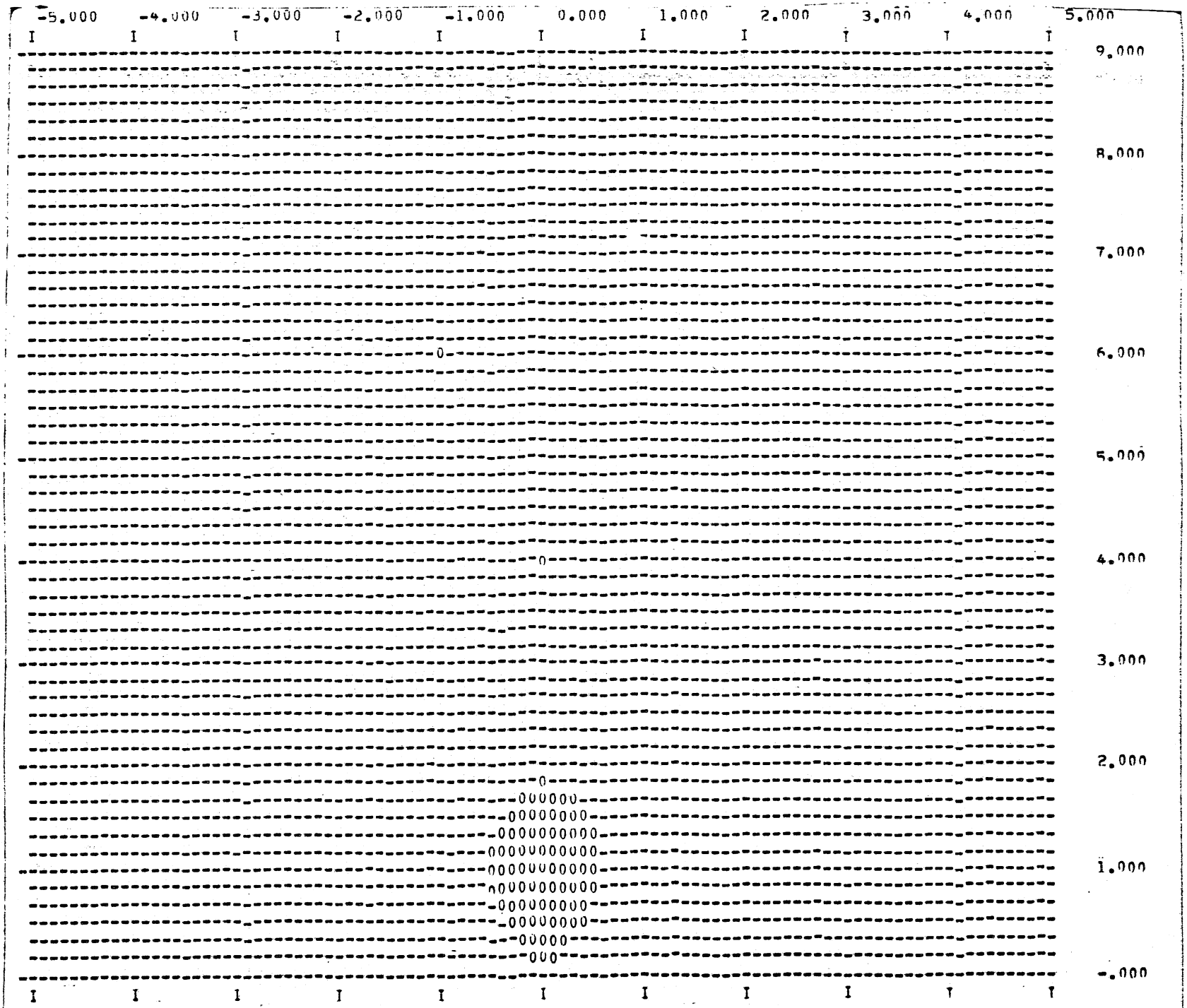

Fig. 33f - Iso-velocity concentrations of u-component for Run 207 (horizontal section for depth z = 0.20 ft)

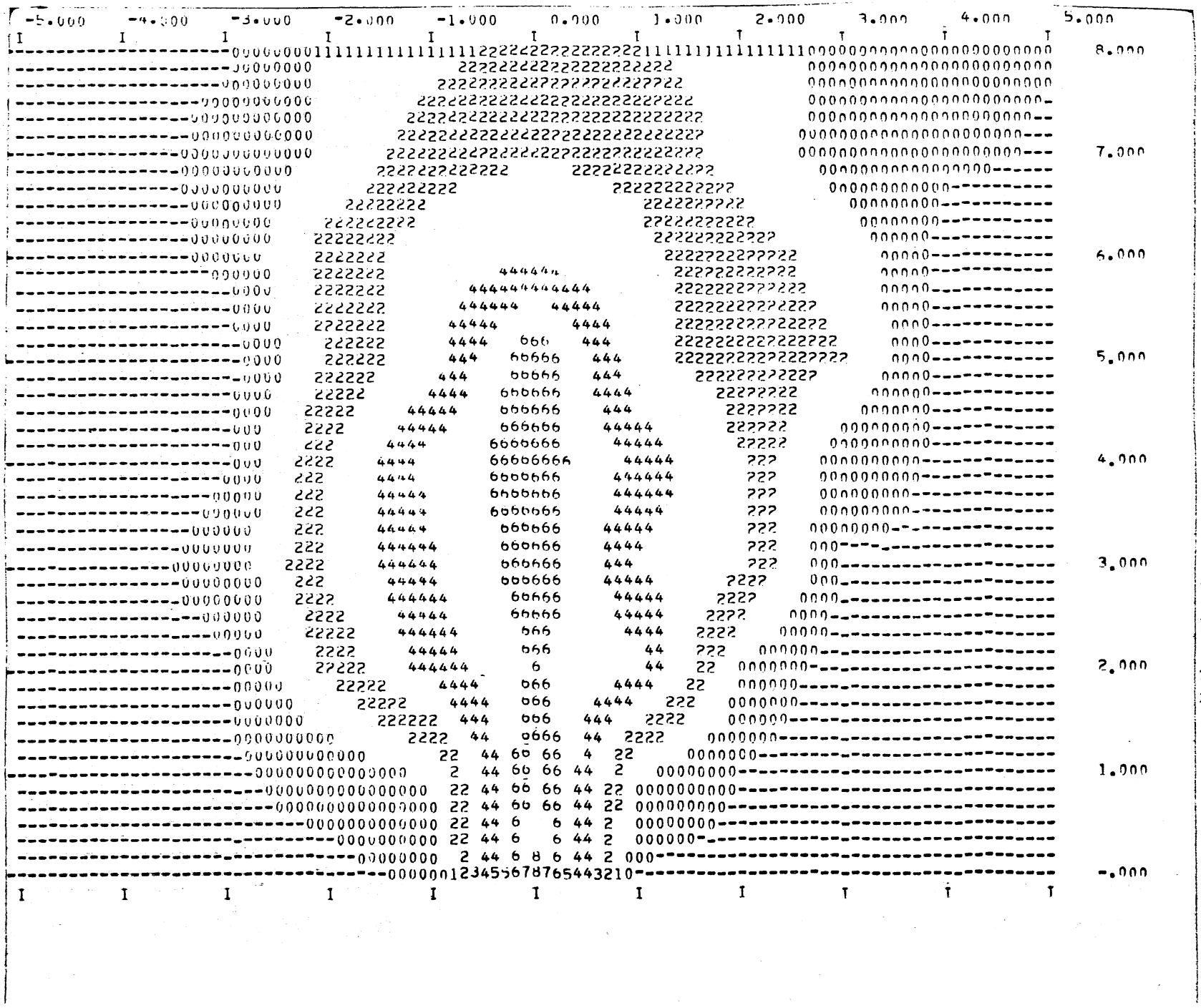

Fig. 33g - Iso-velocity concentrations of u-component for Run 215 (horizontal section for depth z = 0.01 ft)

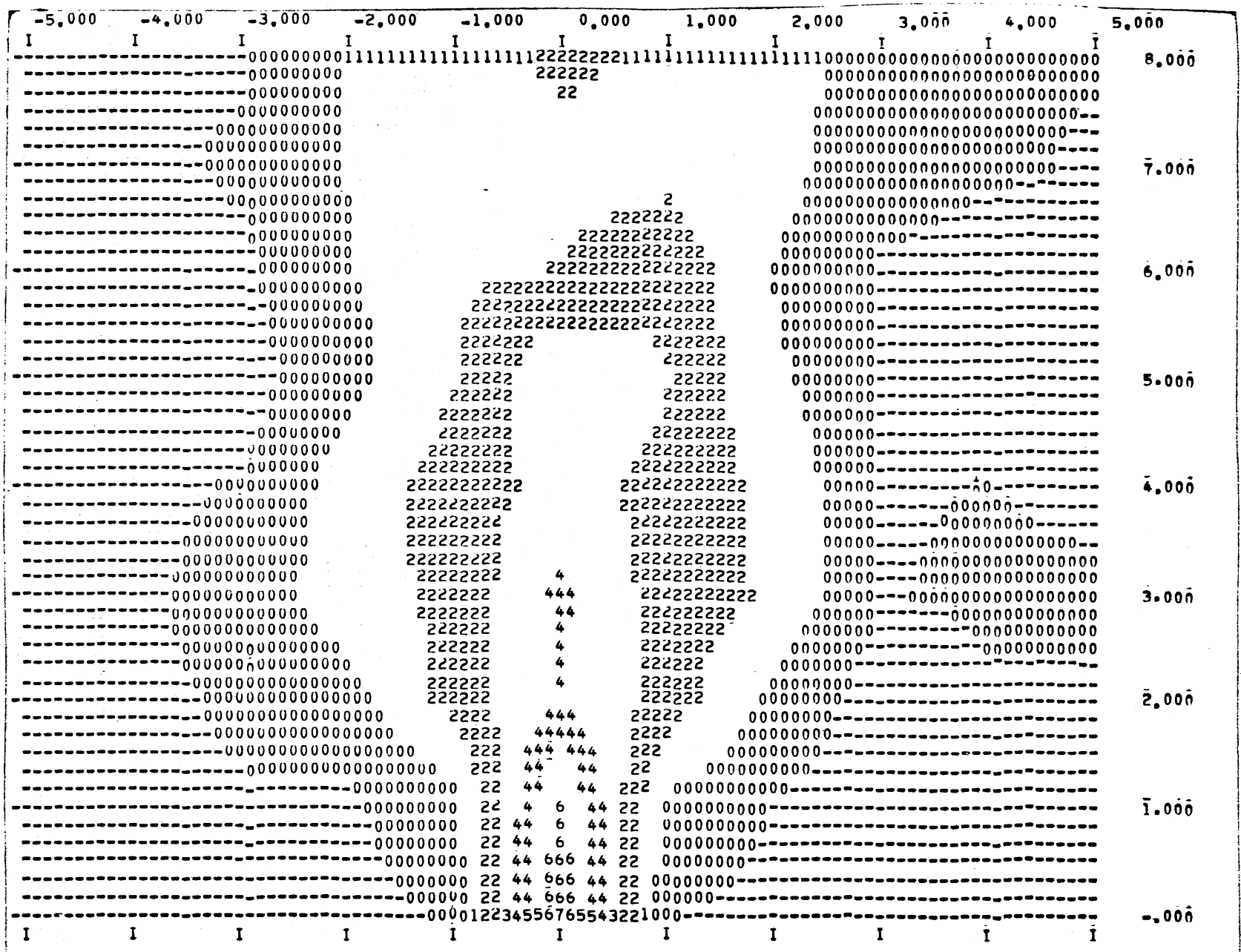

Fig. 33h - Iso-velocity concentrations of u-component for Run 215 (horizontal section for depth z = 0.03 ft)

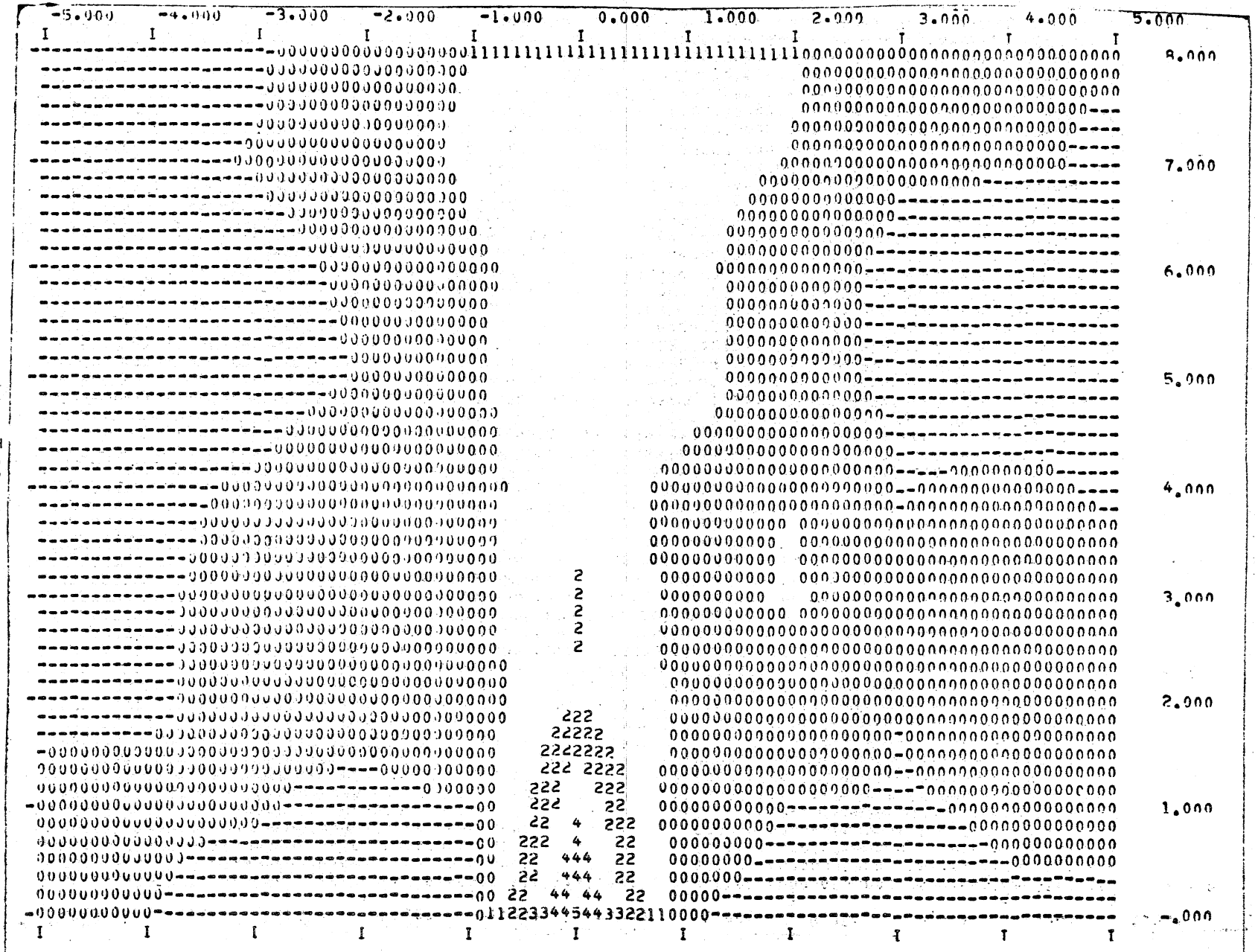

Fig. 33i - Iso-velocity concentrations of u-component for Run 215 (horizontal section for depth z = 0.05 ft)

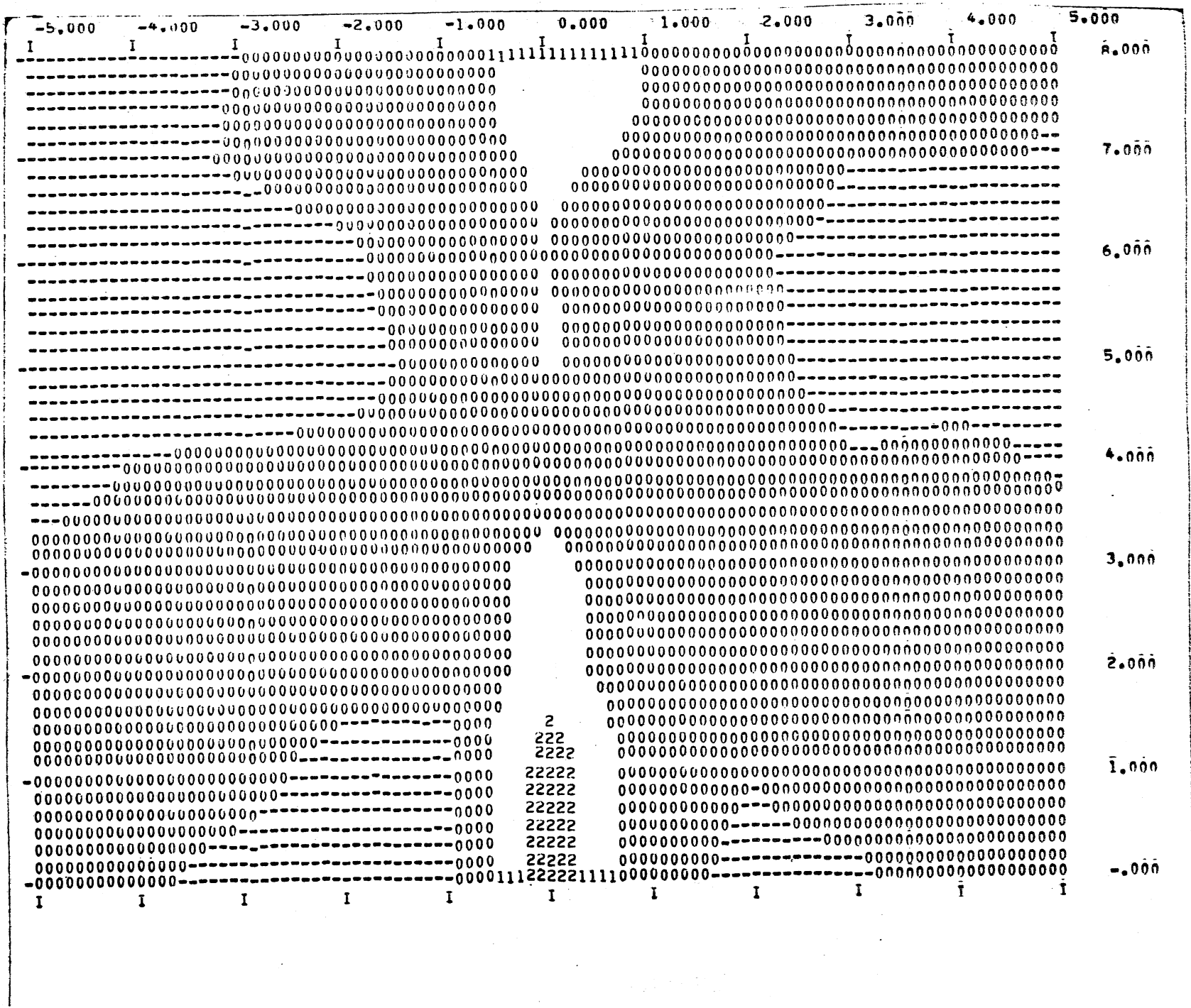

Fig. 33j - Iso-velocity concentrations of u-component for Run 215 (horizontal section for depth z = 0.07 ft)

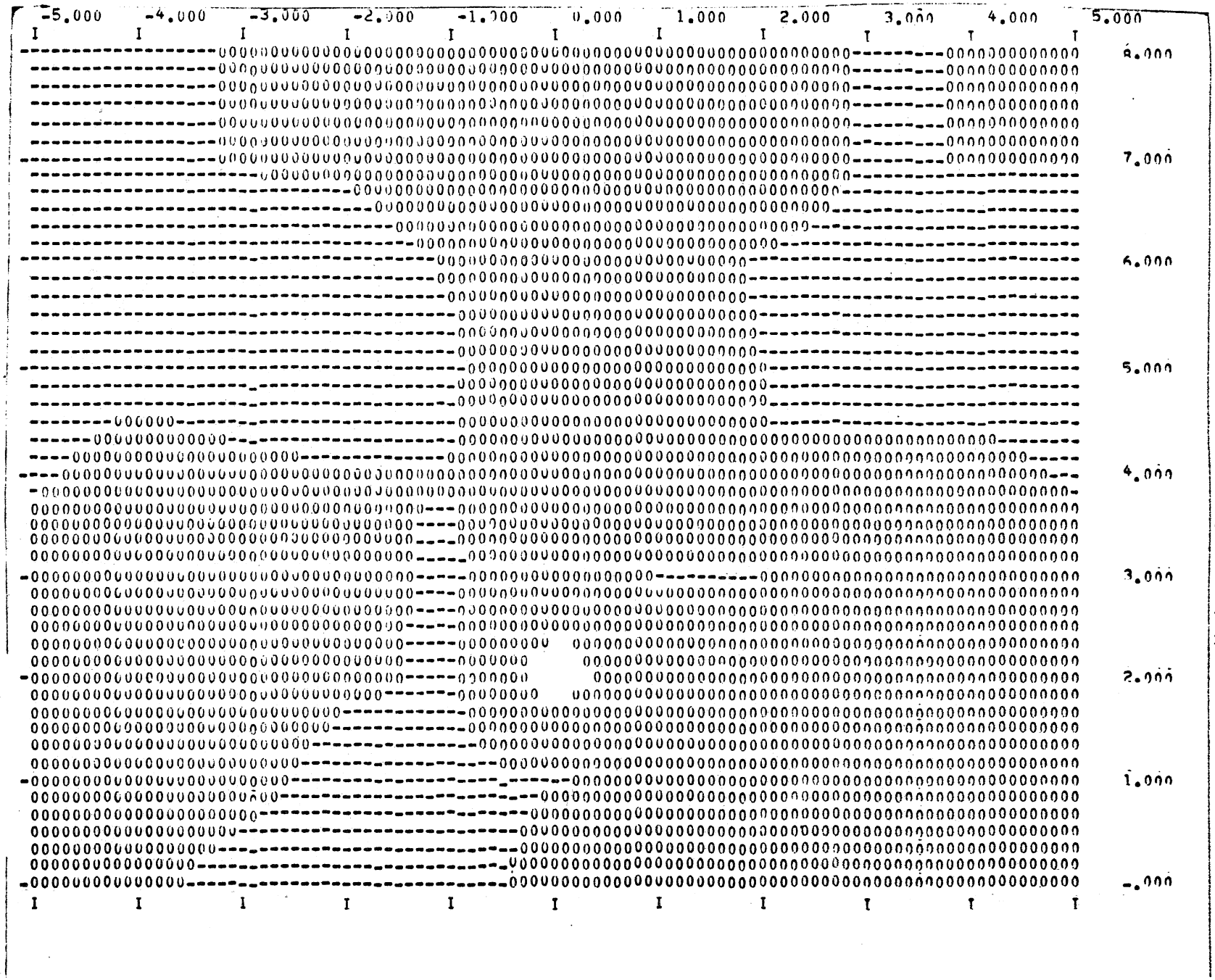

Fig. 33k - Iso-velocity concentrations of u-component for Run 215 (horizontal sectio for depth z = 0.10 ft)

velocity concentrations plotted by CONTOUR for horizontal planes. Again the discharge is at the bottom center of each figure and flow is from the bottom to the top. The symbol table in Fig. 33a gives the significance of each printed number.

The spreading patterns described by iso-velocity-concentration lines are quite similar to those found for iso-temperature concentrations. The following observations can be made:

> Near the outlet the surface jet is surrounded by a flow field with negative velocity. These velocities are part of a large eddy which forms on either side of the warm water jet. Lateral spread appears to depend on outlet densimetric Froude numbers. Smaller numbers are associated with faster spread.
>
> The horizontal shear stresses which the jet exerts on the underlying temperature-stratified fluid appear to produce a sort of low-amplitude standing wave pattern at certain depths. The phenomenon was also apparent in some of the temperature concentration patterns shown in Fig. 31. The distance x_u over which the velocity distribution could be clearly identified as a jet-type flow was estimated and graphed versus F_o in Fig. 34. The results are approximated by the relationship

$$\frac{x_u}{d_o} = 22.5 \sqrt{F_o} \tag{61}$$

> Although the measurements leading to Figs. 32 and 34 are only very crude estimates, it is worthwhile to note that the depth of penetration did not exceed two times the outlet depth and the spreading jet-type flow patterns persisted only over a relatively short distance of fifty times the outlet depth or less.

Iso-velocity concentrations have also been plotted in vertical cross sections perpendicular to the main axis of the experimental tank. Again only u-components of velocities were used. Examples are given in Fig. 35. The profiles show quite nicely the decrease in depth and the lateral spreading of the surface jet with distance. The shape of the profiles justifies Eq. (1).

A velocity concentration map for a vertical section through the main trajectory is given in Fig. 36. Flow is from left to right and distances are given in feet. The stratification is quite apparent.

To obtain velocity concentrations it is necessary to reduce each measurement by a reference velocity. The average discharge velocity at the outlet was chosen as such a value. The resulting concentration

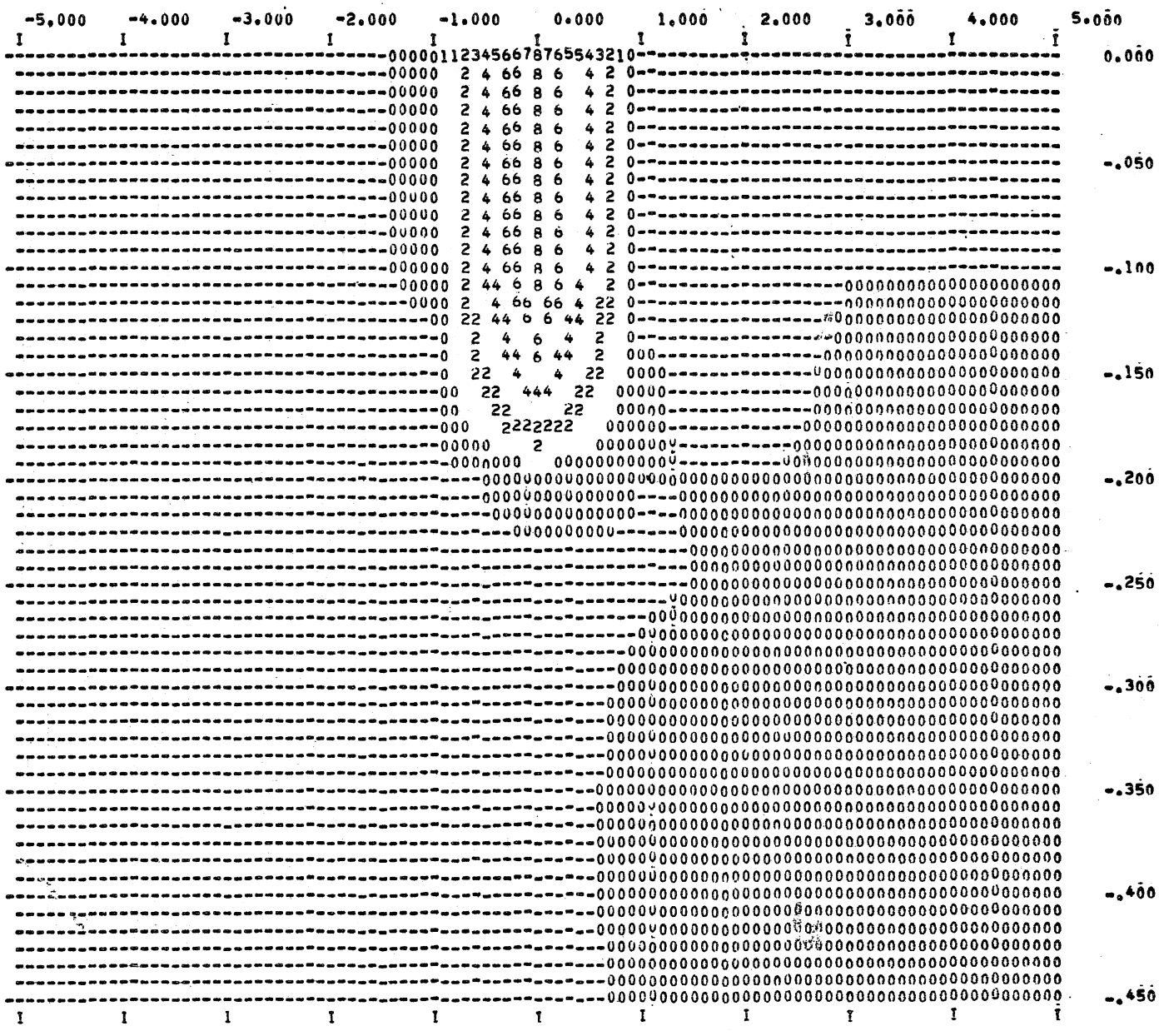

Fig. 35a - Iso-velocity concentrations for Run 215. (Vertical section at x = .5 ft)

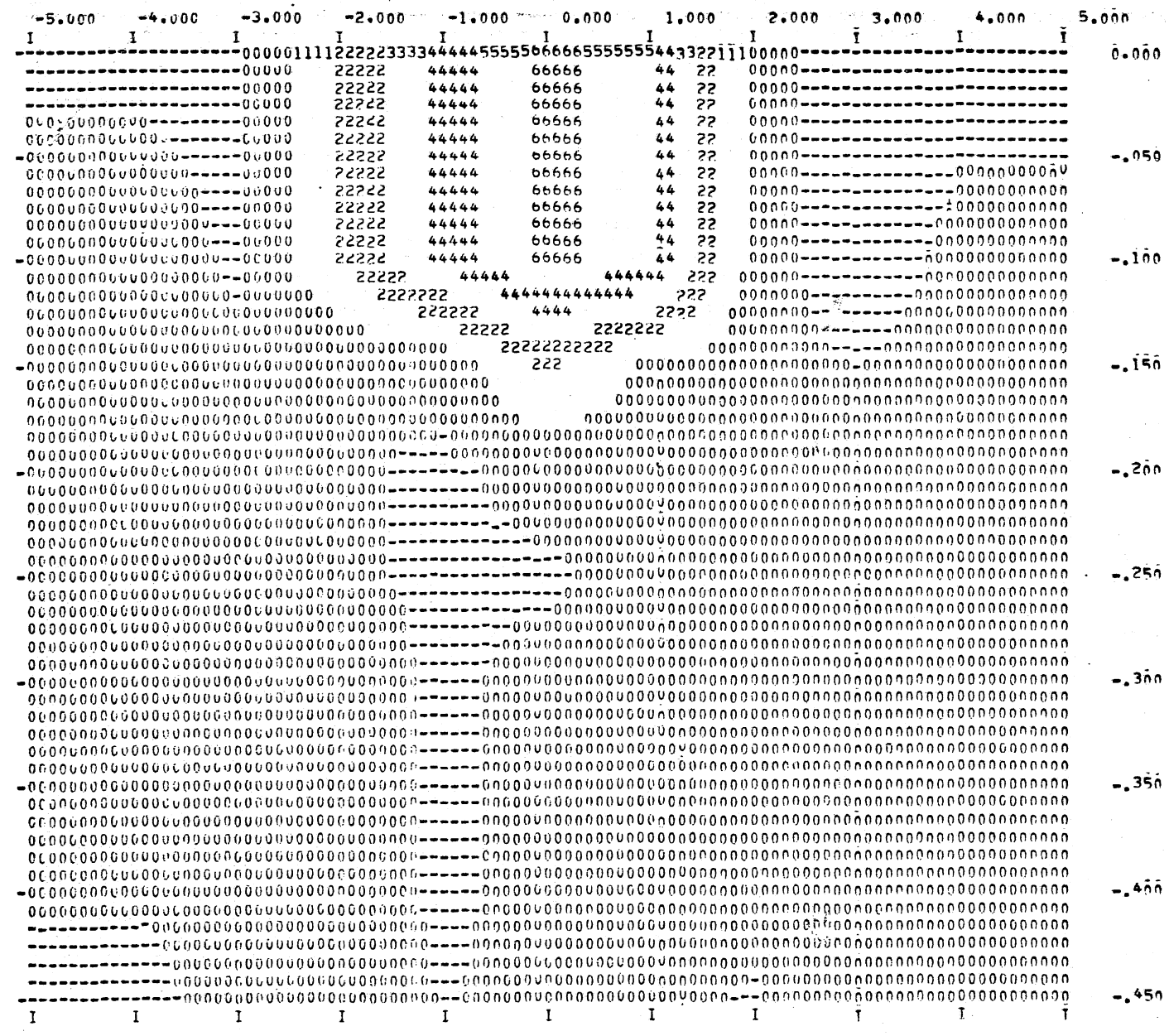

Fig. 35b - Iso-velocity concentrations for Run 215. (Vertical section at x = 1.5 ft)

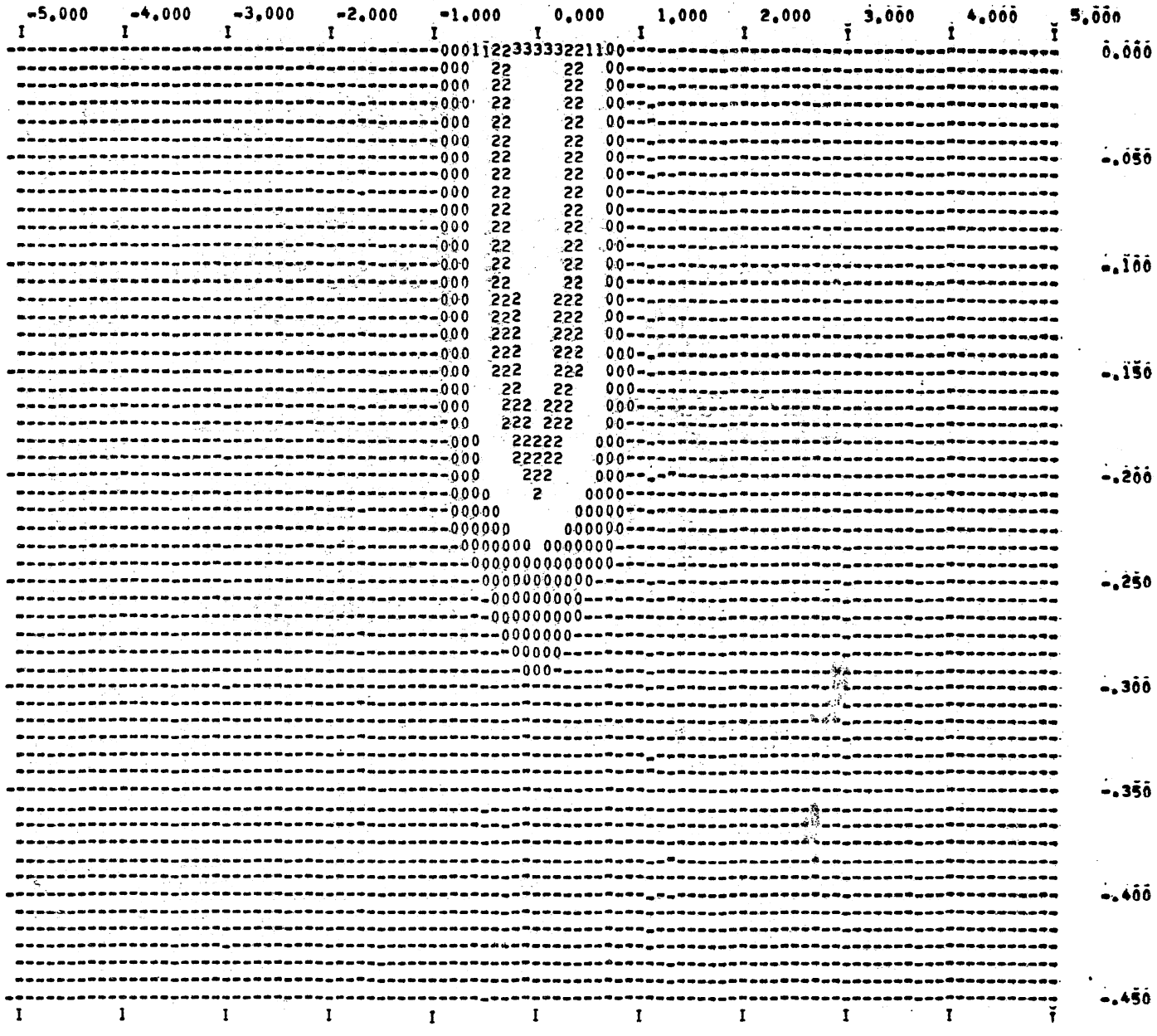

Fig. 35c - Iso-velocity concentrations for Run 207. (Vertical section for x = 0.5 ft)

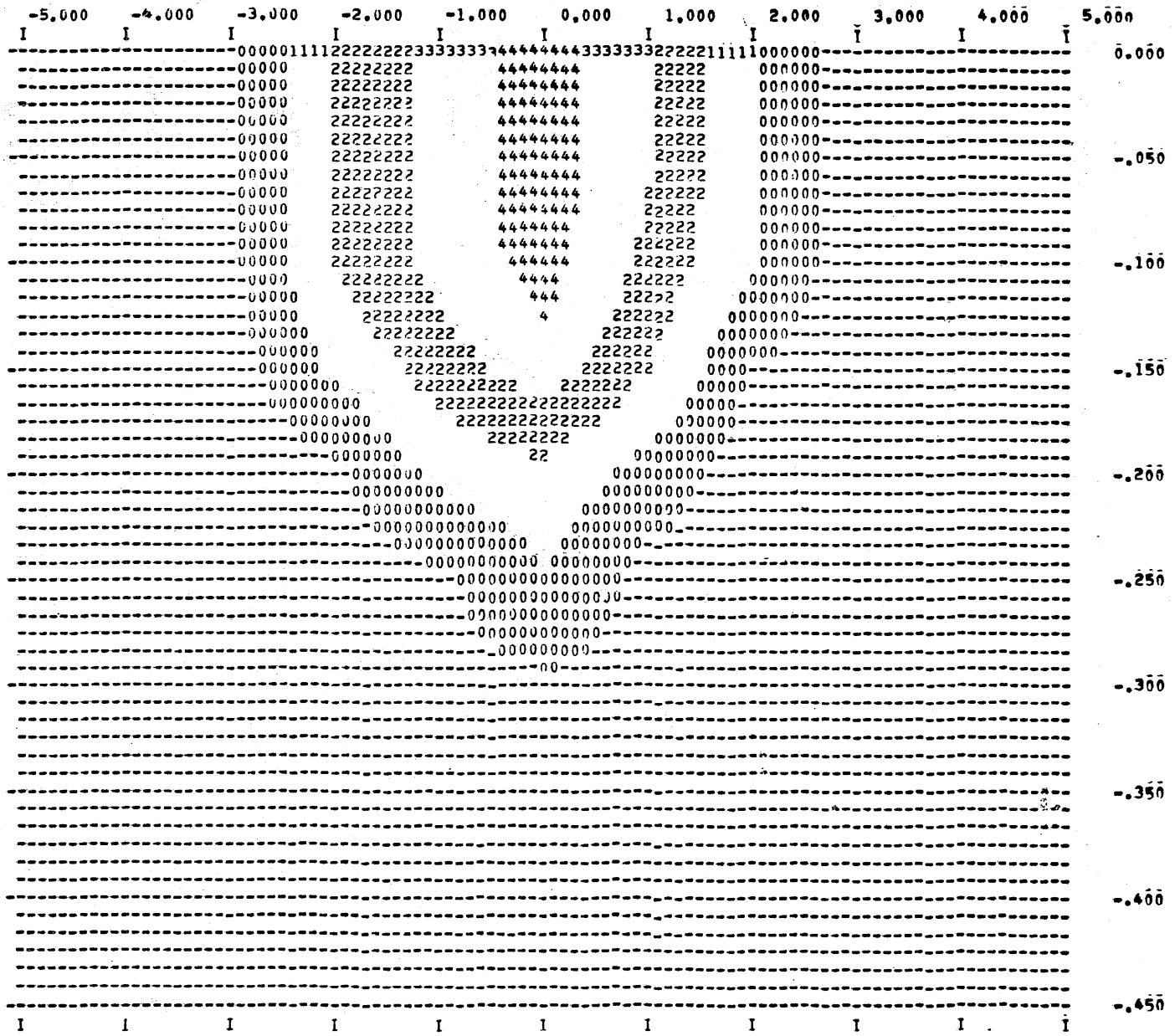

Fig. 35d - Iso-velocity concentrations for Run 207. (Vertical section for x = 3.0 ft)

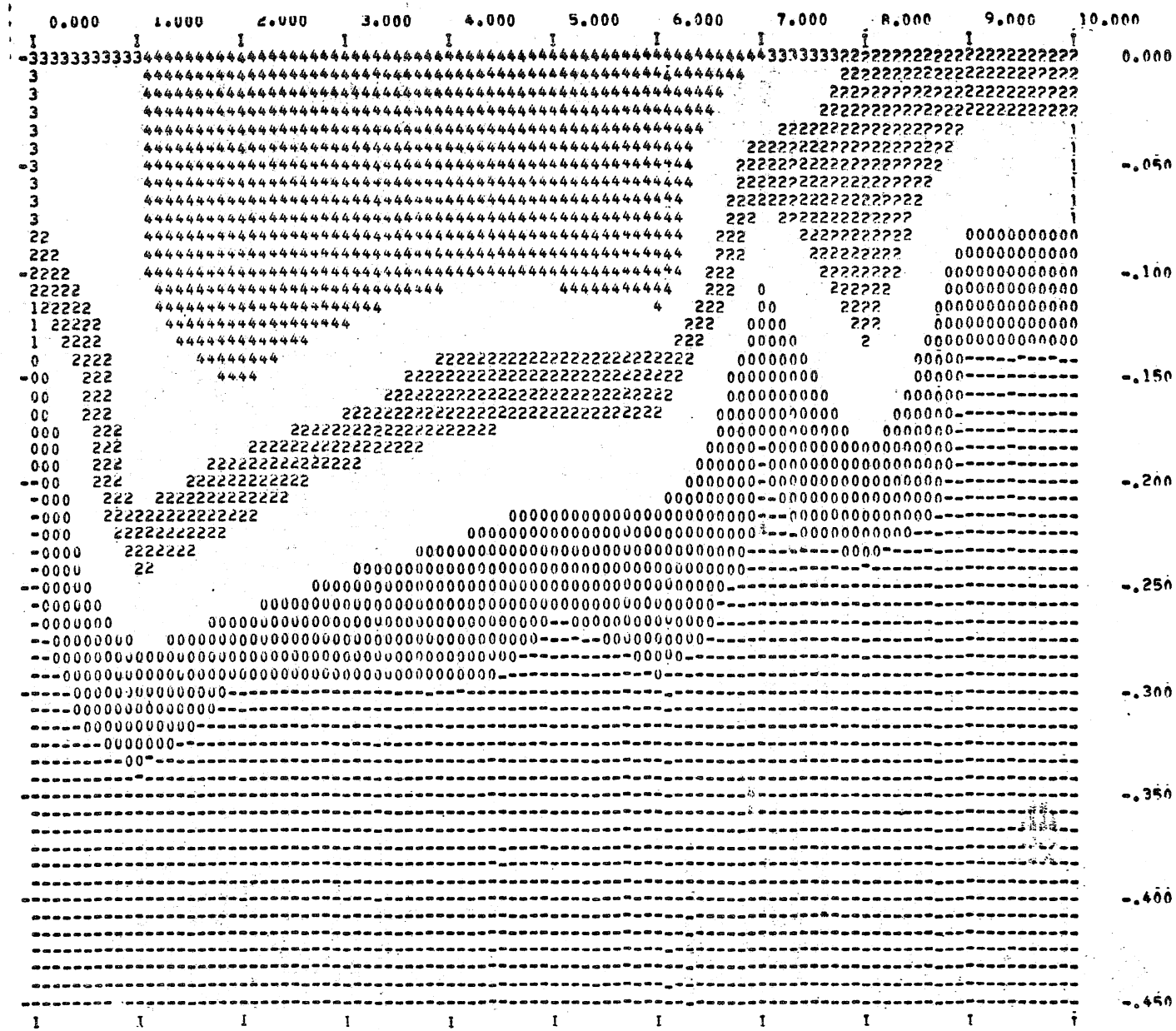

Fig. 36 - Iso-velocity concentrations for Run 207. (Vertical section for y = 0)

values show the velocity decay with distance from the outlet quite well. To illustrate the actual spread of the plume it is helpful to reduce all velocity data with the velocity on the main trajectory as a reference value. Such velocity concentrations then are equal to $u(x,y,z)/u(x,0,0)$. Plots obtained with these concentrations for zero depth were used to find the horizontal standard deviations $b(x)$ by locating the points at which $u(x,b,0)/u(x,0,0) = 0.606$. The results are plotted for three tests in Fig. 37, and a comparison with values predicted by the analytical model is given.

Visual Spread Angles -- In the previous sections the vertical and horizontal spreading of the surface plume were defined quantitatively in terms of spread velocities or the change in standard deviations for temperature and velocity profiles with distance. It is also possible to use visual contours of the buoyant surface jet to measure spread. To define the contour one must use a tracer in the experiment as described in Ref. [53]. Figure 38 is an example of a visual spreading record near the outlet obtained using floating particles and time-exposure photography. More examples can be found in Ref. [53]. The total width of the surface plume measured perpendicular to the main trajectory can easily be recorded as a function of distance from the outlet.

If the shapes of the velocity and temperature distributions in vertical cross sections are approximated by normal distributions such as are specified in Eqs. (1) and (2), the spread of the contour and the spread measured by standard deviations are correlated. If the contour represents a line of iso-velocity concentration of magnitude k, the lateral contour spread at the surface dr_c/ds or dy_c/dx is

$$\frac{dy_c}{dx} = \frac{db}{dx}\left[\ell n \frac{1}{k^2}\right]^{1/2} \tag{62}$$

where db/dx is the standard deviation spread. Contour spreads were measured on plots of visual tracers. However, they are difficult to use because it is uncertain how small a value of k should be used to describe the contour of the plume. Therefore visual records of tracers, isotherms, and iso-velocity concentrations were used only to find the initial angle of spread. The tangents drawn to the contours of available surface spreading records define a horizontal spreading angle ϕ_o as shown in Fig. 39. This angle was measured on available records in Ref. [53]. Part of the scatter is due to the fact that the experimental tank into which the water was discharged was partially temperature stratified. The spread of the jet will depend on that stratification, and an additional parameter is needed to take it into consideration. Considering largely the velocity data, a very approximate relationship between the outlet spreading angle and the outlet densimetric Froude number appears to be

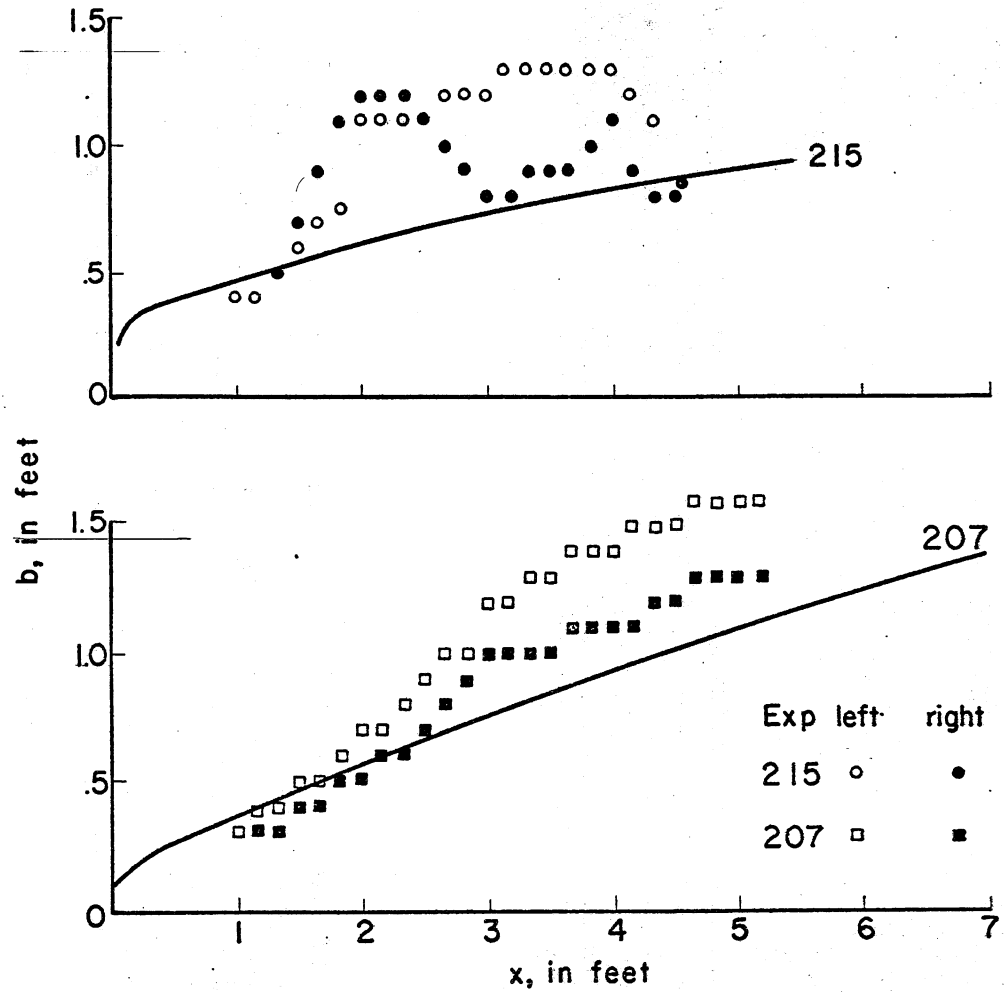

Fig. 37 - Lateral Spread of Heated Water Jet on Water Surface as Illustrated by Values of Standard Deviations b(x) plotted against Distance x from point of Discharge. Analytical Model Predictions (solid lines) and Experimental Data (dotted lines)

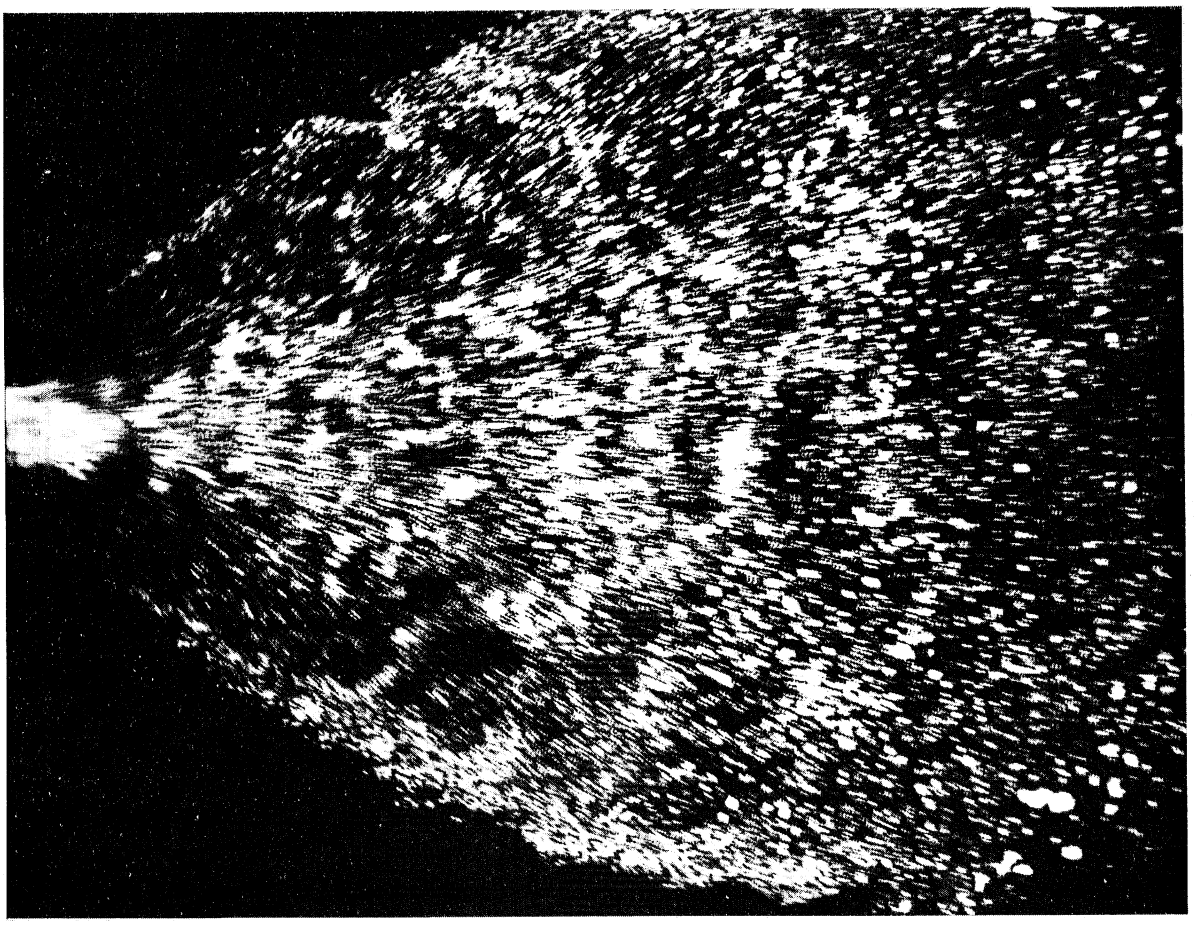

Fig. 38 - Visual Surface Spreading Pattern (Time Exposure of Tracer Particles)

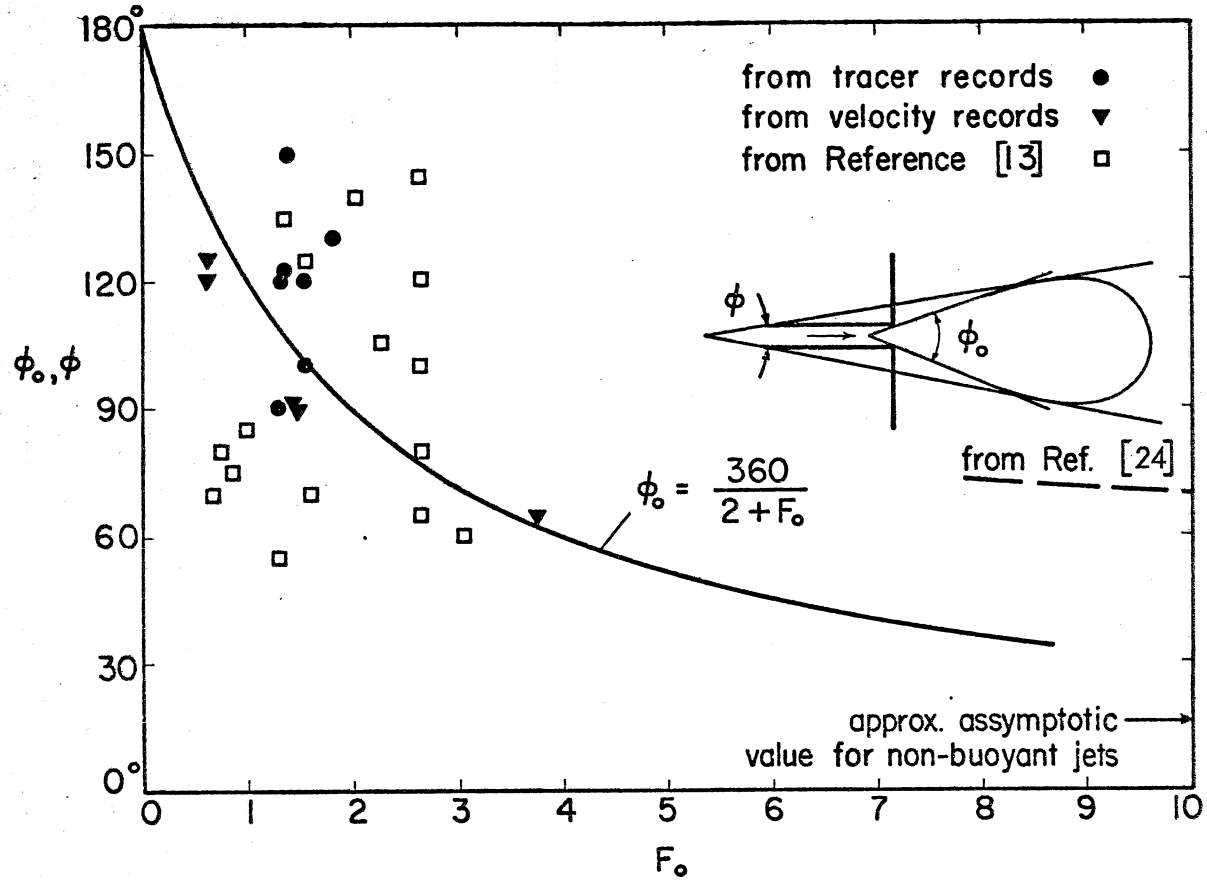

Fig. 39 - Visual Surface Spreading Angle ϕ_o of Heated Water Surface Jet. Experimental Data

$$\phi_o = \frac{360^o}{2 + F_o} \tag{63}$$

where ϕ_o is given in degrees. The data were converted from contour spread values using the simple relationship

$$\phi_o = 2 \arctan\left(\frac{dy_c}{dx}\right) \tag{64}$$

The present data and also those taken from another source show a great deal of scatter, the source of which is believed to be an existing stratification in the tank which was not given sufficient attention. The buoyancy experienced by a jet discharged into a tank will be strongly influenced by an existing temperature stratification.

The same data were also plotted on $\tan \phi_o/2$ versus $1/F_o$ in Fig. 40, and again considerable scatter was obtained. The velocity data appear to fit a straight line with the description

$$\left(\frac{dy_c}{dx}\right)_0 = \frac{c_7}{F_o} + 0.15 \quad \text{for} \quad F_o > 1.0 \tag{65}$$

The boundary or contour of a surface plume was previously estimated to be $y_c \approx mb$, with $m \approx 3$. Thus

$$\left(\frac{db}{dx}\right)_0 = \frac{c_7}{3.0} \frac{1}{F_o} + 0.05 \tag{66}$$

By comparison with Eq. (20) one finds that the second part of the right-hand side of the equation is approximately the turbulent spread and the first part is the buoyancy induced spread. By comparing with Eq. (18) it is found that

$$\frac{c_5}{c_6} = \frac{c_7}{3.0} \quad \text{or} \quad c_5 = e^{-0.5} \frac{c_7}{3.0} = \frac{c_7}{4.95} \tag{67}$$

Here c_7 is of the order of 1.25 to 2.5, and hence c_5 is of the order of from 0.25 to 0.50. These values agree reasonably well with the values found from the lateral velocities in one of the previous sections. A value of $c_5 = 0.40$ was used in the analytical model.

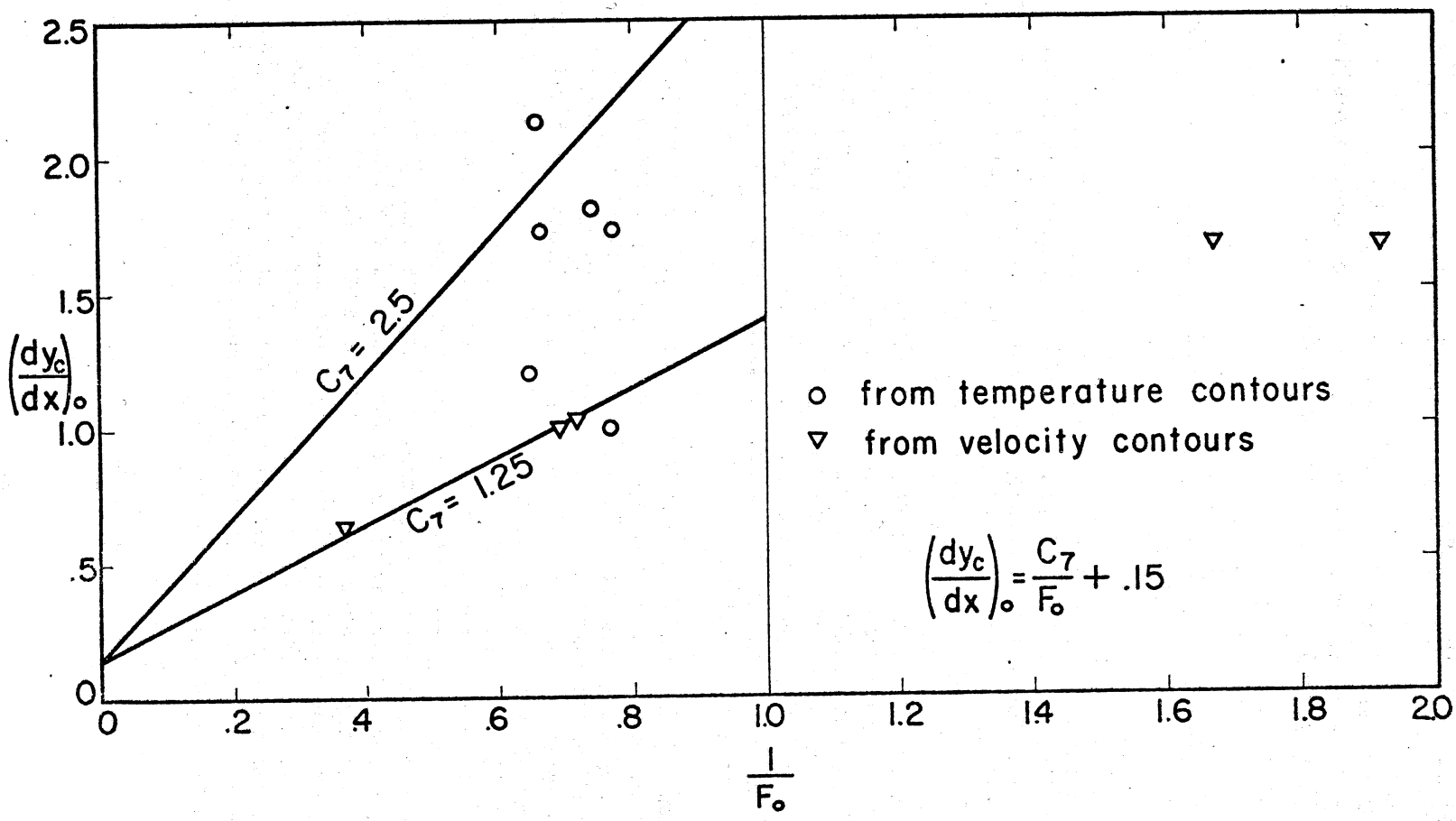

Fig. 40 - Surface Spreading of Visual Contour of Heated Water Surface Jet. Experimental Data

Entrainment and Mixing near the Outlet

Volumetric Fluxes, Heat Fluxes, and Heat Contents -- The volumetric flux, the heat flux, and the heat content along the main trajectory (main axis of the tank) were calculated by integration of the measured velocity and temperature profiles in cross sections perpendicular to the axis of the tank. The theoretical values of the fluxes are given in Eqs. (5), (6), and (68) with the provision $x = s$, $y = r$.

$$C(x) = \varrho c_p \int_{-\infty}^{\infty}\int_{0}^{\infty} T^*(x,y,z)\, dxdy \qquad (68)$$

The limits of integration were changed. Instead of an infinitely large cross section, a finite one defined as that area perpendicular to the main trajectory in which the u-velocity components were all positive was used. The integration was carried out in three steps: integration of individual profiles of velocity (or excess temperature or products of these) with respect to depth; multiplication of each result by distance between midpoints of adjacent profiles; and addition of several of these results for an individual cross section $x = \text{const}$. The results of all integrations were reduced to dimensionless form by using the corresponding outlet values for reference; e.g., Q_o for volumetric flux, $\varrho Q_o c_p (T_o - T_c)$ for heat flux, and $d_o w_o (T_o - T_c)$ for heat content. The results referring to volumetric fluxes are plotted in Fig. 41 versus distances from the outlet.

Primarily because of the small number of vertical profiles measured in each cross section perpendicular to the x-axis, the experimental results show scatter. They show conclusively, however, that there is a substantial amount of entrainment of surrounding water by the heated water jet even if the vertical stratification is strong. Values predicted by the analytical model are also shown in Fig. 41. For further comparison, the theoretical distribution of volume flux for a semi-circular non-buoyant jet is also given. It appears that the measured entrainment was initially larger than that predicted for non-buoyant jets. This observation is quite reasonable considering that the experimental jet had a fully developed velocity distribution at the point of discharge, while the non-buoyant jet theory assumes that the discharge velocity is uniform. The actual zone of flow establishment is therefore much shorter in the experiments than in that theory. For the same reason the analytical model also predicts more initial entrainment than the non-buoyant jet theory. On the other hand, a fully developed non-buoyant circular jet has an entrainment characteristic equal to

$$\frac{Q}{Q_o} = \frac{0.32\, x}{D_o} \qquad (69)$$

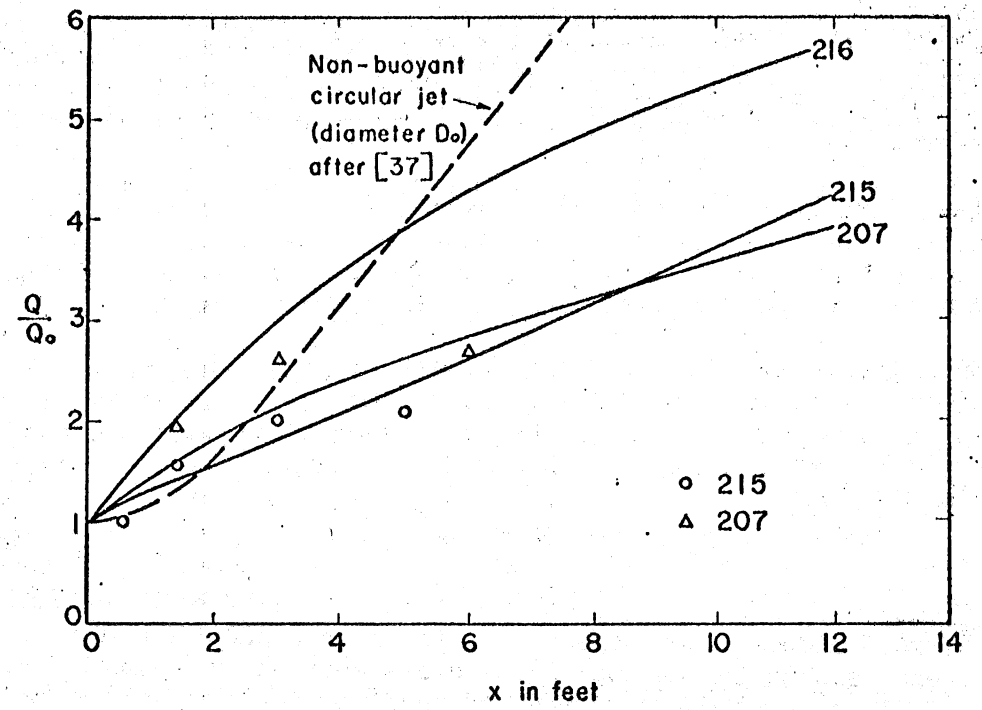

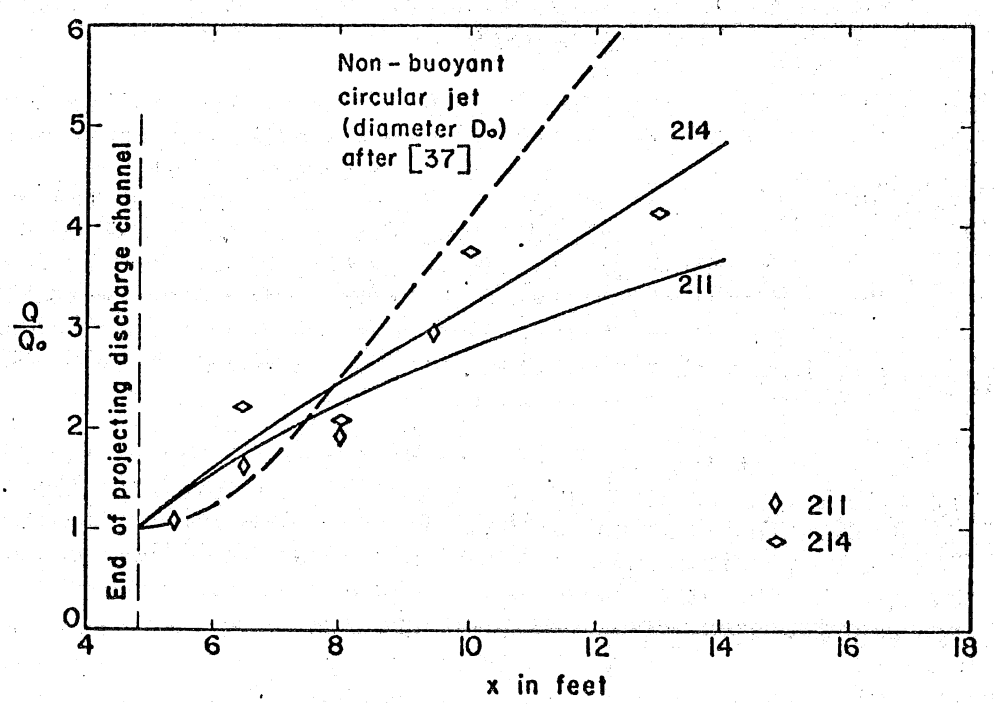

Fig. 41 - Total Volumetric Flow versus Distance from Source of Discharge

In the experiments reported $D_o = 0.4$, and the resulting relationship is shown in Fig. 41. It represents a limiting case of the analytical model ($F_o \longrightarrow \infty$) and is therefore tangent to the result for Exp. 216 ($F_o = 3.75$). It is also evident from Fig. 41 that buoyancy essentially reduces entrainment further downstream from the outlet. Differences in total flow rate between a non-buoyant and a buoyant jet become quite marked.

Heat fluxes, calculated and measured, show only small significant variations with distance. The experiments were carried out in an enclosed and fairly well insulated space. In steady state operation the rate of surface heat transfer was therefore small.

Entrainment and the resulting increase in flow rate as shown in Fig. 41 produce a substantial dilution of the heated effluent and hence a substantial temperature drop. Measured centerline water surface temperatures reported in Fig. 42 show this quite clearly. For comparison, computed temperatures are also shown. The fit between measurements and calculations is strikingly poor, and there are two good reasons for this: first, the failure to account for a zone of flow establishment and second, the stratification of the water in the receiving experimental tank.

It is believed that the length of the zone of flow establishment for velocity distributions is different from that for temperature distributions, because in the discharge cross section the velocity distribution is non-uniform, but the temperature distribution is uniform. The zone of flow establishment for temperature is therefore longer and of the order indicated in Ref. [37]. The zone of flow establishment for velocities is relatively short, if not negligible. The basic analytical model as described does not include a zone of flow establishment.

The second source of disagreement is the temperature stratification in the tank as illustrated by Fig. 31. The water entrained by a surface jet from a temperature stratified reservoir is not of constant temperature. Water entrained laterally is warmer than water entrained vertically. The coldest (bottom) water was taken as a reference, and hence stronger temperature drops have been calculated than were actually measured.

The heat content in a cross section of the plume, as defined by Eq. (68), is a measure of the amount of heat retained in the receiving body of water as a function of location--i.e., distance from the point of discharge. An example of measured results is given in Fig. 43.

Entrainment Mechanisms -- Vertical turbulent mass and momentum transport processes in density stratified fluids depend, as is well known, on the degree of gravitational stability which the fluid shows in the presence of flow induced shear stresses. Generally the Richardson number

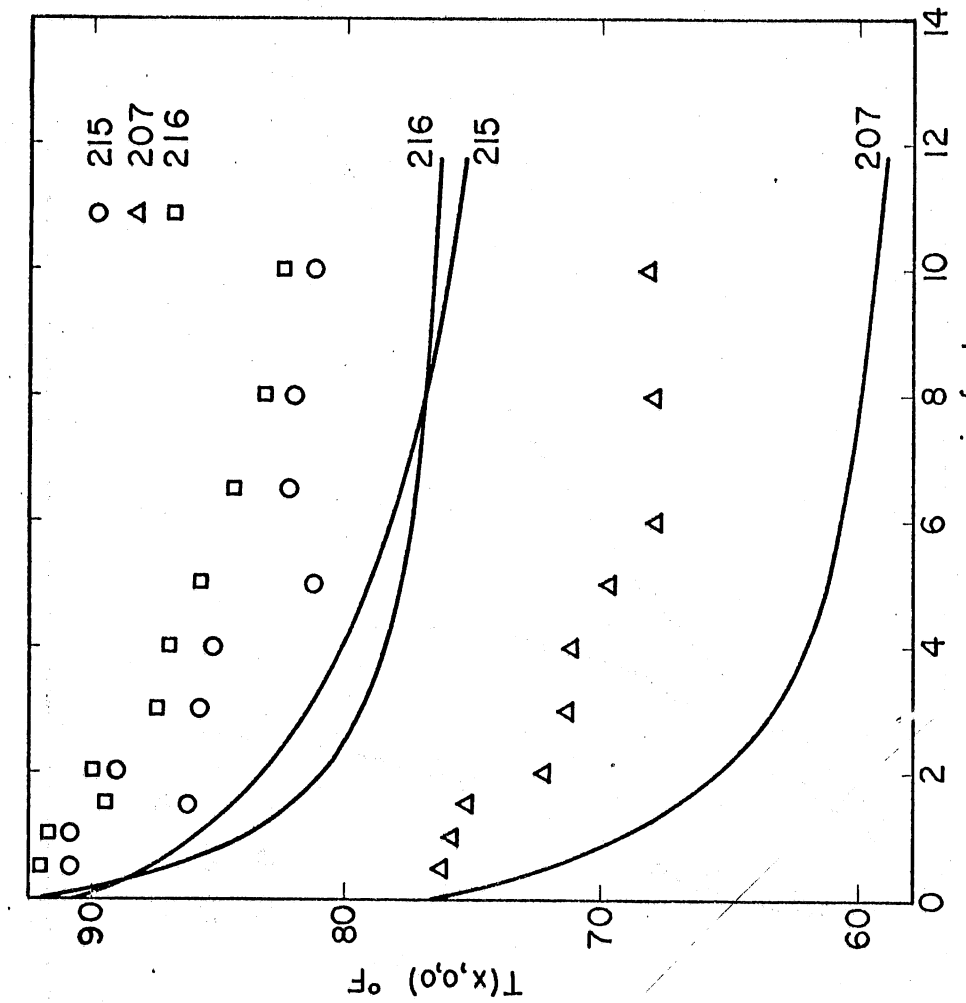

Fig. 42 - Surface Water Temperature Decline along Main Trajectory of Heated Surface Jet

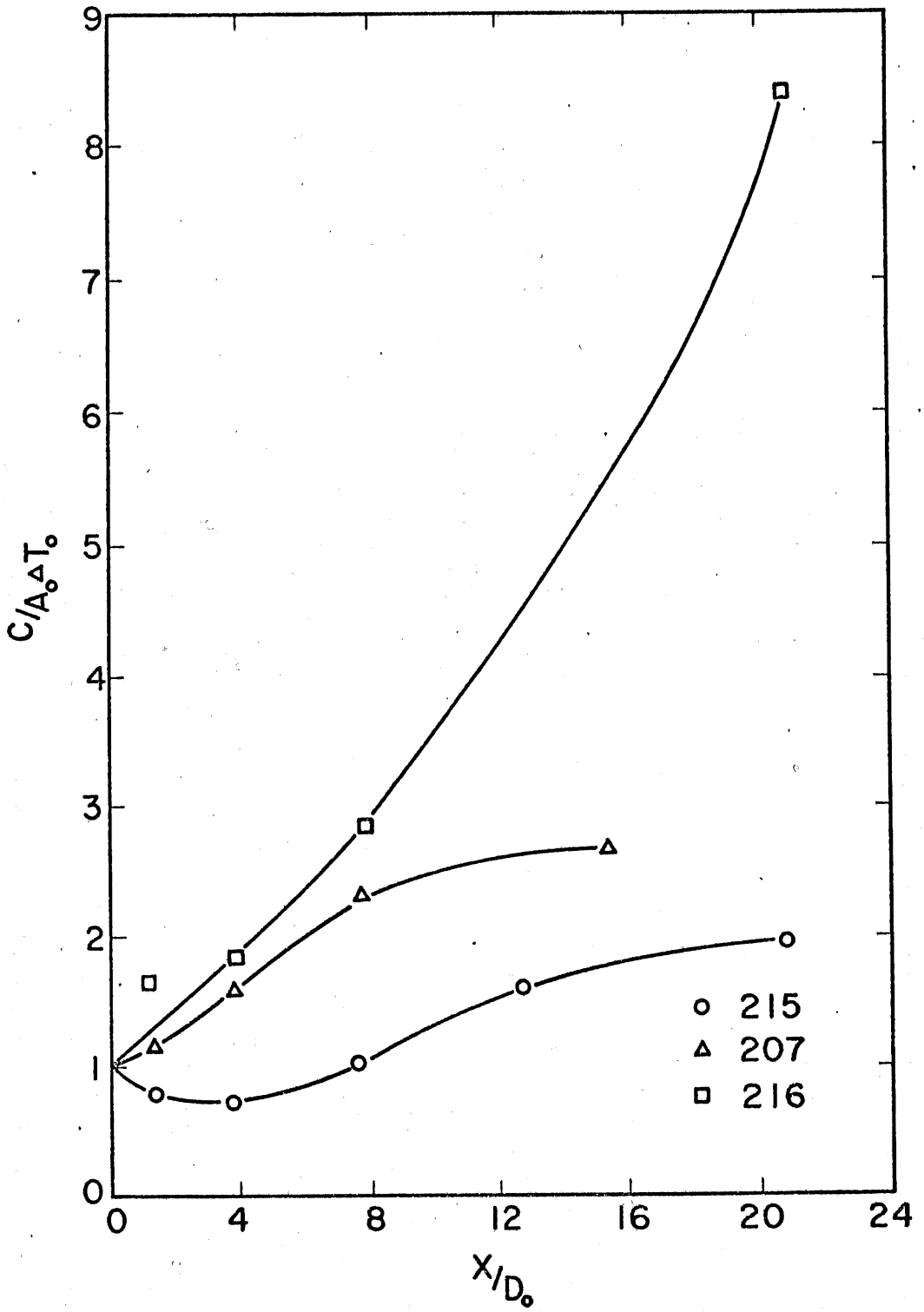

Fig. 43 - Heat Content versus Distance from Source of Discharge

$$Ri = - \frac{g \frac{\partial \varrho}{\partial z}}{\varrho \left(\frac{\partial u}{\partial z}\right)^2} \tag{70}$$

is used as a local stability parameter. The heated water flow from a channel into a reservoir is a density stratified, turbulent flow, and information on the local values of Richardson numbers may shed some light on the vertical mixing process in a plume.

A word of caution is necessary at this point, however, because inherent in the derivation of the Richardson number is the assumption that local turbulence is a function of local mean velocity gradients. This assumption does not necessarily apply to a plume in which the geometrical (depth and width) scale can change drastically with distance from the outlet. There is also turbulence production on the sides of the plume as well as on the bottom. Results given in Ref. [54] suggest caution.

Richardson numbers were calculated numerically. For uniform vertical spacing of measurements, the Richardson number for point i is approximately

$$Ri_i \simeq \frac{-2g}{\varrho_i} \left(\frac{\varrho_i - \varrho_{i-1}}{z_i - z_{i-1}} + \frac{\varrho_{i+1} - \varrho_i}{z_{i+1} - z_i} \right) \left(\frac{u_i - u_{i-1}}{z_i - z_{i-1}} + \frac{u_{i+1} - u_i}{z_{i+1} - z_i} \right)^{-2} \tag{71}$$

Since densities were not measured directly, conversion of the temperature measurements to densities was made using the empirical relationship

$$\varrho = 62.43[1 - (6T^2 - 36T + 47)(0.000001)] \tag{72}$$

where ϱ is obtained in lb_m/ft^3 if T is given in centigrades. Difficulties arose, of course, in the numerical computations when the velocity gradient $\partial u/\partial z$ took a value of zero. It was therefore decided to have the Richardson number assume special designated values if $\partial u/\partial z = 0$ or $\partial \varrho/\partial z = 0$ or both. All results were obtained in tabular form. To facilitate interpretation a graphical presentation of the numerical results with the aid of program CONTOUR is given in Fig. 44. Since the actual values of Richardson numbers covered a very wide range, and the contour plot could differentiate only between ten different symbols, logarithms (base 10) of Richardson numbers instead of actual values were plotted. The numbers actually printed in Figs. 44 and 45 are equal to $\log_{10} Ri + 4$. Using logarithms was desirable also from another point of view: Velocity measurements with the aid of the tethered sphere probe are probably not precise enough to give accurate values of velocity gradients. This problem exists in part also when measurements are being made with other velocity measuring

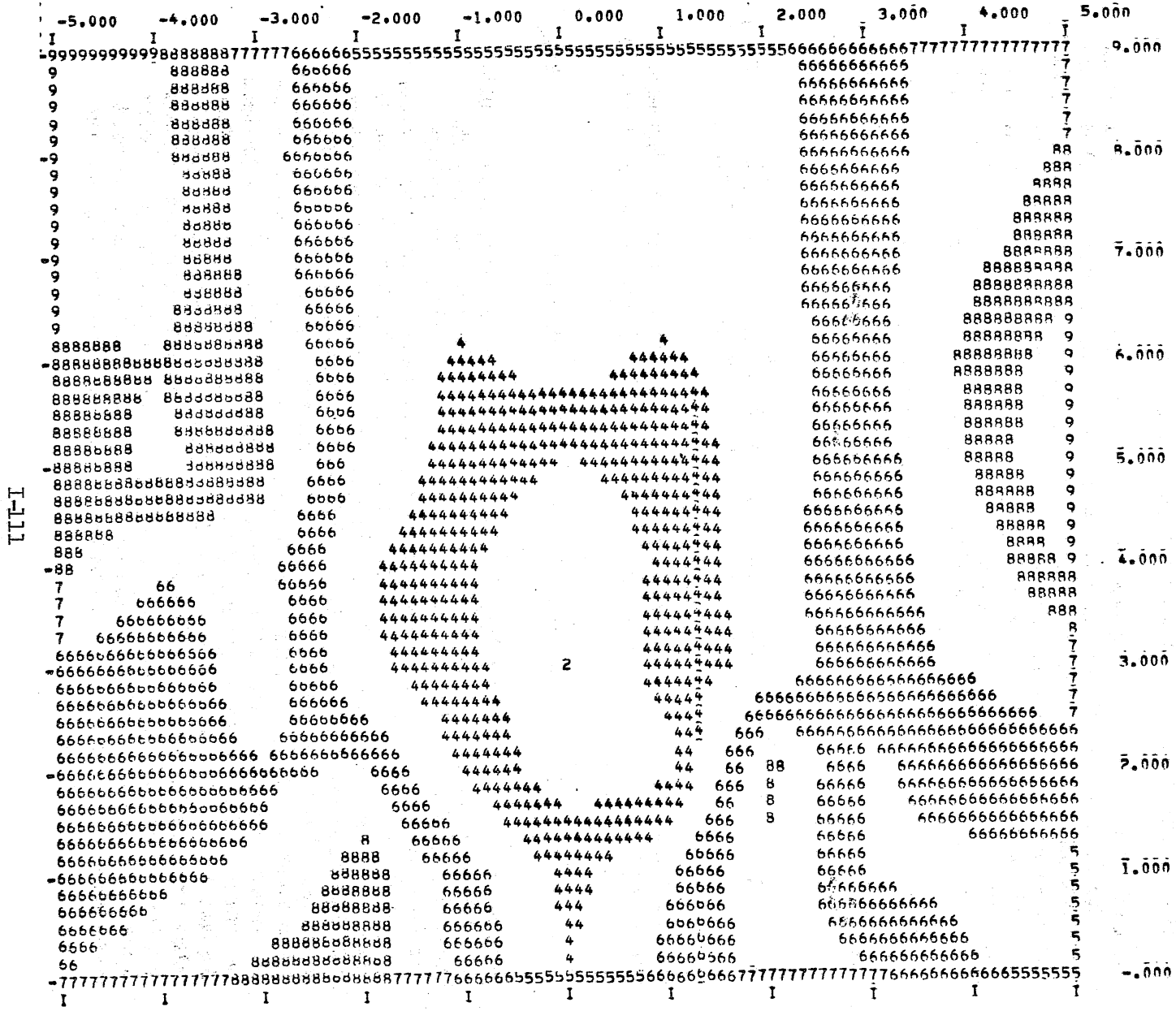

Fig. 44a - Iso-logarithms of Richardson numbers for Run 215. (Horizontal section at z = .05 ft)

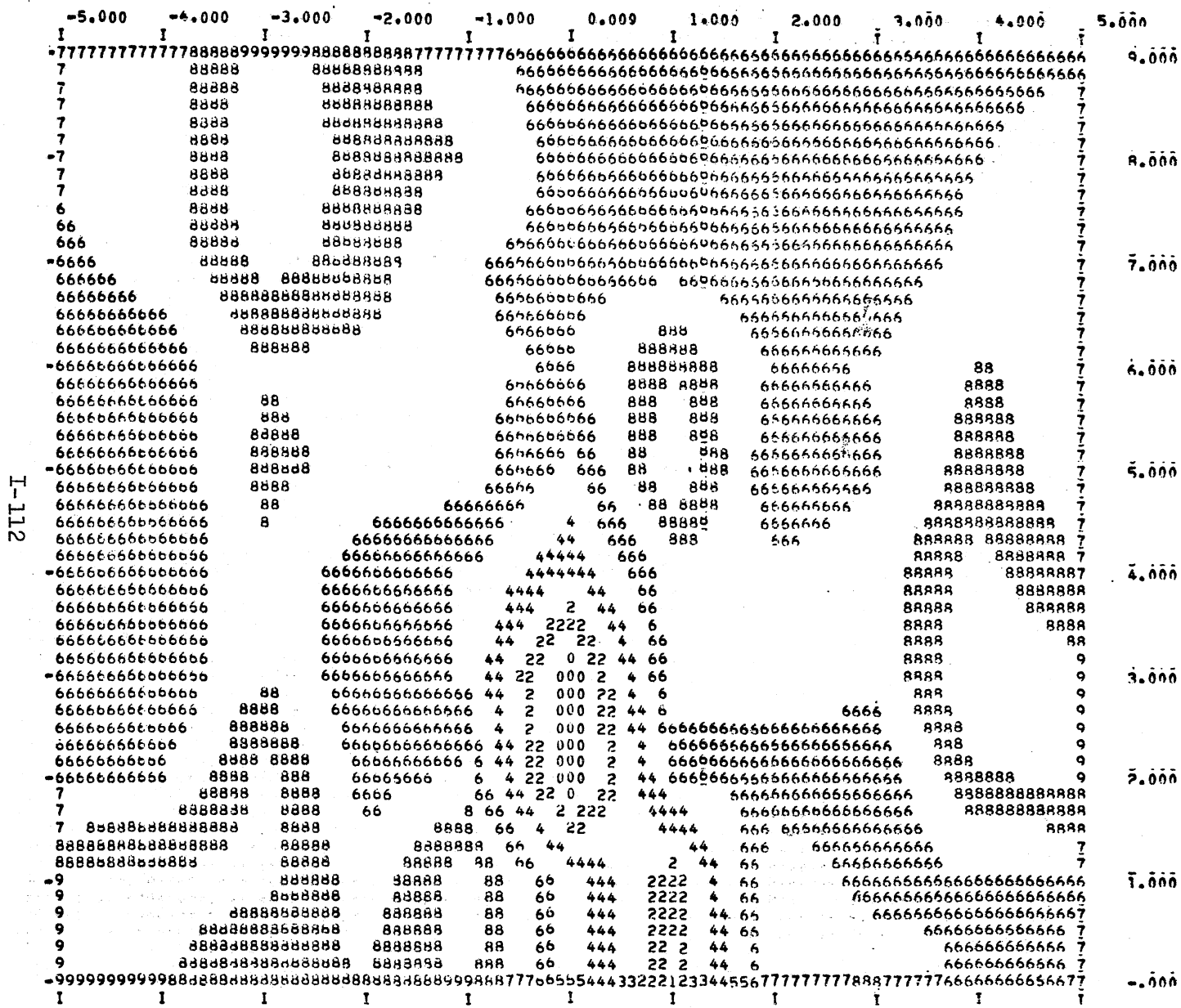

Fig. 44b - Iso-logarithms of Richardson numbers for Run 215. (Horizontal section at z = .14 ft)

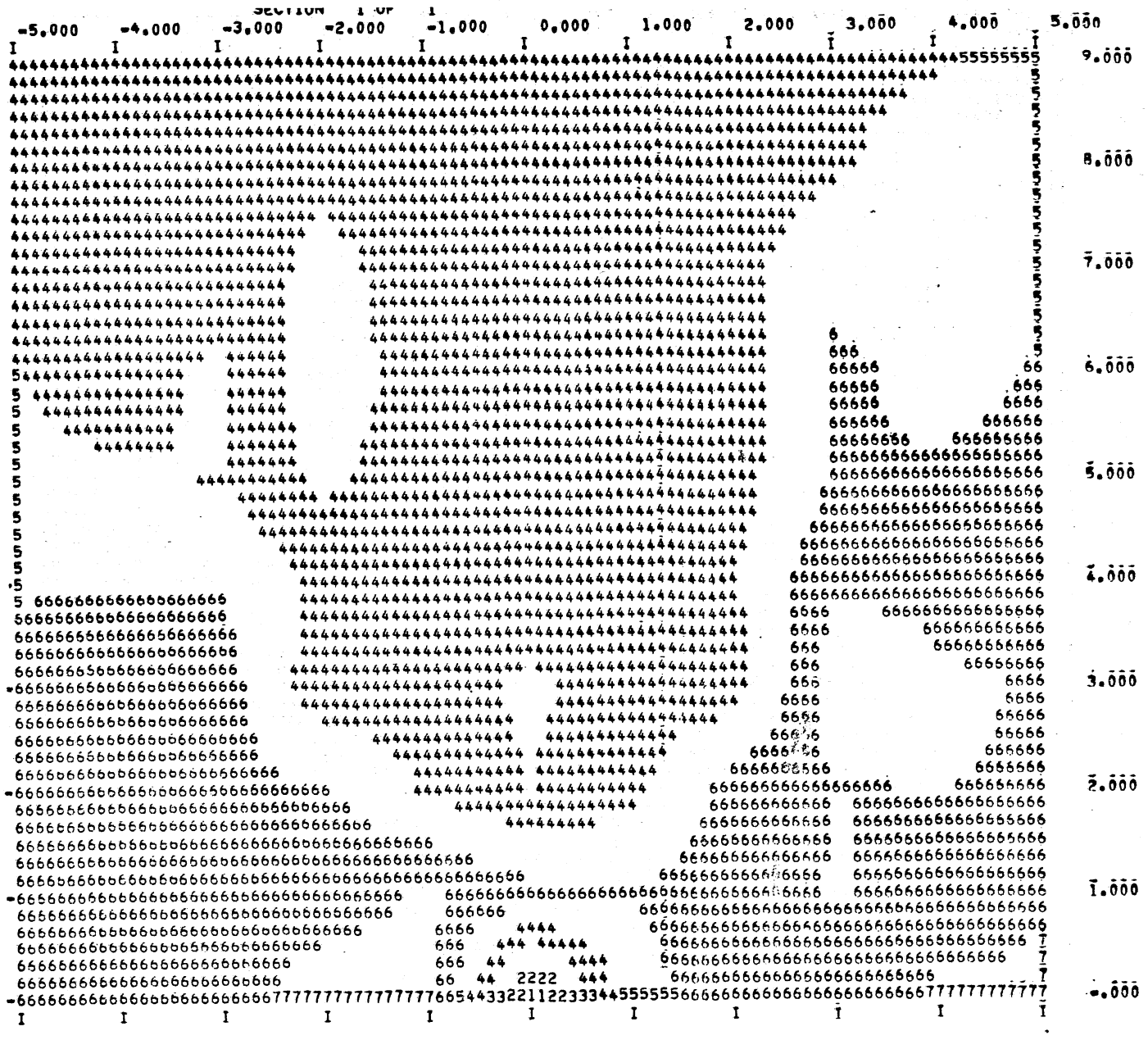

Fig. 44c - Iso-logarithms Richardson numbers for Run 20 (Horizontal sec at z = .05 ft)

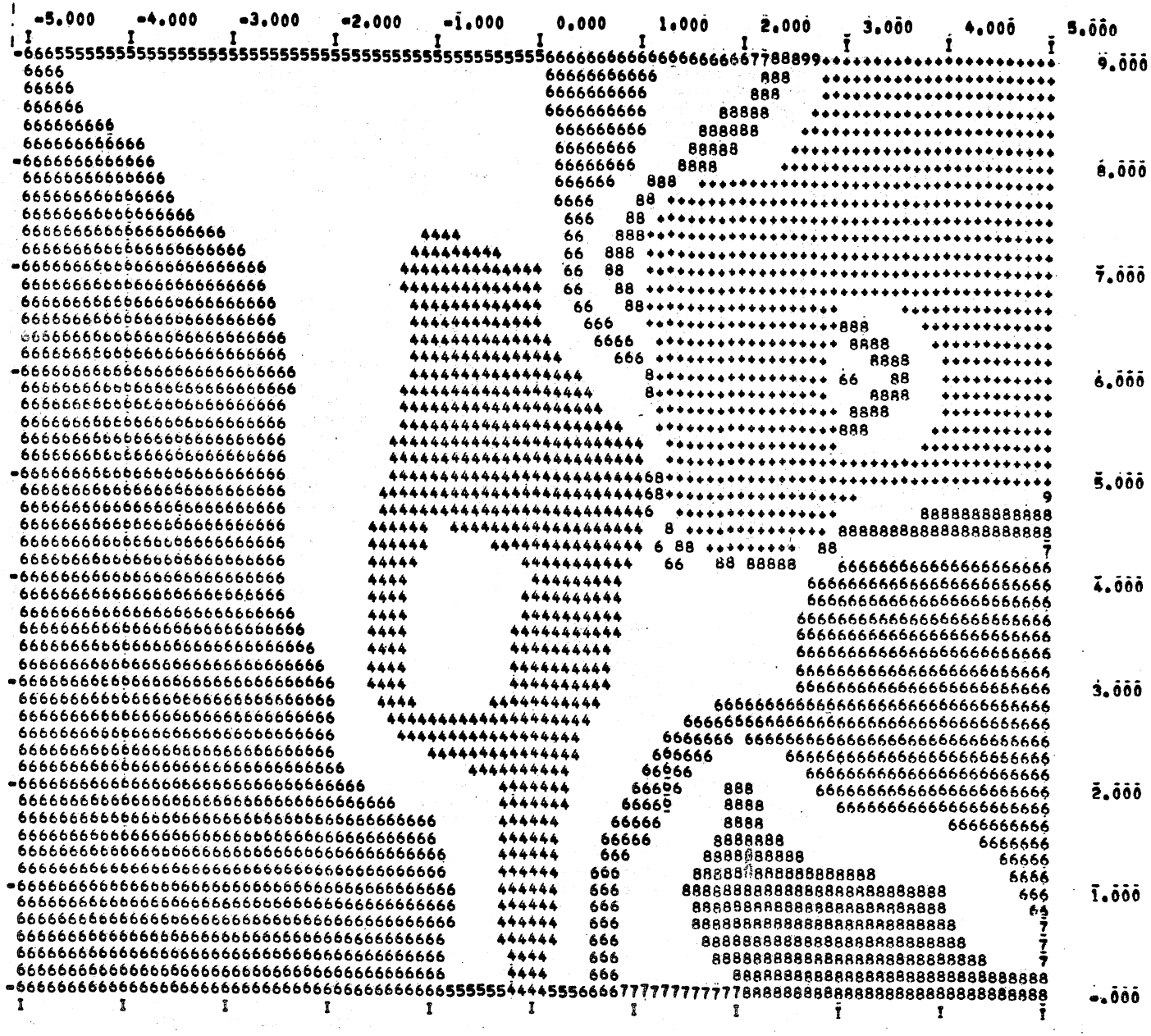

Fig. 44d - Iso-logarithms of Richardson numbers for Run 207. (Horizontal section at z = .14 ft)

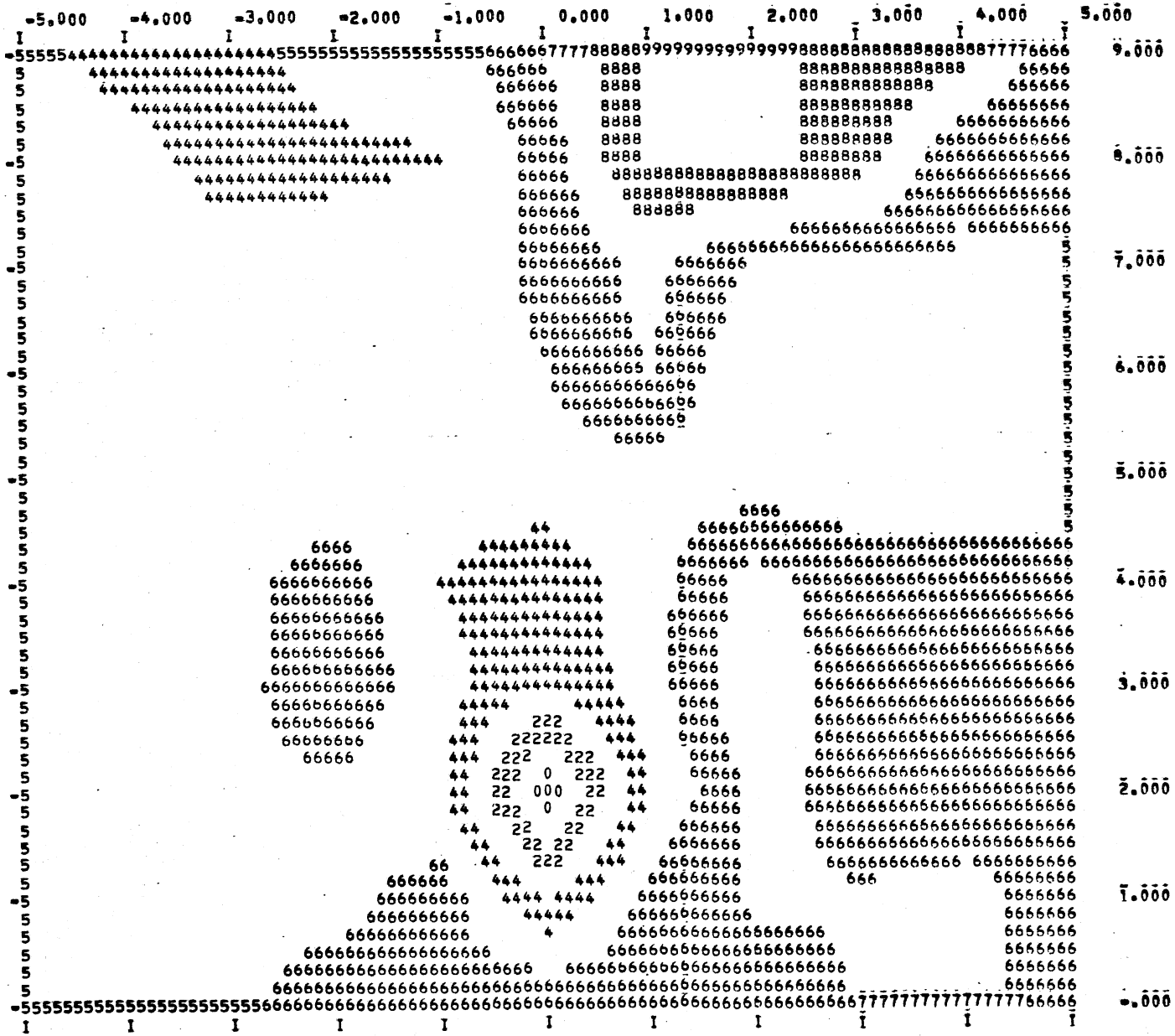

Fig. 44e - Iso-logarithms of Richardson numbers for Run 207. (Horizontal section at z = .20 ft)

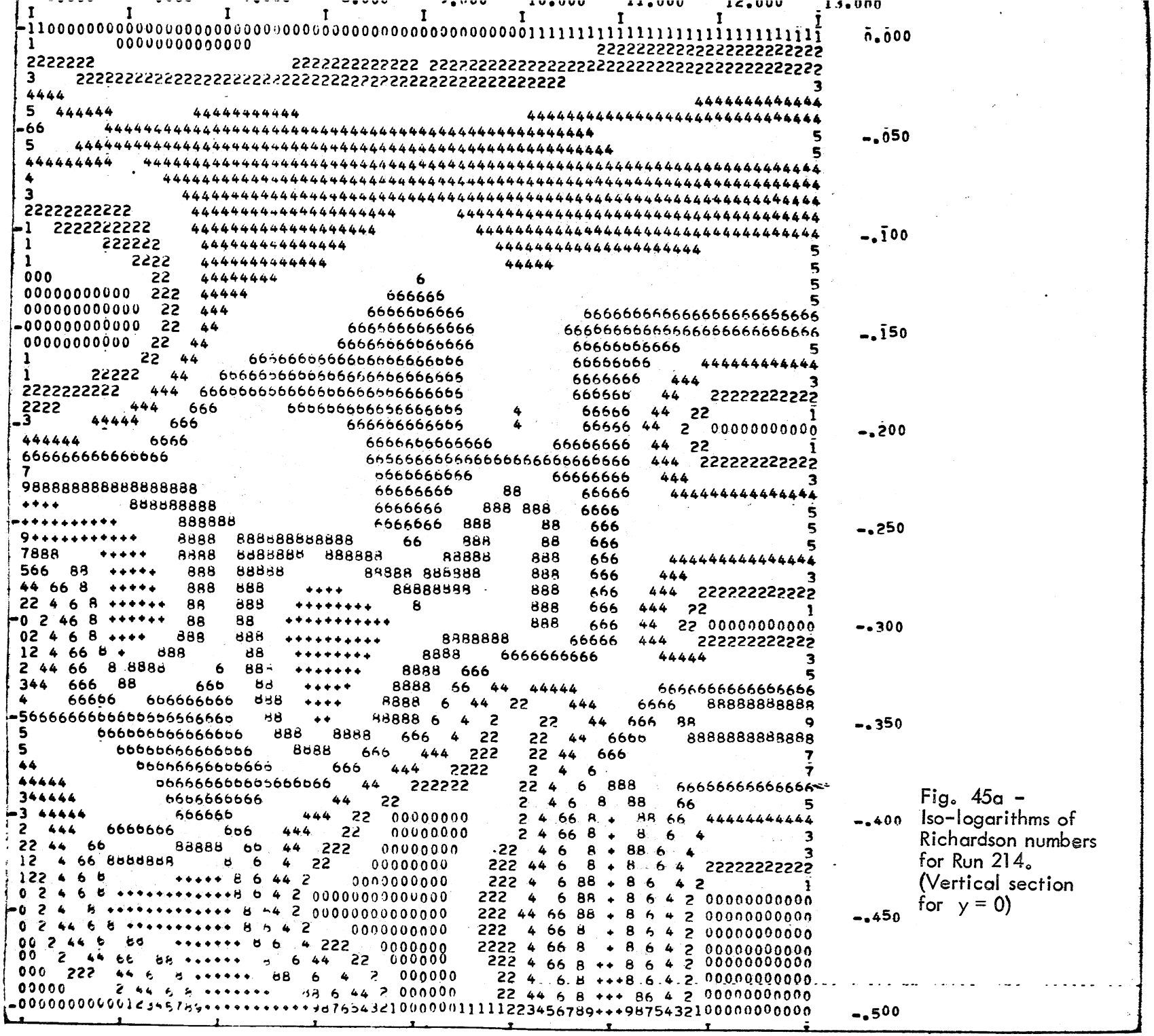

Fig. 45a - Iso-logarithms of Richardson numbers for Run 214. (Vertical section for y = 0)

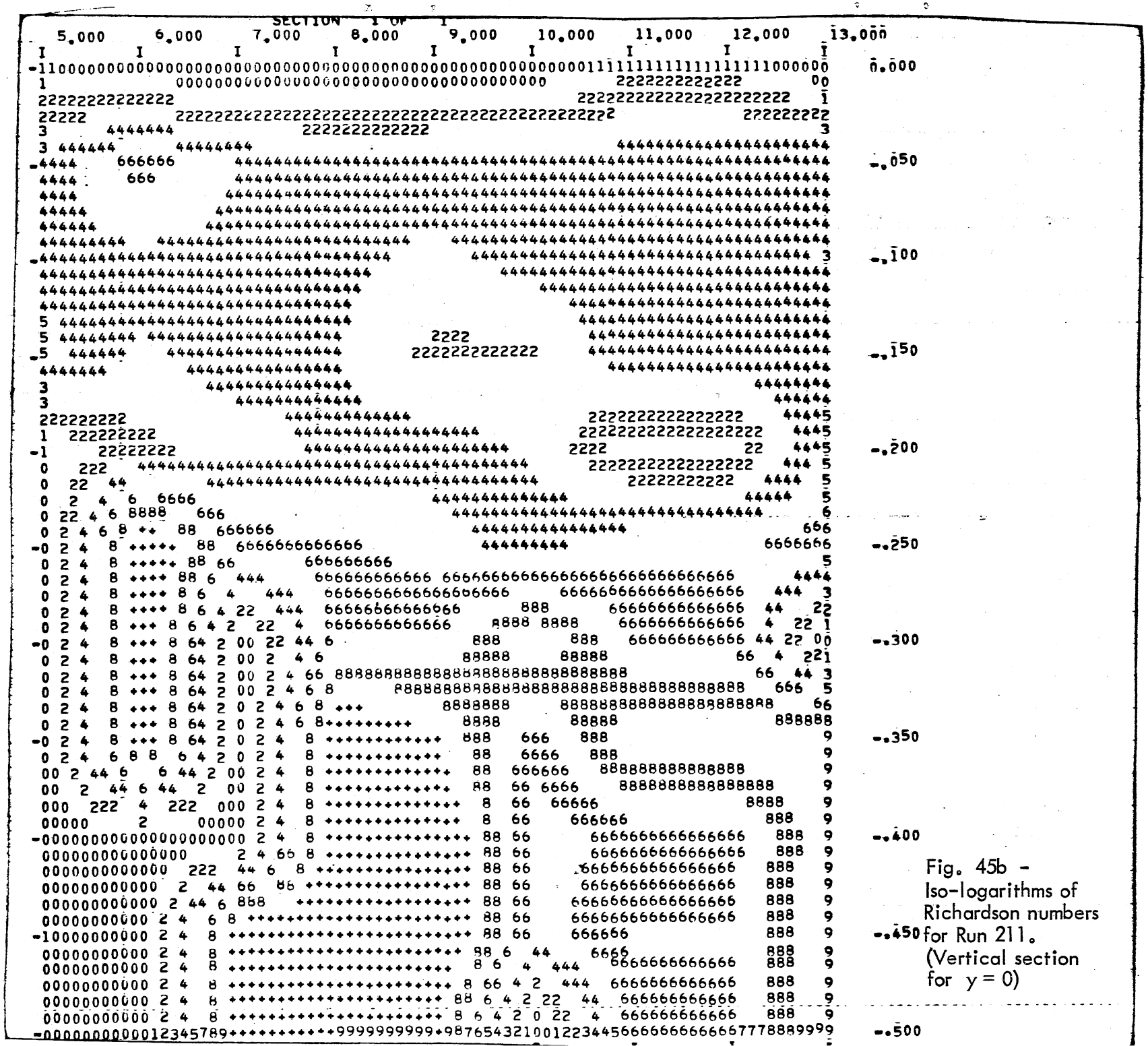

Fig. 45b - Iso-logarithms of Richardson numbers for Run 211. (Vertical section for $y = 0$)

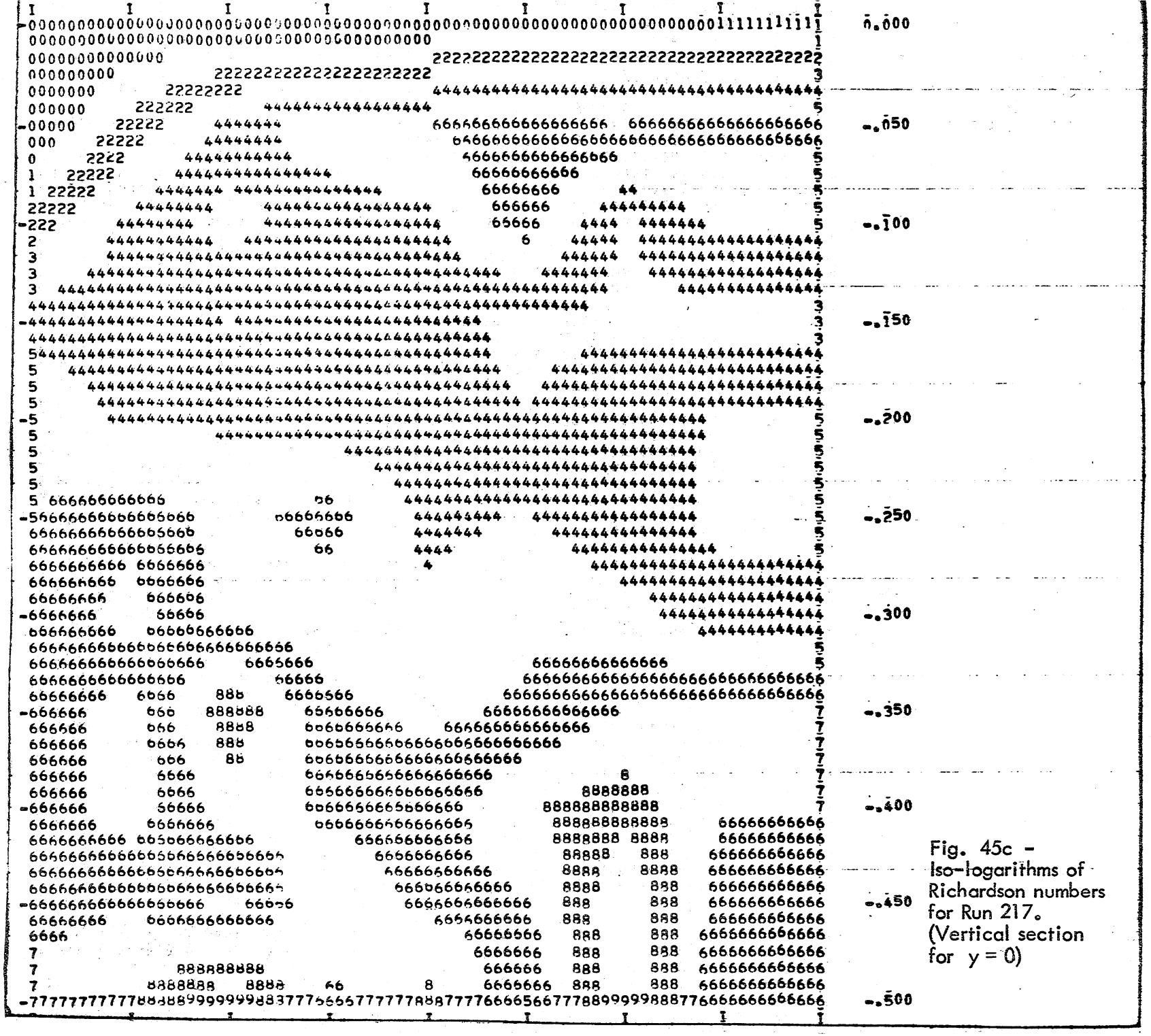

Fig. 45c - Iso-logarithms of Richardson numbers for Run 217. (Vertical section for y = 0)

devices. The logarithm of the Richardson number indicates essentially the order of magnitude and thereby eliminates some of the measurement errors except in those areas in which gradients are very small.

By the above rule Richardson numbers in the range $0.1 < Ri < 1$ obtain the symbol 3. It is generally accepted that a density stratification is stable--i.e., turbulent mixing is absent--when $Ri > 1$. Therefore areas with numbers larger than 3 should represent stably stratified flow regions with little or no vertical mixing. Alternate contour bands have been plotted. Figure 44 represents horizontal cross sections. The outlet is at the middle of the bottom. All scales are in feet.

Figure 45 represents vertical cross sections. The outlet is at the upper left. The first impression of Fig. 45 is of a rather disorganized pattern. A closer examination shows, however, the following typical features:

> Near the surface is a thin layer of weak stratification; underneath, a much thicker layer with fairly stable stratification ($1 < Ri < 10$). The thickness of that layer appears to increase with distance from the outlet; underneath that layer more stably stratified fluid and finally the cold water in the tank with Richardson numbers varying rather randomly. In that last layer the velocity and temperature gradients are very small and Richardson numbers are probably meaningless for that reason, because of errors in temperature and velocity measurements.
>
> Near the outlet the patterns differ depending on the outlet Froude number. In Run 214 ($F_o < 1$) a cold water wedge is formed in the channel and its effect on Richardson numbers is clearly apparent. The flow as it leaves the outlet has a stable thermocline at approximately one-third of the depth, but both the top and the bottom are unstable. In Run 211 the stability near the outlet increases from top to bottom of the outlet channel. The lower two-thirds are stably stratified. In Run 217 ($F_o \simeq 4$) the major portion of the outlet flow is unstably stratified.

Flow Regime of Thermal Plume

It has been shown that the heated water surface jet is subject to inertial and buoyant forces, the interplay of which largely determines the behavior of the jet. This interaction is uninhibited by solid walls, and one might therefore expect that the flow regime which the surface jet assumes is one in accordance with the minimum energy principle. In using the analytical model described it was found that the buoyant surface jet tends toward a regime with a specific local densimetric Froude number as defined in Eq. (4). In the absence of currents and wind this number was found to be

close to 3.0. Figure 46 illustrates the situation for the laboratory experiments. The value of 3.0 must be considered representative for an internally critical flow. Usually critical, gravity controlled flows are associated with Froude numbers equal to unity. The value 3.0 arises because of the definition of F^* (on the main trajectory) as given in Eq. (4). If instead of F^* the ratio of inertial to buoyant forces in a cross section is used, one finds that with

$$I = \frac{\varrho}{2} u_i^2 \, a_i \, b_i \, f_3 \tag{73}$$

for the inertial forces and

$$B = \int_{-nb}^{nb} \int_{0}^{ma} \varrho^*(x,y,z) \, zgdzdr$$

$$= g\varrho_i(x,0,0)\lambda_v \, a_i^2 \, b_i \, f_5\{1 - \exp[-\frac{1}{2}(\frac{m}{\lambda_v})^2]\} \tag{74}$$

for the buoyancy forces, the ratio is equal to 0.545 F^*. The critical value of the ratio then is close to 1.6. Values of $\lambda_v = \lambda_h = 1.05$ and $m = n = 3$ were used to arrive at this result.

Experimental data on densimetric Froude numbers show them to be somewhat smaller than predicted, as is also shown in Fig. 46. A sharp dropoff in experimental values occurs at approximately 6 ft from the outlet, possibly because of density stratification in the tank.

In the absence of wind and cross-currents the heated water jet thus appears to tend toward a very specific flow regime. In the process the flow appears to reduce its overall entrainment coefficient drastically, as shown in Fig. 47.

When a cross-current or wind is present, it is not clear whether the flow regime should be defined in terms of the total densimetric Froude number F or the relative densimetric Froude number F^* as defined in Eq. (4). It is also questionable whether a specific regime is reached in all situations. Therefore the conclusions of the preceding paragraphs should be applied only to situations without wind or current.

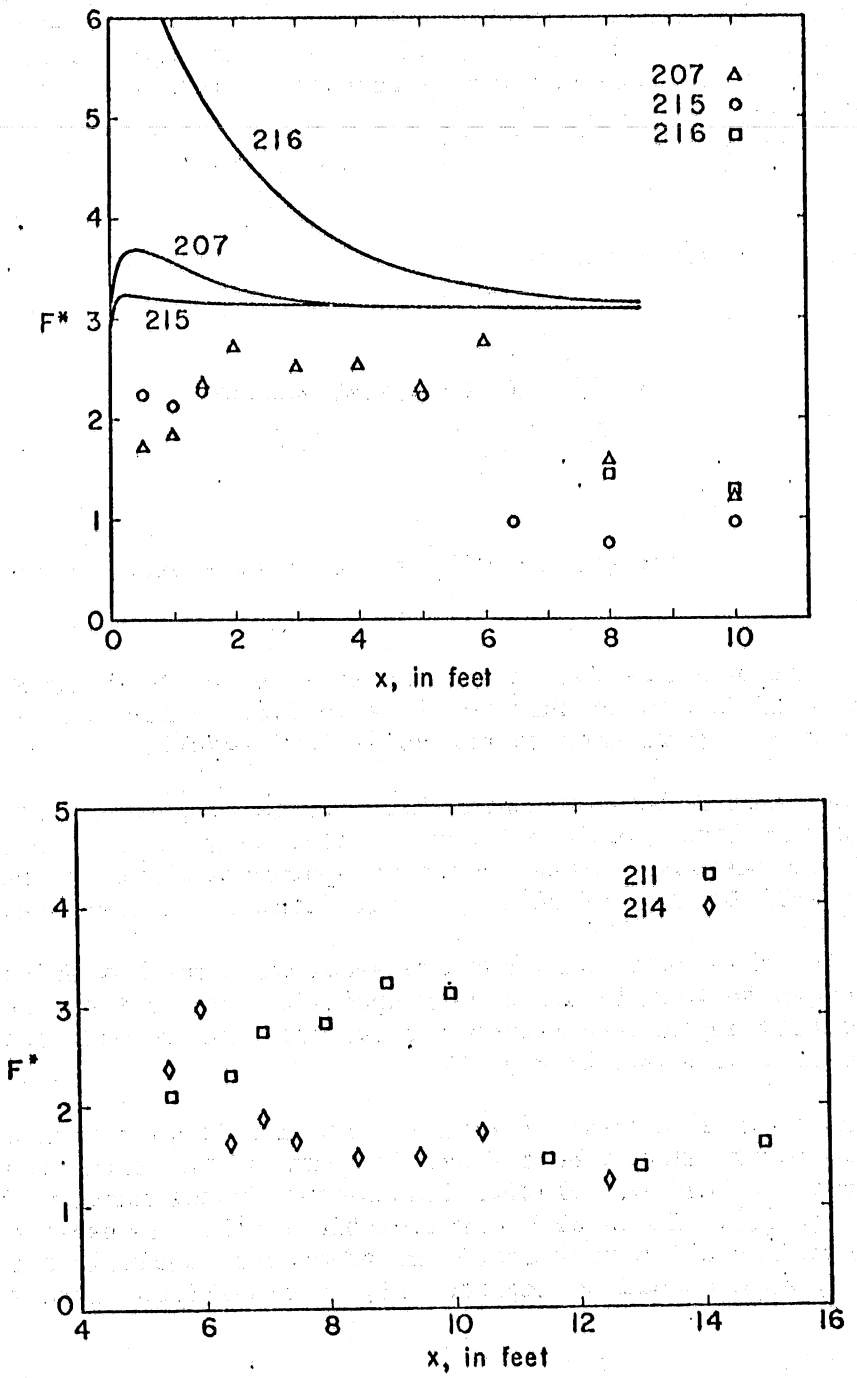

Fig. 46 - Densimetric Froude Numbers versus Distance on Main Trajectory. Analytical Model Predictions (solid lines) and Experimental Data

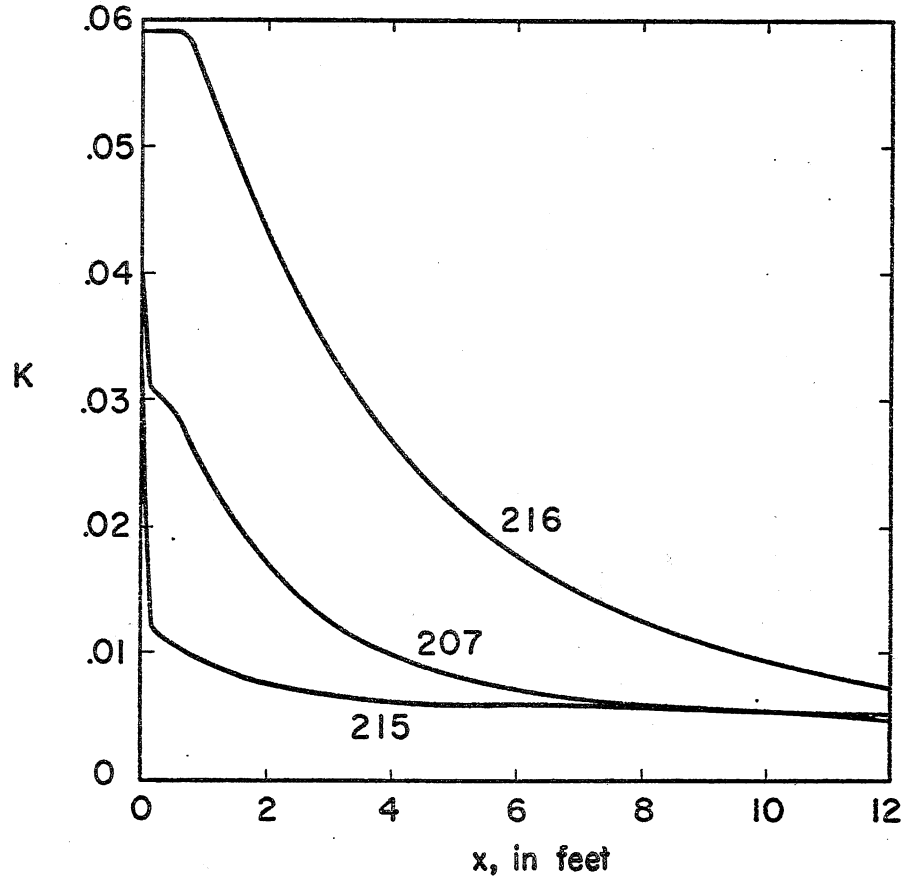

Fig. 47 - Entrainment Coefficients versus Distance along Main Trajectory for several experimental conditions as found from the Analytical Model

SECTION VII

ACKNOWLEDGMENTS

In the course of this study Mr. P. Vaidyaraman, Mr. W. Geiger, Mr. Glen Martin, and Mr. K. Streed provided valuable assistance. Their participation in various phases of the project is gratefully acknowledged. The manuscript of this report was edited and typed by Mrs. Shirley Kii.

The help and encouragement of Dr. Mustafa Shirazi, the Project Officer, are gratefully acknowledged.

SECTION VIII

REFERENCES

[1] "Biological Aspects of Thermal Pollution," edited by P. A. Krenkel and F. L. Parker, Proc. of the National Symposium on Thermal Pollution, Portland, Oregon, June 1968.

[2] Presentation prepared by the staff of the National Water Quality Laboratory of the FWQA, Duluth, Minnesota, for the Joint Commission on Atomic Energy, November 1969.

[3] Jensen, L. D.; Davies, R. M.; Brooks, A. S., and Meyers, C. D. The Effects of Elevated Temperature upon Aquatic Invertebrates, A Review of the Literature, Res. Rep. No. 4, Res. Proj. RP-49, Department of Geography and Environmental Engineering, The Johns Hopkins University, September 1969.

[4] Parker, F. L. and Krenkel, P. A., Thermal Pollution, Status of the Art, Rep. No. 3, Dept. of Environmental and Water Resources Engineering, Vanderbilt University, December 1969.

[5] Thermal Pollution - 1968, hearings before the Subcommittee on Air and Water Pollution of the Committee on Public Works, U.S. Senate, Parts 1, 2, 3, and 4.

[6] Edinger, J. E. and Polk, E. M., Initial Mixing of Thermal Discharges into a Uniform Current, Rep. No. 1, Department of Environmental and Water Resources Engineering, Vanderbilt University, October 1969.

[7] Wada, A., A Study on Phenomena of Flow and Thermal Diffusion Caused by Outfall of Cooling Water, Tech. Rep. C-66006, Central Research Institute of Electric Power Industry, Tokyo, January 1967.

[8] Wada, A., Numerical Analysis of Distribution of Flow and Thermal Diffusion Caused by Outfall of Cooling Water, Tech. Rep. C-67004, Central Research Institute of Electric Power Industry, Tokyo, January 1969.

[9] Hoopes, J. A.; Zeller, R. W.; and Rohlich, G. A., Heat Dissipation and Induced Circulation from Condenser Cooling Water Discharges into Lake Monona, Rep. No. 35, Eng. Exp. Station, Univ. of Wisconsin, February 1968. (See also Zeller, R. W., Hoopes, J. A. and Rohlich, G. A., "Heated Surface Jets in Steady Cross Current," Proc. ASCE, Jrl. Hydr. Div., September 1971, pp. 1403-1426.)

[10] Carter, H. H., A Preliminary Report on the Characteristics of a Heated Jet Discharged Horizontally into a Traverse Current - Part I - Constant Depth, Tech. Rep. No. 61, Chesapeake Bay Institute, Johns Hopkins University, November 1969.

[11] Motz, L. H. and Benedict, B. A., Heated Surface Jet Discharged into a Flowing Ambient Stream, Rep. No. 4, Dept. of Environmental and Water Resources Engineering, Vanderbilt University, August 1970.

[12] Cederwall, K., "Dispersion Phenomena in Coastal Environments," reprint from the Journal of the Boston Society of Civil Engineers, January 1970.

[13] Hayashi, T. and Shuto, N., "Diffusion of Warm Water Jets Discharged Horizontally at the Water Surface," Proc. 12th Congr., IAHR, Colorado, Vol. 4, September 1967.

[14] Stolzenbach, K. D. and Harleman, D. R. F., An Analytical and Experimental Investigation of Surface Discharges of Heated Water, Rep. No. 135, Ralph M. Parsons Laboratory for Water Resources and Hydrodynamics, Mass. Inst. of Tech., February 1971.

[15] Koh, R. C. Y. and Fan, L. N., Mathematical Models for the Prediction of Temperature Distributions Resulting from the Discharge of Heated Water into Large Bodies of Water, 16130 DWO 10/70, Water Pollution Control Research Series, EPA, October 1970.

[16] Platten, J. L. and Keffer, J. F., Entrainment in Deflected Axisymmetric Jets at Various Angles to the Stream, Mech. Eng. T.P. 6808, Univ. of Toronto, June 1968.

[17] Bowley, W. W. and Sucec, J., "Trajectory and Spreading of a Turbulent Jet in the Presence of a Cross Flow of Arbitrary Velocity Distribution," Tech. Paper 69-GT-33, ASME, March 1969.

[18] Silberman, E. and Stefan, H., Physical (Hydraulic) Modeling of Heat Dispersion in Large Lakes: A Review of the State of the Art, Report ANL/ES-2, Argonne National Laboratory, August 1970.

[19] Wiegel, R. L.; Mobarek, I.; and Jen, Y., Discharge of Warm Water Jet over Sloping Bottom, Rep. HEL 3-4, Hydraulic Engineering Laboratory, Univ. of California, November 1964.

[20] Jen, Y.; Wiegel, R. L.; and Mobarek, I., "Surface Discharge of Horizontal Warm Water Jets," Proc. ASCE, Jrl. Power Div., April 1966.

[21] Tamai, N.; Wiegel, R. L.; and Tornberg, G. F., "Horizontal Discharge of Warm Water Jets," Proc. ASCE, Jrl. Power Div., October 1969.

[22] Stefan, H. and Schiebe, F. R., "Heated Discharge from Flume into Tank," Proc. ASCE, Jrl. Sanitary Eng. Div., December 1970.

[23] Kashiwamura, M. and Yoshida, S., "Outflow Pattern of Fresh Water Issued from a River Mouth," Coastal Engineering in Japan, Vol. 10, 1967.

[24] Wood, I. R. and Wilkinson, D. L., discussion of "Surface Discharge of Horizontal Warm-Water Jet," by Jen, Wiegel, and Mobarek, Proc. ASCE, Jrl. Power Div., Vol. 93, No. PO1, March 1967, pp. 149-151.

[25] Cheney, W. O. and Richards, G. V., Ocean Temperature Measurements for Power Plant Design, Pacific Gas and Electric Company, date not shown.

[26] Fitch, N. R., Temperature Surveys of St. Croix River, 1969-1970, Environmental Monitoring Program, Northern States Power Company, December 31, 1970.

[27] Squire, James L., Jr., Surface Temperature Gradients Observed in Marine Areas Receiving Warm Water Discharges, Tech. Paper No. 11, Bureau of Sport Fisheries and Wildlife, January 1967.

[28] Ackers, P., "Modeling of Heated Water Discharges," Chapter 6 of Engineering Aspects of Thermal Pollution, edited by F. L. Parker and P. A. Krenkel, Proc. of the National Symposium on Thermal Pollution, Vanderbilt University, 1968.

[29] Asbury, J. G.; Grench, R. E.; Nelson, D. M.; Prepejchal, W.; Romberg, G. P.; and Siebold, P., A Photographic Method for Determining Velocity Distributions within Thermal Plumes, Rep. ANL/ES-4, Argonne National Laboratory, February 1971.

[30] Fan, L. N. and Brooks, N. H., Numerical Solutions of Turbulent Buoyant Jet Problems, Rep. No. KH-R-18, W. M. Keck Laboratory of Hydraulics and Water Resources, January 1969.

[31] Rouse, H.; Yih, C. S.; and Humphreys, H. W., "Gravitational Convection from Boundary Source," Tellus, Vol. 4, No. 3, August 1952, pp. 201-210.

[32] Abraham, G., "Horizontal Jets in Stagnant Fluid of Other Density," Proc. ASCE, Jrl. Hydr. Div., July 1965, pp. 139-154.

[33] Fan, L. N. and Brooks, N. H., discussion of "Horizontal Jets in Stagnant Fluid of Other Density," Proc. ASCE, Jrl. Hydr. Div., March 1966.

[34] Abramovich, G. N., The Theory of Turbulent Jets, Massachusetts Institute of Technology Press, Cambridge, Mass., 1963.

[35] Gordier, R. L., Studies on Fluid Jets Discharging Normally into Moving Liquid, Technical Paper No. 28-B, St. Anthony Falls Hydraulic Laboratory, Univ. of Minnesota, 1959.

[36] Stefan, H., "Stratification of Flow from Channel into Deep Lake," Proc. ASCE, Jrl. Hydr. Div., July 1970.

[37] Albertson, M. L.; Dai, Y. B.; Jensen, R. A.; and Rouse, H., "Diffusion of Submerged Jets," Trans. ASCE, Vol. 115, 1950, pp. 639-697.

[38] Folsom, R. G. and Ferguson, C. K., "Jet Mixing of Two Liquids," Trans. ASME, January 1949, pp. 73-77.

[39] Rossby, C. G. and Montgomery, R. B., "The Layer of Frictional Influence in Wind and Ocean Currents," Papers in Physical Oceanography and Meteorology, Vol. 3, No. 3, 1935.

[40] Parr, A. E., "On the Probable Relationship between Vertical Stability and Lateral Mixing Processes," Conseil Permanent International pour l'exploration de la Mer, Jrl. du Conseil, Vol. 11, No. 3, 1936.

[41] Munk, W. H. and Anderson, E. R., "Notes on a Theory of the Thermocline," Jrl. of Marine Research, Vol. 7, 1948.

[42] Ellison, T. H. and Turner, J. S., "Turbulent Entrainment in Stratified Flows," Jrl. of Fluid Mechanics, Vol. 6, Part 3, October 1959.

[43] Kato, H. and Phillips, O. M., "On the Penetration of a Turbulent Layer into a Stratified Fluid," Jrl. of Fluid Mechanics, Vol. 37, Part 4, July 1969.

[44] Wada, A., Numerical Analysis of Distribution of Flow and Thermal Diffusion Caused by Outfall of Cooling Water, Tech. Rep. C 67004, Central Res. Inst. of Electric Power Industry, January 1969.

[45] Sundaram, T. R. and Rehm, R. G., "Formation and Maintenance of Thermoclines in Stratified Lakes Including the Effects of Power-Plant Thermal Discharges," AIAA 8th Aerospace Science Meeting, New York, January 1970.

[46] Fan, Loh-Nien, Turbulent Buoyant Jets into Stratified or Flowing Ambient Fluids, Rep. No. KH-R-15, W. M. Keck Laboratory of Hydraulics and Water Resources, June 1967.

[47] Abbott, M. B., "On the Spreading of One Fluid over Another," La Houille Blanche, Vol. 16, No. 6, 1961, pp. 827-846.

[48] Edinger, J. E.; Duttweiler, D. W.; and Geyer, J. C., "The Response of Water Temperatures to Meteorological Conditions," Water Resources Research, Vol. 4, No. 5, October 1968, pp. 1137-1143.

[49] Roll, H. U., Physics of the Marine Atmosphere, International Geophysics Series, Vol. 7, Academic Press, New York, 1965.

[50] Wada, A., Effect of Winds on a Two-Layered Bay, Tech. Rep. C-66002, Central Research Institute of the Electric Power Industry, Tokyo, September 1966.

[51] Brady, D. K.; Graves, W. L., Jr.; and Geyer, J. C., Surface Heat Exchange at Power Plant Cooling Lakes, Report No. 5, Project RP-49, Department of Geography and Environmental Engineering, Johns Hopkins University, November 1969.

[52] Wilkinson, D. L. and Wood, I. R., "A Rapidly Varied Flow Phenomenon in a Two-Layer Flow," Jrl. of Fluid Mechanics, Vol. 47, Part 2, May 1971, pp. 241-256.

[53] Stefan, H. and Schiebe, F. R., Experimental Study of Warm Water Flow into Impoundments. Part III: Temperature and Velocity Fields Near a Surface Outlet in Three-Dimensional Flow, Project Report No. 103, St. Anthony Falls Hydraulic Laboratory, Univ. of Minnesota, December 1968.

[54] Wada, A., "A Study of Mixing Process in the Sea Caused by Outfall of Industrial Warm Water," Coastal Engineering in Japan, Vol. XII, 1969, pp. 147-158.

Appendix A

COMPUTER PROGRAM FOR ANALYTICAL MODEL
(FORTRAN IV)

```
      PROGRAM PLUME (INPUT,OUTPUT)
C ST CROIX FIELD DATA,  SEPTEMBER 4,1969
      DIMENSION Q(200),T(200),U(200),A(200),B(200),DELRO(200),H(200),
     1 ALFA(200),X(200),Y(200),XL(200),YL(200),XR(200),YR(200),K(200),
     2 MO(200),F(200),AREA(200)
      REAL M,N,L,K1,KS,KH,K,KV,MO,MOO,KRATIO
      N=3.0
      M=3.0
      L=1.05
C INTEGRATION COEFFICIENTS
      F1=3.1415*(ERFN(N/SQRT(2.)))*(ERFN(M/SQRT(2.)))
      F2=F1*(L**2./(L**2.+1.))
      F3= 3.1415*(ERFN(N))*(ERFN(M))/2.
      F4=F1*L**2.
      F5=L*(ERFN(N/SQRT(2.)))*(SQRT(3.1415*2.))
      F6=EXP(-.5)
      PRINT 32
   32 FORMAT (1H1,//,52X,*HEATED WATER PLUME CHARACTERISTICS*,///)
      PRINT 11
   11 FORMAT( //,8X,*F1*,11X,*F2*,11X,*F3*,11X,*F4*,11X,*F5*,11X,*F6*)
      PRINT 20,F1,F2,F3,F4,F5,F6
   20 FORMAT(/,6F13.3,//)
C EMPIRICAL COEFFICIENTS
      C4=0.081
      C5=0.4
      KHAMB=0.082
C DRAGCOEFFICIENT
      CD=1.
C STEP LENGTH
      DS=10.
      NSTEP=200
C CURRENT VELOCITY
      US=.033
C WIND CONDITIONS
      WIND=10.
      BETA=9.*3.1415/8.
C WIND SHEAR STRESS
      ROAIR=0.0030
      W=WIND*(5280.0/3600.)
      IF(W.LE.30.5) GO TO 1
      IF(W.GT.30.5) GO TO 2
    1 STRECO=0.0010
      GO TO 3
    2 STRECO=0.0021
    3 TAUW=STRECO*ROAIR*W**2
      PRINT 53
   53 FORMAT (40X,*US(FT/SEC)*,10X,*W(FT/SEC)*,10X,*TAUW(LBS/SQ. FT)*,/)
      PRINT 104,US,W,TAUW
  104 FORMAT (40X,1F8.2,10X,1F8.3,10X,1F8.4,///)
C SOLAR RADIATION AND DEW POINT TEMPERATURE
      HS=87./3600.
      TD=74.
C INITIAL CONDITIONS
      RINV=1.0E-30
      ALFAO=3.1415/2.
      QO=660.
      TO=93.1
```

```
      TC=77.5
      DPO=10.
      WIDO=195.
C INITIAL SURFACE HEAT TRANSFER PARAMETERS
      TM=(T(1)+TC+TD)/2.
      BET=.255-.0085*TM+.000204*TM**2.
      FUWI=70.+.7*WIND**2.
      KS=(15.7+(BET+.26)*FUWI)/(3600.*24.)
      EQU=TD+HS/KS
      PRINT 51
   51 FORMAT(40X,*KS (BTU/SQFT SEC DEGF)*,5X,*EQUILIBRIUM TEMP (DEG F)*)
      PRINT 60,KS,EQU
   60 FORMAT(/,33X,2G25.4,//)
C COLD WATER DENSITY
      TCC=(5./9.)*(TC-32.)
      RHOCC=1.-(6.*TCC**2.-36.*TCC+47.)*.0000001
      RHOTC=RHOCC*62.43/32.17
C INITIAL DENSITY DIFFERENTIAL
      TCEL=(5./9.)*(TO-32.)
      RHOC=1.-(6.*TCEL**2.-36.*TCEL+47.)*.0000001
      RHO=62.43*RHOC/32.17
      DELROO=RHOTC-RHO
C INITIAL PARAMETERS
   96 UO=QO/(DPO*WIDO)
      FO =UO/(((DELROO/1.94)*32.2*DPO)**.5)
      MOO=1.94*QO**2/(WIDO*DPO)
C STARTING CONDITIONS
      ALFA(1)=ALFAO
      Q(1)=QO
      T(1)=TO-TC
C INITIAL STANDARD DEVIATIONS
      AA=1.94*Q(1)*F3
      BB=2.*1.94*Q(1)*US*COS(ALFA(1))*F1-MOO*F1
      CC=0.5*1.94*3.1415*US**2*(COS(ALFA(1)))**2*M*N*Q(1)-0.5*MOO*3.1415
     1*US*COS(ALFA(1))*M*N
      CX=BB**2-4.*AA*CC
      U(1)=(-BB+SQRT(CX))/(2.*AA )
      A(1)=DPO/L
      B(1)=Q(1)/(A(1)*(U(1)*F1+0.5*3.1415*US*COS(ALFA(1))*M*N ))
C INITIAL COORDINATES
      X(1)=.0
      Y(1)=.0
C INITIAL HEAT AND MOMENTUM FLUXES
      H(1)=U(1)*T(1)*A(1)*B(1)*F2+US*COS(ALFA(1))*T(1)*A(1)*B(1)*F4
      MO(1)=(U(1)**2.*A(1)*B(1)*F3+2.*US*COS(ALFA(1))*A(1)*B(1)*F1*U(1)
     1+US**2.*COS(ALFA(1))**2.*N*M*A(1)*B(1)*3.1415/2.)*1.94
      I=1
C DENSITY DIFFERENTIAL
  150 TCEL=(5./9.)*(T(I)+TC-32.)
      RHOC=1.-(6.*TCEL**2.-36.*TCEL+47.)*.000001
      RHO=62.43*RHOC/32.17
      DELRO(I)=RHOTC-RHO
C DENSIMETRIC FROUDE NUMBER
      F(I)=U(I)/(((DELRO(I)/1.94)*32.2*L*A(I))**.5)
      IF (F(1) .GE. 3.0)  GO TO 95
      DPO=.95*DPO
      GO TO 96
   95 IF (I .GT. 1) GO TO 97
```

```
  501 FORMAT (50X,*U0(FT/SEC)*,10X,*F0*,/)
      PRINT 500,U0,F0
  500 FORMAT (47X,2G15.3,/)
C ENTRAINMENT COEFFICIENTS
   97 IF(U(I)/(US*COS(ALFA(I))).LE.0.1) KH=KHAMB
      KV=(1.0-1.33*ALOG(6.32/F(I)))
      IF (KV.GT.1.0) KV=1.0
       IF(KV.LT.0.0) KV=0.0
      KH=.059
      KV=KH*KV
      K(I)=(KH*A(I)+KV*B(I))/ (A(I)+B(I))
C PRINTOUT OPTION 1
      IF (I .GT.1) GO TO 555
      PRINT 31
   31 FORMAT (3X,*N*,6X,*X(FT)*,6X,*Y(FT)*,6X,*Q(CFS)*,5X,*T(DEG F)*,3X,
     1*A(FT)*,6X,*B(FT)*,6X,*U(FT/SEC)*,2X,*H(BTU/SEC)*,2X,*MO(LBS)*,5X,
     2*ALFA*,10X,*FR*,//)
  555 PRINT 40, I,X(I),Y(I),Q(I),T(I),A(I),B(I),U(I),H(I),MO(I),ALFA(I),
     1F(I)
   40 FORMAT (1X,I3,3X,9F11.2,1F11.4,1F11.2)
C NEW FLOW RATE
      DQ=K(I)*U(I)*(A(I)+B(I))*3.1415*DS*SQRT(2.0)/2.
      Q(I+1)=Q(I)+DQ
C SURFACE HEAT TRANSFER COEFFICIENTS
      TM=(T(I)+TC+TD)/2.
      BET=.255-.0085*TM+.000204*TM**2.
      FUWI=70.+.7*WIND**2.
      KS=(15.7+(BET+.26)*FUWI)/(3600.*24.)
      EQU=TD+HS/KS
C HEATLOSS
      HLOSS=(F5*B(I)*T(I)+(TC-EQU)*2.*N*B(I))*DS*KS/62.4
      H(I+1)=H(I)-HLOSS
C FIND FRICTION FORCE DF
      VISC=.000019142/(.471101+.0143454*(T(I)+TC)+.0000682074*
     1(T(I)+TC)**2.)
      DFLAM=- VISC*EXP(-0.5)*(A(I)**2+B(I)**2)/(A(I)*B(I))*1.965*U(I)
      DF=(KH-K(I))*DFLAM/KH*(-1.)
C FIND WIND FORCE FW
      FW=TAUW*2.*N*B(I)*DS
C NEW MOMENTUM AT I+1
      GAMA=BETA-ALFA(I)
      DMO=DF+FW*COS(GAMA)
      MO(I+1)=MO(I)+DMO
C NEW ANGLE OF MAIN TRAJECTORY AT I+1
      DD=CD*1.94*(US*SIN(ALFA(I)))**2.*M*A(I)*DS/2.
      RINV=(DD-FW*SIN(GAMA))/MO(I)
      DALFA= (ABS(RINV)**.667)*DS*COS(ALFA(I))*RINV/ABS(RINV)
      ALFA(I+1)=ALFA(I)-DALFA
C FIND NEW AREA AT I+1
      K1=US*COS(ALFA(I+1))*2.*N*M
      Z1=F3
      Z2= F1*(K1/(N*M)-MO(I+1)/(1.94*Q(I+1)))
      Z3= 3.1415*K1*(K1/(8.*N*M)-MO(I+1)/(4.*1.94*Q(I+1)))
      ZZ=ABS(Z2)**2.-4.*Z1*Z3
      IF(ZZ.LE.0.0) GO TO 4
      U(I+1)=(-Z2+SQRT(ZZ))/(2.*Z1)
      AREA(I+1)=Q(I+1)/(U(I+1)*F1+K1*3.1415/4.)
```

Appendix B

ZONE OF FLOW ESTABLISHMENT

The analytical method of plume analysis described previously starts with a fully developed jet. Obviously, this condition will not be found at the real point of discharge. The starting point of the analysis presented has therefore been called the virtual origin ($s = 0$). Between the real origin and the virtual origin of the jet is the outlet region or zone of flow establishment. An analytical treatment of the outlet region is possible only if the geometry is not too complicated. Structures such as levees, as well as the bottom topography in shallow receiving waters, may interfere with the formation of a zone of flow establishment. In many cases it may be necessary to resort to physical experimentation to find the location of the virtual origin and the initial flow conditions of the analytical model. Only if the outlet geometry is fairly regular will it be possible to treat the outlet region analytically. In that case it is possible to draw to some extent on information obtained through studies of non-buoyant jet flows. Buoyancy does introduce some important modifications, however. The zone of flow establishment for neutrally buoyant submerged circular jets with initially uniform velocity and temperature has been well documented [37]. The length of the zone of flow establishment was found to be of the order of 6.2 times the diameter of the discharge nozzle. This value can be found from experimental data; for example, by plotting centerline velocities versus distance. Over the length of the zone of flow establishment the velocity will be constant.

The heated water half-jet under consideration is non-circular, buoyant, and non-uniform with respect to velocity at the point of discharge. Typically it may have the features of a fully developed channel flow before entering the reservoir. The initial conditions for the zone of flow establishment are a temperature distribution of the form

$$T^*(0,r,z) = T^*(0,0,0) = \text{const} \tag{75}$$

$$\text{for} \quad r \leq \frac{w_o}{z} \quad \text{and} \quad z \leq d_o$$

and a velocity distribution

$$u(0,r,z) = u(0,0,0)\ f(r,z) \tag{76}$$

where $f(r,z)$ may be any function suitable for describing the discharge velocity profile, for example

$$f(r,z) = \left[1 - \left(\frac{z}{d_o}\right)^{n_1}\right]\left[1 - \left(\frac{r}{w_o/2}\right)^{n_2}\right] \qquad (77)$$

for a rectangular channel, with n_1 and n_2 being constants.

In the zone of flow establishment the temperature profile will transit from the form given by Eq. (75) to that given by Eq. (2), while the velocity distribution will transit from Eq. (76) to Eq. (1). The details will be governed largely by the free-shear turbulence generated by shear stresses between discharged and ambient water.

The length of the zone of flow establishment (x_o) for buoyant surface jets cannot be measured as easily as for non-buoyant ones, because buoyancy induces an acceleration in the longitudinal direction near the outlet which masks the end of the zone of flow establishment. To obtain information on (x_o) one must therefore examine velocity distributions rather than centerline velocities. Figure 33 illustrates some of the velocity distributions obtained by computer plotting. For the evaluation of x_o these are not accurate enough due to interpolation errors. Instead, graphs of actually measured velocities such as are given in Figs. 29 through 34 of Ref. [53] must be used. These measurements, all of which refer to strongly buoyant jets, indicate that it takes less than six times the width of the outlet channel to develop a horizontal velocity profile and less than six times the depth to develop a vertical velocity profile. The measurements were not sufficiently detailed to enable evaluation of a dependence between densimetric Froude number at the discharge F_o, as defined in Eq. (45), and x_o. It appears that for experiments 215, 207, 214, and 211, summarized in Table 1, x_o was very approximately equal to three times the outlet width.

The mechanism which produces this result is probably not horizontal momentum transfer by eddy diffusivity, but rather a secondary effect of the buoyancy-induced horizontal currents shown in Fig. 28. The currents move high-momentum fluid from the center of the plume toward the edges, where the shallow thickness of the flow activates shear stresses in horizontal planes which reduce the momentum of the flow rapidly. The same horizontal transport mechanism applies in part also to heat. Thus the zone of flow establishment for velocity and temperature is shortened by buoyancy effects, as stated earlier.

From some of the data on spreading angles at the outlet presented in Fig. 39 it might be gathered that buoyancy effects become small if $F_o > 10$. Zones of flow establishment for temperature may be somewhat longer than those for velocity. All the above results apply to straight jets rather than curved ones.

Once the length of the zone of flow establishment has been determined, an approximate analytical treatment of the zone of flow establishment can be given analogous to that found in treatments of non-buoyant jet

flows [37]. For high values of F_o ($F_o > 10$ perhaps) results regarding the flow rate and the dimensions of the jet at the end of the zone of flow establishment can be taken directly from the literature [37]. In the intermediate range ($1 < F_o < 10$) the velocity distribution can be approximated by a function of the form

$$u^*(s,r,z) = u^*(0,0,0) = U_o \tag{78}$$

for the inner core region ($r < w/2$ and $z < d$) and

$$u^*(s,r,z) = u^*(0,0,0) \exp\left[\frac{-(z-d)^2}{2a^2}\right] \exp\left[\frac{-(r-w)^2}{2b^2}\right] \tag{79}$$

for the turbulent diffusion region ($r > w/2$ and $z > d$). The dimensions of the core region can be assumed to decrease linearly with distance such that

$$\frac{w}{w_o} = 1 - \frac{x}{x_o} \tag{80}$$

and

$$\frac{d}{d_o} = 1 - \frac{x}{x_{o,d}} \tag{81}$$

where x_o and $x_{o,d}$ are the lengths of the zone of flow establishment for width and depth, respectively, for velocity. Turbulent entrainment in the zone of flow establishment is different from that in fully developed flow. In a turbulent, non-buoyant, circular jet the entrainment coefficient varies linearly from virtually zero to $K = 0.059$ over the length of the zone of flow establishment. A similar variation can be introduced for the zone of flow establishment for buoyant surface jets.

In the total picture the computational scheme developed for fully developed jets can be extended to include a zone of flow establishment. For very low densimetric Froude numbers (tentatively $F_o < 3$) the zone of flow establishment is very short and the computational scheme developed is applicable without further extension. For high densimetric Froude numbers (tentatively $F_o > 10$) the zone of flow establishment can be treated as non-buoyant. Only in the intermediate range would the extension of the analytical model as presented be of value.